



University of Kentucky  
UKnowledge

---

University of Kentucky Doctoral Dissertations

Graduate School

---

2005

## INVESTIGATION OF RECTANGULAR CONCRETE COLUMNS REINFORCED OR PRESTRESSED WITH FIBER REINFORCED POLYMER (FRP) BARS OR TENDONS

Ching Chiaw Choo  
*University of Kentucky*

[Right click to open a feedback form in a new tab to let us know how this document benefits you.](#)

---

### Recommended Citation

Choo, Ching Chiaw, "INVESTIGATION OF RECTANGULAR CONCRETE COLUMNS REINFORCED OR PRESTRESSED WITH FIBER REINFORCED POLYMER (FRP) BARS OR TENDONS" (2005). *University of Kentucky Doctoral Dissertations*. 309.

[https://uknowledge.uky.edu/gradschool\\_diss/309](https://uknowledge.uky.edu/gradschool_diss/309)

This Dissertation is brought to you for free and open access by the Graduate School at UKnowledge. It has been accepted for inclusion in University of Kentucky Doctoral Dissertations by an authorized administrator of UKnowledge. For more information, please contact [UKnowledge@lsv.uky.edu](mailto:UKnowledge@lsv.uky.edu).

ABSTRACT OF DISSERTATION

Ching Chiaw Choo

The Graduate School

University of Kentucky

2005

INVESTIGATION OF RECTANGULAR CONCRETE COLUMNS REINFORCED OR  
PRESTRESSED WITH FIBER REINFORCED POLYMER (FRP) BARS OR TENDONS

---

ABSTRACT OF DISSERTATION

---

A dissertation submitted in partial  
fulfillment of the requirements for  
the degree of Doctor of Philosophy  
in the College of Engineering at the  
University of Kentucky

By

Ching Chiaw Choo

Lexington, Kentucky

Director: Issam Elias Harik, Professor of Civil Engineering

Lexington, Kentucky

2005

Copyright © Ching Chiaw Choo 2005

## ABSTRACT OF DISSERTATION

### INVESTIGATION OF RECTANGULAR CONCRETE COLUMNS REINFORCED OR PRESTRESSED WITH FIBER REINFORCED POLYMER (FRP) BARS OR TENDONS

Fiber reinforced polymer (FRP) composites have been increasingly used in concrete construction. This research focused on the behavior of concrete columns reinforced with FRP bars, or prestressed with FRP tendons. The methodology was based the ultimate strength approach where stress and strain compatibility conditions and material constitutive laws were applied.

Axial strength-moment ( $P$ - $M$ ) interaction relations of reinforced or prestressed concrete columns with FRP, a linearly-elastic material, were examined. The analytical results identified the possibility of premature compression and/or brittle-tension failure occurring in FRP reinforced and prestressed concrete columns where sudden and explosive type failures were expected. These failures were related to the rupture of FRP rebars or tendons in compression and/or in tension prior to concrete reaching its ultimate strain and strength. The study also concluded that brittle-tension failure was more likely to occur due to the low ultimate tensile strain of FRP bars or tendons as compared to steel. In addition, the failures were more prevalent when long term effects such as creep and shrinkage of concrete, and creep rupture of FRP were considered. Barring FRP failure, concrete columns reinforced with FRP, in some instances, gained significant moment resistance. As expected the strength interaction of slender steel or FRP reinforced concrete columns were dependent more on column length rather than material differences between steel and FRP.

Current ACI minimum reinforcement ratio for steel ( $\rho_{\min}$ ) reinforced concrete columns may not be adequate for use in FRP reinforced concrete columns. Design aids were developed in this study to determine the minimum reinforcement ratio ( $\rho_{f,\min}$ ) required for rectangular reinforced concrete columns by averting brittle-tension failure to a failure controlled by concrete crushing which in nature was a less catastrophic and more gradual type failure. The proposed method using  $\rho_{f,\min}$  enabled the analysis of FRP reinforced concrete columns to be carried out in a manner similar to steel reinforced concrete columns since similar provisions in ACI 318 were consistently used in developing these aids. The design aids produced accurate estimates of  $\rho_{f,\min}$ . When creep and shrinkage effects of concrete were considered, conservative  $\rho_{f,\min}$  values were obtained in order to preserve an adequate margin of safety due to their unpredictability.

KEYWORDS: Fiber-Reinforced Polymer, Concrete Columns, Premature Compression Failure, Brittle-Tension Failure, Minimum Required Reinforcement Ratio

*Ching Chiau Choo*

March 23, 2005

INVESTIGATION OF RECTANGULAR CONCRETE COLUMNS REINFORCED OR  
PRESTRESSED WITH FIBER REINFORCED POLYMER (FRP) BARS OR TENDONS

By

Ching Chiaw Choo

*Issam Elias Harik*

Director of Dissertation

*Kamyar Mahboub*

Director of Graduate Studies

March 23, 2005

DISSERTATION

Ching Chiaw Choo

The Graduate School

University of Kentucky

2005

INVESTIGATION OF RECTANGULAR CONCRETE COLUMNS REINFORCED OR  
PRESTRESSED WITH FIBER REINFORCED POLYMER (FRP) BARS OR TENDONS

---

DISSERTATION

---

A dissertation submitted in partial  
fulfillment of the requirements for  
the degree of Doctor of Philosophy  
in the College of Engineering at the  
University of Kentucky

By

Ching Chiaw Choo

Lexington, Kentucky

Director: Dr. Issam Elias Harik, Professor of Civil Engineering

Lexington, Kentucky

2005

Copyright © Ching Chiaw Choo 2005



(This page is purposely left blank)

*To my parents Chong Ted Choo and Hung Kiew Ngui  
For their love, support, and patience*

*To my dearest brothers and sisters  
For their love, encouragement and support*

*To my wife Chiau Wei Law with love and gratitude  
For her patience and understanding throughout this endeavor*

*Their love and encouragement made this a reality.*

## ACKNOWLEDGMENTS

The following dissertation, while an individual work, benefited from the insights and direction of a great many persons.

My long time mentor and dissertation chair, Issam E. Harik, exemplifies the high quality scholarship to which I aspire to. Professor Harik provided timely and instructive comments and evaluation at every stage of the dissertation process, allowing me to complete this project on schedule. I thank him for his advice, guidance, support, and encouragement throughout my dissertation effort.

I also wish to thank Professor Hans Gesund, for his wise advice, his technical leadership, and his many acts of assistance and kindness. It is no exaggeration to say that without him this dissertation would not be as complete.

Thanks are also due to my Ph.D. advisory members, in no particular order, Dr. George Blandford, Dr. Kamyar Mahboub, and Dr. Mark Hanson, who provided time and support, and gave me constructive criticisms.

Graduate school is not free, and I appreciate the Department of Civil Engineering, the Graduate School, and other organizations that have provided financial support.

## TABLE OF CONTENTS

Acknowledgments.....		iii
List of Tables.....		vii
List of Figures.....		viii
Chapter 1 INTRODUCTION		
1.1	Corrosion in Concrete Structures	1
1.2	Alternative Reinforcement for Concrete Construction	2
1.3	Fiber Reinforced Polymer (FRP)	3
1.4	Research Objective	6
1.5	Research Significance	6
1.6	Organization of Dissertation Report	6
Chapter 2 MATERIAL PROPERTIES		
2.1	Introduction	8
2.2	Concrete	8
2.2.1	Short Term Concrete Stress/Strain Model	9
2.2.2	Typical Long Term Concrete Stress/Strain Model	10
2.2.3	Realistic Long Term Concrete Stress/Strain Model	13
2.3	Reinforcing Steel Grade 60 (A706)	15
2.4	Prestressing Steel	17
2.5	Fiber Reinforced Polymer (FRP) Composites	20
2.5.1	Tensile Properties of FRP Rebars	22
2.5.2	Compressive Properties of FRP Rebars	25
2.5.3	Long Term Properties of FRP Rebars	28
Chapter 3 FRP REINFORCED CONCRETE COLUMNS: COLUMN CROSS SECTIONAL (SHORT COLUMN) STRENGTH		
3.1	Introduction	31
3.2	Basic Assumptions	31
3.3	Reinforced Concrete Column Cross Section Strength	32
3.3.1	Concrete Compressive Forces	33
3.3.2	Reinforcement Tensile and Compressive Forces	34
3.3.3	Concrete Compressive Force Displaced by Reinforcement	35
3.3.4	Reinforced Concrete Column Cross Section ( <i>P-M</i> ) Strength	36
3.4	Strength Interaction of Reinforced Concrete Column Cross Sections	37
3.5	Concluding Remarks	52

Chapter 4	FRP REINFORCED CONCRETE COLUMNS: SLENDER COLUMN STRENGTH	
4.1	Introduction	54
4.2	Review of ACI 318-02: Moment Magnification Method in Non-Sway Frames	56
4.3	Deflection Method for Reinforced Concrete Columns	60
	4.3.1 Development of Axial Load-Moment-Curvature ( $P-M-\phi$ ) Relationship	62
	4.3.2 Numerical Computation of Column Deflection	63
4.4	Slender Reinforced Concrete Column Strength	65
Chapter 5	PRESTRESSED CONCRETE (PC) COLUMNS WITH FRP COMPOSITES	
5.1	Introduction – Prestressing Concrete Columns with Steel Tendons	74
5.2	Prestressing Concrete Columns with FRP Tendons	75
5.3	Derivation of the Strength Interaction Relation of Prestressed Concrete Columns in Bonded Application	76
	5.3.1 Concrete Compressive Forces	76
	5.3.2 Prestressing Reinforcement Forces	77
5.4	Strength Interaction Relation of PC columns with FRP Reinforcement	80
	5.4.1 Influence of Effective Prestress Force on Strength Interaction	82
	5.4.2 Influence of Concrete Compression Strength on Strength Interaction	85
	5.4.3 Influence of Reinforcement Ratio on Strength Interaction	87
	5.4.4 Influence of Long Term Loading on Strength Interaction	88
5.5	Slender Prestressed Concrete Columns with FRP Prestressing Reinforcement	90
5.6	Concluding Remarks	94
Chapter 6	A RATIONAL APPROACH TOWARDS THE DESIGN OF CONCRETE COMPRESSION MEMBERS WITH FRP REBAR	
6.1	Introduction	96
6.2	Strength Interaction ( $P-M$ ) Analysis of Concrete Columns Reinforced with FRP Rebar	98
6.3	Prevention of Brittle-Tension Failure	101
	6.3.1 Influence of Concrete Compressive Strength ( $f'_c$ )	106
	6.3.2 Influence of $\gamma$	108
	6.3.3 Influence of Long Term Concrete Loadings	110
	6.3.4 Application of the $E_{ft}-\epsilon_{ft}$ Interaction Design Aids	112
6.4	Effect of Internal Prestressing	119
6.5	Summary and Conclusions	121

Chapter 7	SUMMARY AND CONCLUSION	
7.1	Introduction	124
7.2	Summary and Conclusion of Chapters	124
7.3	Financial Viability of Fiber Reinforced Polymer	128
7.3	Future Research	129
Bibliography		130
Vita		140

## LIST OF TABLES

Table 2.1	Typical values of creep coefficients, $C_{cr}$ (Nilson 1997)	11
Table 2.2	Typical densities of FRP and steel bars, lbs/ft <sup>3</sup> (kg/m <sup>3</sup> ) (ACI 440 2001)	20
Table 2.3	Tensile properties of FRP bars (ACI 440 2001)	23

## LIST OF FIGURES

Fig. 2.1	The short term (ST) concrete stress/strain curve based on Hognestad expressions	10
Fig. 2.2	Second-order polynomial interpolation of creep coefficient and ultimate concrete compressive strength based on Nilson's values	12
Fig. 2.3	The typical long term (TLT) concrete stress/strain curve (Choo et al. 2003)	13
Fig. 2.4	The realistic long term (RLT) concrete stress/strain curve (Choo et al. 2003)	14
Fig. 2.5	A composite of short and long term concrete loadings	15
Fig. 2.6	Stress/strain curve of ASTM A706 Grade 60 rebar (CALTRANS 1999)	16
Fig. 2.7	Modified stress/strain model for Grade 60 steel	17
Fig. 2.8	Stress/strain curves of 7-wire low relaxation prestressing steel strands (PCI 1999)	19
Fig. 2.9	Typical tensile and compressive test setups	21
Fig. 2.10	Typical tensile failure mode of FRP rebars	22
Fig. 2.11	Tensile failure of ECS rebars	23
Fig. 2.12	Tensile stress/strain curves of CFRP bars (Hill et al. 2003)	24
Fig. 2.13	Typical compressive failure of short FRP specimens	26
Fig. 2.14	Typical compressive failure of short steel specimens	26
Fig. 2.15	Compressive stress/strain curves of GFRP bars (Deitz et al. 2003)	27
Fig. 2.16	Creep behaviors of (a) AFRP rod; (b) CFRP rod; and (c) GFRP rod (Yamaguchi et al. 1997)	29
Fig. 3.1	Typical rectangular concrete column cross section	32
Fig. 3.2	Typical strength ( $P_u$ - $M_u$ ) interaction of steel reinforced concrete column cross sections	37



Fig. 3.3	Short term non-dimensional interaction diagram of Grade 60 steel reinforced concrete column cross sections	38
Fig. 3.4	Short term non-dimensional interaction diagram of aramid (AFRP) reinforced concrete column cross sections	40
Fig. 3.5	Short term non-dimension interaction diagram of carbon (CFRP) reinforced concrete column cross sections	40
Fig. 3.6	Short term non-dimension interaction diagram of glass (GFRP) reinforced concrete column cross sections	41
Fig. 3.7	The effect of reduced elastic compression modulus on FRP RC column cross sectional strength	42
Fig. 3.8	A composite of the short and long term concrete loading	45
Fig. 3.9	Long term strength interaction diagrams of steel reinforced concrete column cross sections	46
Fig. 3.10	Long term strength interaction diagrams of AFRP reinforced concrete column cross sections	48
Fig. 3.11	Long term strength interaction diagrams of CFRP reinforced concrete column cross sections	49
Fig. 3.12	Long term strength interaction diagrams of GFRP reinforced concrete column cross sections	50
Fig. 4.1	Column strength due to slenderness effect	55
Fig. 4.2	Effective length factor ( $k$ ) of columns	56
Fig. 4.3	Secondary moment due to the lateral deflection of a column subjected to a constant eccentricity ( $e$ )	60
Fig. 4.4	Numerical integration for column deflection	63
Fig. 4.5	The axial load-moment interaction curves of Phrang and Siess (1964) for steel reinforced concrete columns bent in single curvature	66
Fig. 4.6	Short term interaction responses of the axial load-moment and moment-curvature relationships ( $P^* - M^* - \phi^*$ ), and the ultimate axial load-moment ( $P_u^* - M_u^*$ ) relationships of Grade 60 steel	

	RC concrete columns	68
Fig. 4.7	Short term interaction responses of the axial load-moment and moment-curvature relationships ( $P^*-M^*-\phi^*$ ), and the ultimate axial load-moment ( $P_u^*-M_u^*$ ) relationships of AFRP RC concrete columns	69
Fig. 4.8	Short term interaction responses of the axial load-moment and moment-curvature relationships ( $P^*-M^*-\phi^*$ ), and the ultimate axial load-moment ( $P_u^*-M_u^*$ ) relationships of CFRP RC concrete columns	70
Fig. 4.9	Short term interaction responses of the axial load-moment and moment-curvature relationships ( $P^*-M^*-\phi^*$ ), and the ultimate axial load-moment ( $P_u^*-M_u^*$ ) relationships of GFRP RC concrete columns	71
Fig. 4.10	Slender axial load-moment responses of various RC columns due to long term loading	73
Fig. 5.1	Effect of prestressing on the column strength interaction	74
Fig. 5.2	Effect of concrete strength on the column strength interaction	75
Fig. 5.3	Typical strength interaction of a steel prestressed concrete column	78
Fig. 5.4	Strength interaction diagram of steel RC column (Navy 1996)	80
Fig. 5.5	Influence of effective prestresses ( $f_{pc}$ ) in concrete on strength interactions of FRP column cross sections	83
Fig. 5.6	Influence of concrete compression strength on strength interactions of FRP column cross sections	85
Fig. 5.7	Influence of reinforcement ratio on strength interactions of FRP column cross sections	87
Fig. 5.8	Effect of long term loadings on strength interactions of FRP column cross sections	89
Fig. 5.9	Typical axial load-moment-curvature responses of prestressed concrete columns with AFRP as prestressing reinforcement	91
Fig. 5.10	Typical axial load-moment-curvature responses of prestressed concrete columns with CFRP as prestressing reinforcement	92

Fig. 5.11	Ultimate strength interaction diagrams of prestressed concrete columns with AFRP and CFRP as prestressing reinforcement	93
Fig. 6.1	Brittle-tension failures of concrete columns with FRP rebars	97
Fig. 6.2	Schematic strength interactions of concrete columns reinforced with FRP rebars	99
Fig. 6.3	Strength interaction of concrete columns reinforced with GFRP rebars	100
Fig. 6.4	Tensile elastic modulus-strain ( $E_{ft}-\varepsilon_{ft}$ ) interaction charts of concrete columns of rectangular shapes reinforced with FRP rebar having linearly-elastic stress/strain behavior	103
Fig. 6.5	The effect of concrete strength on reinforcement tensile strain	107
Fig. 6.6	The effect of $\gamma$ on $E_{ft}-\varepsilon_{ft}$ interaction	109
Fig. 6.7	Instantaneous (ST) and realistic long term (RLT) concrete stress/strain models	111
Fig. 6.8	(Fig. 6.4.c) Application of $E_{ft}-\varepsilon_{ft}$ graph for Example 6.1	114
Fig. 6.9	(Fig. 6.4.b) Application of $E_{ft}-\varepsilon_{ft}$ graph for Example 6.2	116
Fig. 6.10	(Fig. 6.4.b) Application of $E_{ft}-\varepsilon_{ft}$ graph for Example 6.3	118
Fig. 6.11	Effect of prestressing on the minimum required reinforcement ratio	119

# CHAPTER 1

## INTRODUCTION

### 1.1 Corrosion in Concrete Structures

Corrosion of the reinforcement is one of the major reasons for deterioration of reinforced or prestressed concrete structures with conventional steel. Corrosion is generally associated with a reduction of the effective reinforcement. This usually leads to a reduced in strength and stiffness, and the eventual loss of serviceability of the structural element in question. Potential remedies for the problem may include repairing and strengthening of the existing structures. In cases where the existing structures have been severely deteriorated or damaged, replacement may also be required. Irregardless of the measures taken, these will require resources in the form of time, labor, cost, and other factors.

The corrosion process and its modeling are complex (Thoft-Christensen 2002). The initiation of the corrosion process involves exposing the steel reinforcement to oxygen ( $O_2$ ) and moisture or water ( $H_2O$ ). It has been reported that the accumulation of the chloride ions ( $CL^+$ ), present in seawater and deicing chemical, in concrete also accelerated the electrochemical process (Brown 2002; Clemeña 2002; and Thomas 2002). Because durability of concrete is a major issue, Section 4.4 of ACI318-02 (2002) prescribes limits of maximum chloride ion content that can exist, depending on the type of constructions and conditions, for corrosion protection of steel reinforcement. Additional protection provided by specifying a minimum concrete cover (ACI318-02 section 7.7) of concrete protection for the underlying reinforcement is also prescribed.

Concrete, however, due to its porosity, is still permeable allowing the penetration and infiltration of corrosion agents to initiate the electrochemical process. Therefore, concrete itself may not be able to totally provide the complete protection to shield steel in all environments. Even though, low-permeability concrete, produced by adding pozzolanic materials such as fly ash, silica fume, etc., has been suggested (Knoll 2002; and Rosenberg 1999) for concrete construction, the tendency of concrete to crack would still render reinforcing steel be left

unprotected. Hence, the use of corrosion-resistance material may be the only effective and preventive alternative.

## **1.2 Alternative Reinforcement for Concrete Construction**

In general, coatings prevent the corrosion of reinforcing steel. Epoxy-coated steel (ECS) is one such example. The use of ECS bars started in the 70s and is still widely available and extensively used. However, the problems with ECS rebars are that the coating can be easily damaged or nicked during fabrication, transportation, and handling. Furthermore, it has been reported that delamination or debonding of the coating from the steel bar can occur, which leave the steel bar unprotected (Brown 2002; Clemeña 2002; Pape and Fanous 1998; Rosenberg 1999; Sohaghpurwala and Scannell 1999; & Wioleta et al. 2000). For example, a chloride attack was reported on the Florida Long Key Bridge (Wioleta et al. 2000; & Rosenberg 1999) in which the steel under the coating had eroded away while the protective coating was left intact.

Many types of solid stainless steels, e.g. stainless 304 and 316 (Austenitic group) or 430 (Ferritic group) or 318 (Ferritic-Austenitic or Duplex) steels, and stainless steel clad (SSC) have also been developed to resist different corrosion environments and working conditions. In general, stainless steels are essentially low carbon steels that contain chromium (Cr) at 10% or more by weight. Chromium in steel allows the formation of a rough, adherent, invisible, corrosion-resisting chromium oxide film on the steel surface, and this protective film, if damaged, is self-healing. SSC reinforcing bars are essentially steel bars coated with a thin layer of stainless steel. Solid stainless steel reinforcing bars have as many as 100 times higher chloride threshold level than conventional steels (Hurley and Scully 2002). Hence, solid stainless steels and SSC rebars can potentially be used as corrosion-resistant reinforcement. However, similar to ECS rebars, corrosion of SSC rebars can also be problematic as corrosion can still be initiated at ends where coating is generally not provided.

In addition to stainless steel bars or SSC bars, the MMFX steel corporation has also developed a corrosion-resistance steel known as the microcomposite multistructural formable steel (MMFX). Clemeña (2003) carried out corrosion-resistance tests of the MMFX bars, and

reported that MMFX bars have increased resistance to chloride-induced corrosion as compared to traditional black steel. Thus far, the properties and provisions for the MMFX bars are still being investigated and developed.

### **1.3 Fiber Reinforced Polymer (FRP)**

In general, a material that does not undergo electrochemical reaction with its environments is the solution to the corrosion problem, and fiber reinforced polymer (FRP) is one such material. In addition to be corrosion-free, FRP composites possess other attractive attributes (ACI 440.4R 2004; ACI 440.1R 2003; ACI 440.2R 2002; and ACI 440R 1996):

- Strength advantage – FRP composites depending on the types have strength comparable or greater to that of steel. FRP composites are synthetically designed and developed therefore they can be configured to have specific strength as desired.
- Weight advantage – FRP composites are light, hence can be easily handled and transported.
- Other advantages – Composites are non-conductive and are magnetic-free which is favorable in structures where electric and magnetic interference is undesirable (i.e. magnetic resonance imaging or MRI, computer industries, etc).

The common types of FRP composites for concrete construction include aramid fiber reinforced polymer (AFRP), carbon (C) FRP, and glass (G) FRP. The versatility of the manufacturing process allows FRP composites to be made into different shapes or forms such as bars, sheets, fabrics, laminates, sections, etc. In addition, the different grades of fibers and epoxy allow FRP systems of similar shape to be processed and be tailored for different construction applications. In general the use of FRP systems in concrete applications can be found in the following two areas:

- Design of new structures – FRP composites have been used as flexural and shear reinforcements in reinforced and prestressed beams/girders, slabs or bridge decks, etc (Zou 2003; Deitz et al. 1999; Tacchino and Brown 1999; and Guadagnini et al. 1999).

- Repair and strengthen existing structures – FRP composites have been used in repairing and strengthening of existing infrastructures to account for added weight, damaged, or deterioration. These examples of FRP applications include, amongst others, repairing and strengthening of decks in parking structures, strengthening of un-reinforced concrete and masonry walls, etc. (Alagusundaramoorthy et al. 2003; Deniaud and Cheng 2003; Tavakkolizadeh and Saadatmanesh 2003; Harik et al. 2003; Zhao et al. 2002; Mutsuyoshi et al. 2000; Dortzbach 2000; and Hamilton et al. 2000).

FRP systems have also been used in areas of strengthening and repairing concrete columns (Iacobucci et al. 2003; Sheikh and Yau 2002; Masuo 1999; & Fukuyama et al. 1999). This is typically done by wrapping of concrete columns using circumferential FRP reinforcement in the forms of sheets, strands or cloths, to enhance the column's strength, ductility, and energy absorption capacity. Thus far, the practical applications of FRP as primary reinforcement in concrete columns has never been documented, and relatively few related resources are found in the literature. FRP reinforcing bars were in fact not recommended to resist compression stresses for the following reasons (ACI 440 2003, 1996):

- Lower strength and stiffness in compression when compared with strength and stiffness in tension. In most applications, the compressive strength is not of primary concern as the contribution of the bars is frequently small and negligible.
- Compression properties of the FRP bars are difficult to predict from testing standpoint as issues related to alignment and gripping are hard to overcome. Moreover, the lack of stability of individual fibers in a bar complicates testing and can produce inaccurate measurements of compression properties. While a test method for tensile properties of FRP bars has been established (refer to ACI 440.3R-04, Section B.1), test methods for compression properties of FRP bars are not yet proposed.

Some of the notable studies in FRP reinforced concrete columns are summarized chronologically as follows:

- Kawaguchi (1993) cast twelve 6 x 8 x 24 in. (150 x 200 x 600 mm) concrete specimens reinforced with four braided AFRP rods having a nominal diameter of 12 mm; testing them under eccentric tension and compression. The results from the experiments showed that all specimens in compression failed due to concrete crushing. No AFRP rods rupture was observed in either the eccentric tension or compression tests. Kawaguchi (1993) concluded that the ultimate strength of FRP concrete members subjected to axial forces and bending can be evaluated using the conventional beam theory.
- Paramanatham (1993) tested seventeen 8 x 8 x 72 in. (200 x 200 x 1800 mm) concrete beam-columns reinforced with GFRP bars. He reported that GFRP bars would be stressed up to 20 to 30 percents of its ultimate strength in compression, and up to 70 percent in pure flexure.
- Amer et al. (1996) tested eight 6 x 6 x 72 in. (150 x 150 x 1800 mm) concrete columns reinforced with four 7.5 mm diameter carbon reinforcing bars under various eccentric loads, and developed an experimental diagram.
- Alsayed et al. (1999) tested fifteen 18 x 10 x 48 in. (450 x 250 x 1200 mm) concrete columns under concentric loads to investigate the effect of replacing longitudinal and/or lateral steel bars by an equal volume of GFRP bars. They showed that replacing steel bars with GFRP bars in columns reduced their capacity by about 13 percent. They also showed that replacing steel ties with GFRP ties reduced the columns capacity by 10 percent regardless of the type of longitudinal bars. They also noted that ACI 318-99 might overestimate the capacity of GFRP RC columns.
- Mirmiran et al. (2001) performed an analytical study on slender FRP columns using a cosine function to estimate the deflection shape. They concluded RC columns with low-stiffness FRP are more susceptible to slenderness effect and hence recommended that the ACI slenderness limit for steel reinforced concrete columns of 22 be reduced to 17 for FRP reinforced concrete columns bent in single curvature. They also cited that the ACI moment magnification method can be extended to FRP reinforced concrete columns by introducing a reduced stiffness factor.

Though rare, the use of CFRP as cables in prestressed concrete pile for waterfront structures has also been recorded (Iyer and Lampo 1998). Iyer and Lampo (1998) reported that



the Construction Productivity Advancement Research (CPAR) program cast and tested twelve frictional piles prestressed with CFRP cables in Rapid City, South Dakota. The CPAR conducted the pile driver analysis and the results indicated that the prestressed piles with CFRP cables performed satisfactorily. Arockiasamy and Amer (1998) and Schiebel and Nanni (2000) conducted CFRP prestressed pile tests similar to the one conducted by Iyer and Lamp (1998), and concluded that the performance of FRP prestressed piles is comparable to steel prestressed piles.

#### **1.4 Research Objective**

This study investigates the behavior of concrete columns reinforced or prestressed with fiber reinforced polymer (FRP) bars or tendons; use as the primary longitudinal reinforcement. The behavior of these columns will be quantified by conducting axial load–moment–curvature ( $P$ - $M$ - $\phi$ ) and axial load–deflection ( $P$ - $\Delta$ ) response analysis, the latter is used to study the secondary column effect. Additionally, the failure mechanisms of these columns will also be identified and quantified. Ultimately, design recommendation and design aids will be developed pertaining to the use of FRP bars in concrete columns.

#### **1.5 Research Significance**

This study aims at providing a better understanding of the behavior of concrete columns reinforced or prestressed with fiber reinforced polymer (FRP) bars. The study will determine if the current ACI318 provisions for concrete columns with steel are equally applicable for concrete columns with FRP. Ultimately, better understanding of the column's behavior and failure mechanisms will lead to a rational approach to the design and analysis of concrete columns internally reinforced or prestressed with FRP.

#### **1.6 Organization of Dissertation Report**

A brief summary of each chapter contained in this dissertation is as follows:

- An overview of the problems associated with the concrete structures with steel is presented in this chapter. Amongst other reinforcement types, fiber reinforced polymer (FRP) composites appear to be a viable alternative due to their non-corrosive nature and other attractive attributes. Various applications of FRP composites currently being used in concrete construction are also highlighted in this chapter. The objective and the significance of this research are also included.
- Understanding the behavior of constituent materials is the fundamental of this investigation. Chapter Two presents the stress-strain relations of concrete, steel, prestressing steel strand, and FRP bars. The development of the two long-term concrete stress-strain relations is described. Experimental procedures to determine the mechanical properties of the FRP bars are also presented. Experimental results on various FRP bars performed at the University of Kentucky are also included.
- Chapter Three presents the analytical procedures and equations to conduct the strength interaction relations of concrete columns reinforced with FRP bars. Assumptions pertaining to the analysis are also included. Short and long term strength interaction behaviors, failure mechanisms, and their implications are examined and discussed.
- Chapter Four presents the numerical integration approach for the examination of slenderness effect of concrete columns. The primary parameter studied in the chapter is the slenderness ratio, in addition to other governing factors described in Chapter Three.
- Chapter Five studies concrete columns prestressed (PC) with FRP tendons. In addition to developing the analytical procedures for the strength interaction relations of such columns, the approach developed in Chapter Four will also be used to examine the slenderness effect.
- Recommendations for design of concrete columns with FRP bars will be presented in Chapter Six. A rational approach is discussed and design aids are presented to facilitate the determination of the minimum required reinforcement ratio for concrete columns reinforced with FRP bars. Several numerical examples are also presented to illustrate the use of the design aids. General observations, findings, and conclusions pertaining to the approach are also discussed.
- Chapter Seven provides the overall summary and conclusions of the study. Several related research areas are also identified and proposed for future study.

## CHAPTER 2

### MATERIAL PROPERTIES

#### 2.1 Introduction

Knowledge of stress/strain characteristics of the individual constituents (e.g. concrete and reinforcing bar) in a reinforced concrete member is essential and is required when detailed analyses are to be performed, in order to understand and better predict the behavior of such concrete elements. In this chapter, three concrete stress/strain models are presented. One of which is the short term (ST) parabolic-linear concrete stress/strain relationship. Additionally, the two long term concrete stress/strain relationships are the typical long term (TLT) and realistic long term (RLT) models. Mechanical characteristics of reinforcing materials such as steel, prestressing steel tendon, and FRP rebars are also introduced and discussed in the following sections:

#### 2.2 Concrete

Concrete is a composite material. It is produced from a large number of constituent materials – cementitious materials, fine and coarse aggregates, water, and admixtures (Mehta and Monteiro 1993; Nawy 1996). The structural behavior of concrete can be expressed in terms of its stress/strain relationships. The standard US test for measuring the compressive strength of concrete consists of short-term compression tests on cylinders 6 in. (150 mm) in diameter by 12 in. (300 mm) high, made, cured, and tested in accordance with ASTM C 469. The concrete compressive strength can be influenced by the water/cementitious material ratio, type of cementitious materials, aggregate, moisture and temperature during curing, and rate of loading (MacGregor 1997). The tensile strength of concrete varies between 8 and 15% of the compressive strength (MacGregor 1997). Two types of tests are widely used to measure the tensile strength of concrete: the *modulus of rupture* or flexural test (ASTM C 78), and the *split cylinder test* (ASTM C 496). Since the tension strength of concrete is relatively low, it is commonly ignored in the analysis and design of concrete elements, and in the study it will also be omitted from the analyses herein.

### 2.2.1 Short-Term Concrete Stress/Strain Model

Concrete generally behaves nonlinearly. In this study, the short term concrete compression stress/strain model (ST-curve) suggested by Hognestad (Ford et al. 1981) for short-term monotonic loading is adopted. This stress/strain model is presented in Fig. 2.1. The initial stress/strain curve of the ST-curve is expressed by a parabolic equation with its vertex at the maximum compression strength of concrete,  $f'_c$ , and followed by a linear-straight line portion to its ultimate:

$$f_c = 0.85f'_c \left[ \frac{2\varepsilon_c}{\varepsilon_o} - \left( \frac{\varepsilon_c}{\varepsilon_o} \right)^2 \right], \quad 0 \leq \varepsilon_c < \varepsilon_o \quad (2.1.a)$$

$$f_c = 0.85f'_c [1 - m(\varepsilon_c - \varepsilon_o)], \quad \varepsilon_o \leq \varepsilon_c \leq \varepsilon_{cu} \quad (2.1.b)$$

$f_c$  is the concrete stress in compression (ordinate axis) as depicted in Fig. 2.1.  $m$  is the slope of the linear-straight line portion (Equation 2.1.b) and is taken to be 20 to generally match the experimental results of cylinder tests (Ford et al. 1981).  $\varepsilon_c$  is the short-term concrete strain in compression (abscissa axis in Fig. 2.1).  $\varepsilon_{cu}$  is the ultimate concrete compression strain and for short term loading it is typically the ACI maximum usable strain of 0.003 in/in.  $\varepsilon_o$  is the concrete strain corresponding to the maximum concrete compression stress,  $f'_c$  (Fig. 2.1) and is expressed as

$$\varepsilon_o = \frac{1.7f'_c}{E_c} \quad (2.2)$$

$E_c$  is the secant modulus of elasticity of concrete determined at a service stress of  $0.45 f'_c$ . ACI 318-02 gives the following expression for calculating  $E_c$

$$E_c = 33w_c^{1.5} \sqrt{f'_c}, \quad 90 \text{ lb/ft}^3 \leq w_c \leq 155 \text{ lb/ft}^3 \quad (2.3)$$

$w_c$  is the density of concrete in pounds per cubic foot ( $1 \text{ lb/ft}^3 = 16.02 \text{ kg/m}^3$ ). For normal-weight concrete ( $w_c = 150 \text{ lb/ft}^3$ ), the modulus of elasticity of concrete can be calculated using this alternative equation:

$$E_c = 57,000 \sqrt{f'_c} \quad (\text{lb/in}^2) \quad (2.4)$$

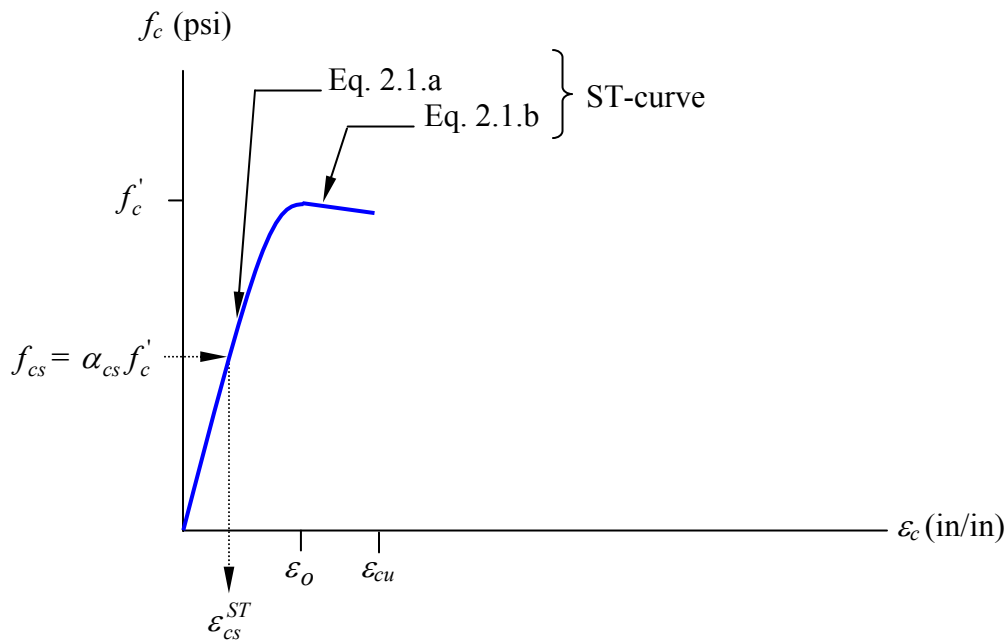


**Fig. 2.1 – The short-term (ST) concrete stress/strain curve based on Hognestad expressions**

## 2.2.2 Typical Long-Term Concrete Stress/Strain Model

Creep is the increase in strain with time due to a sustained load. It is stress dependent. Creep is a complex phenomenon and is affected by a number of variables such as age of concrete at initial loading, environmental humidity, size of member, and water/cement content (Branson 1977). Creep strain,  $\epsilon_{cr}$ , is estimated in this study by multiplying the short term concrete strain,  $\epsilon_c$ , by a creep coefficient,  $C_{cr}$ , as the following linear expression (Nilson 1997):

$$\varepsilon_{cr} = C_{cr} \cdot \varepsilon_c \quad (2.5)$$

$C_{cr}$  is assumed to be dependent on the maximum concrete compressive strength,  $f'_c$  (Nilson 1997). Typical values of  $C_{cr}$  are presented in Table 2.1. A second-order polynomial expression relating  $C_{cr}$  to magnitude of  $f'_c$  (lb/in<sup>2</sup>) ranging from 3,000 to 12,000 psi (21 to 83 MPa) based on the values given by Nilson (1997) is given as follows and shown in Fig. 2.2

$$C_{cr} = 0.01 \left( \frac{f'_c}{1000} \right)^2 - 0.32 \left( \frac{f'_c}{1000} \right) + 4.02 \quad (2.6)$$

**Table 2.1. Typical values of creep coefficient,  $C_{cr}$  (Nilson 1997)**

Ultimate Concrete Compressive Strengths, $f'_c$ (psi)	Creep Coefficients, $C_{cr}$
3,000	3.1
4,000	2.9
6,000	2.4
8,000	2.0
10,000	1.6
12,000	1.4

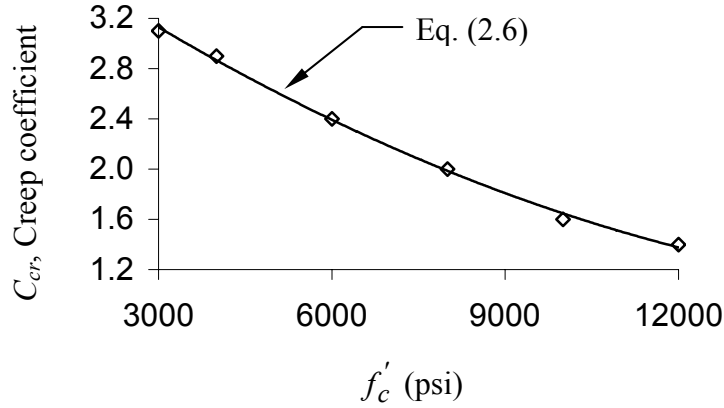


**Fig. 2.2 – Second-order polynomial interpolation of creep coefficient and ultimate concrete compressive strength based on Nilson’s values (see Table 2.1).**

Shrinkage is assumed to be independent of load or stress. Shrinkage in concrete depends to a great extent on the quantity of water in the mix and the relative humidity of the surrounding air (MacGregor 1997; Nilson 1997). Shrinkage strains,  $\varepsilon_{sh}$ , are reported to range from  $2 \times 10^{-4}$  to  $12 \times 10^{-4}$  in/in (MacGregor 1997; Nilson 1997). In this study, the magnitude of shrinkage strain will be assumed to be uniform across the uncracked part of a reinforced column cross-section.

Vandevelde (1968) modified the Hognestad expression to account for creep strain and devised a modified elastic stress/strain curve. A similar concept was applied in this study, and the resulting long-term concrete stress/strain curve (TLT-curve) that includes creep and shrinkage strains is shown in Fig. 2.3 (Choo et al. 2003). The TLT-curve is expressed by Eqs. 2.7. a – c:

$$f_c = 0, 0 \leq \varepsilon_c < \varepsilon_{sh} \quad (2.7.a)$$

$$f_c = 0.85 f'_c \left\{ \frac{2(\varepsilon_c - \varepsilon_{sh})}{[\varepsilon_o(1 + C_{cr}) + \varepsilon_{sh}]} - \left[ \frac{\varepsilon_c - \varepsilon_{sh}}{\varepsilon_o(1 + C_{cr}) + \varepsilon_{sh}} \right]^2 \right\}, \varepsilon_{sh} \leq \varepsilon_c < \varepsilon_o(1 + C_{cr}) + \varepsilon_{sh} \quad (2.7.b)$$

$$f_c = 0.85 f'_c \{1 - m[\varepsilon_c - (\varepsilon_o(1 + C_{cr}) + \varepsilon_{sh})]\}, \varepsilon_o(1 + C_{cr}) + \varepsilon_{sh} \leq \varepsilon_c \leq \varepsilon_{cu}(1 + C_{cr}) \quad (2.7.c)$$

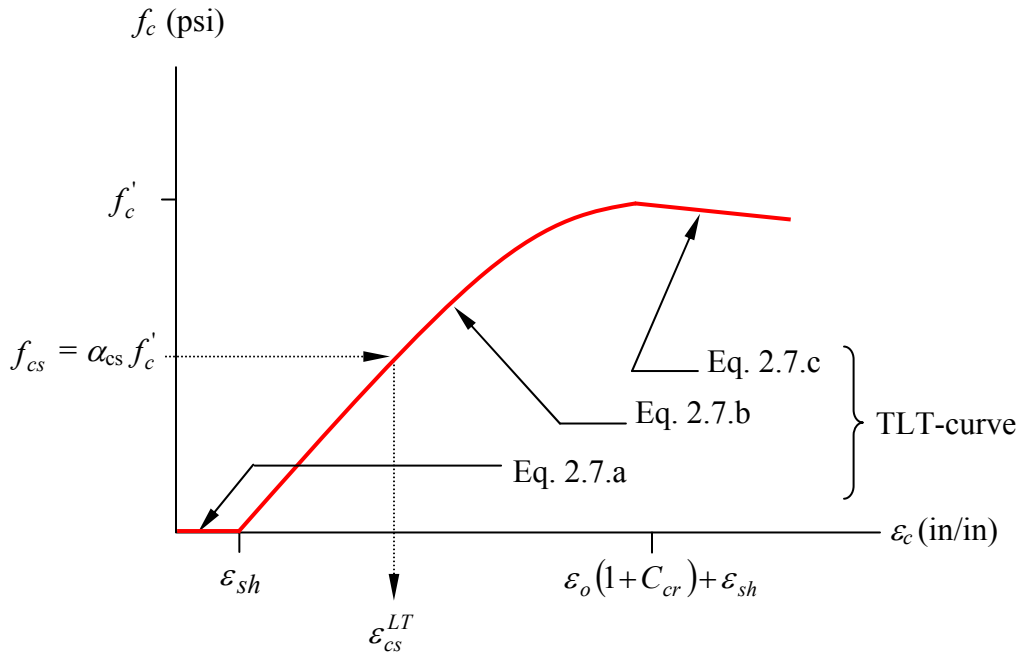


**Fig. 2.3 – The typical long-term (TLT) concrete stress/strain curve (Choo et al. 2003).**

### 2.2.3 Realistic Long-Term Concrete Stress/Strain Model

In addition to the typical long-term (TLT) concrete model, a realistic long-term (RLT) concrete model which considers a realistic load path for a concrete in compression was also devised for this study. In this model, creep and shrinkage will only occur in concrete columns under long-term *service* load conditions, as supposed to the TLT model which assumes creep and shrinkage occurred under *ultimate* load conditions. Eventually, the service load would be increased by a relatively quick, catastrophic loading to failure (e.g. sudden increase in load due to earthquake) – a path that simulates instantaneous short term loading shown in Fig. 2.1. The actual long term service load stress,  $f_{cs} = \alpha_{cs} \cdot f'_c$ , of concrete frequently varies between 30 and 60 percent of the concrete strength. Therefore,  $\alpha_{cs}$  ranges between 0.3 and 0.6 with a value of 0.45 used here. See Fig. 2.4, and Eqs. 2.8 – 2.11, which are combinations of the previous expressions:

$$f_c = 0, \quad 0 \leq \varepsilon_c < \varepsilon_{sh} \quad (2.8.a)$$



$$f_c = f_c' \left\{ \frac{2(\varepsilon_c - \varepsilon_{sh})}{[\varepsilon_o(1+C_{cr}) + \varepsilon_{sh}] - \left[ \frac{\varepsilon_c - \varepsilon_{sh}}{\varepsilon_o(1+C_{cr}) + \varepsilon_{sh}} \right]^2} \right\}, \text{ when } \varepsilon_{sh} \leq \varepsilon_c < \varepsilon_{cs}^{LT} \quad (2.8.b)$$

$$f_c = f_c' \left[ \frac{2(\varepsilon_c - \Delta\varepsilon_{cs})}{\varepsilon_o} - \left( \frac{\varepsilon_c - \Delta\varepsilon_{cs}}{\varepsilon_o} \right)^2 \right], \text{ when } \varepsilon_{cs}^{LT} \leq \varepsilon_c < (\varepsilon_o + \Delta\varepsilon_{cs}) \quad (2.8.c)$$

$$f_c = f_c' \{1 - m[\varepsilon_c - (\varepsilon_o + \Delta\varepsilon_{cs})]\}, \text{ when } (\varepsilon_o + \Delta\varepsilon_{cs}) \leq \varepsilon_c \leq (\varepsilon_{cu} + \Delta\varepsilon_{cs}) \quad (2.8.d)$$

where,

$$\varepsilon_{cs}^{ST} = \varepsilon_o - \sqrt{\varepsilon_o^2(1 - \alpha_{cs})} \quad (2.9)$$

$$\varepsilon_{cs}^{LT} = 2\varepsilon_{sh} + \varepsilon_o(1 + C_{cr}) - \varepsilon_o\sqrt{1 - \alpha_{cs}} - \varepsilon_o C_{cr}\sqrt{1 - \alpha_{cs}} - \varepsilon_{sh}\sqrt{1 - \alpha_{cs}} \quad (2.10)$$

$$\Delta\varepsilon_{cs} = \varepsilon_{cs}^{LT} - \varepsilon_{cs}^{ST}, \quad (2.11)$$

and  $m = 20$  (Ford et al 1981)

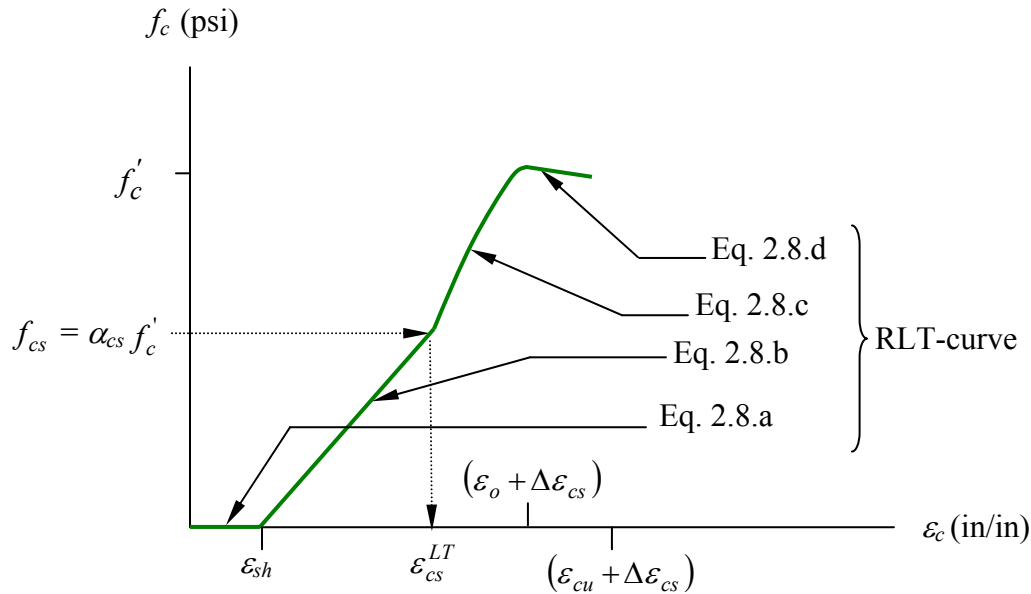


**Fig. 2.4 – The realistic long-term (RLT) concrete stress/strain curve (Choo et al 2003).**

A composite of the three concrete models (ST, TLT, and RLT) is presented in Fig. 2.5.

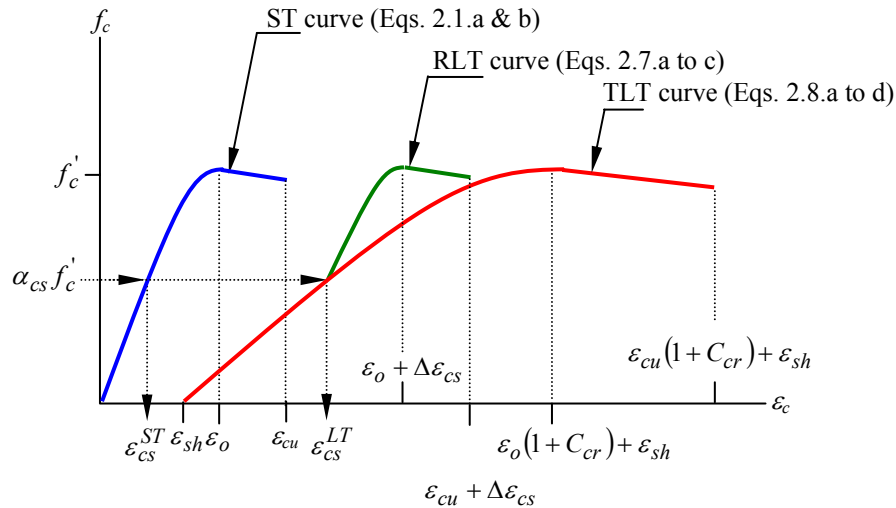


**Fig. 2.5 – A composite of short and long term concrete loadings.**

### 2.3 Reinforcing Steel Grade 60 (A706)

The properties of a typical Grade 60 steel reinforcing bar are introduced in this section, which will be used later for comparative purposes in the analyses of concrete columns. The stress/strain curve and the properties of several ASTM A706 Grade 60 rebars are shown in Fig. 2.6. The curve typically exhibits an initial linear elastic portion, a yield plateau, and a nonlinear strain hardening range in which stress increases with strain (CALTRANS 1999).

<i>Ultimate tensile strain</i>	$\epsilon_{su} = \begin{cases} 0.12 & \#10 \text{ (\#32m) bars and smaller} \\ 0.090 & \#11 \text{ (\#36m) bars and larger} \end{cases}$
<i>Reduced ultimate tensile strain (25% reduction)</i>	$\epsilon_{su}^R = \begin{cases} 0.090 & \#10 \text{ (\#32m) bars and smaller} \\ 0.060 & \#11 \text{ (\#36m) bars and larger} \end{cases}$
<i>Onset of strain hardening</i>	$\epsilon_{ssh} = \begin{cases} 0.0150 & \#8 \text{ (\#25m) bars} \\ 0.0125 & \#9 \text{ (\#29m) bars} \\ 0.0115 & \#10 \text{ \& \#11 (\#32m \& \#36m) bars} \\ 0.0075 & \#14 \text{ (\#43m) bars} \\ 0.0050 & \#18 \text{ (\#57m) bars} \end{cases}$

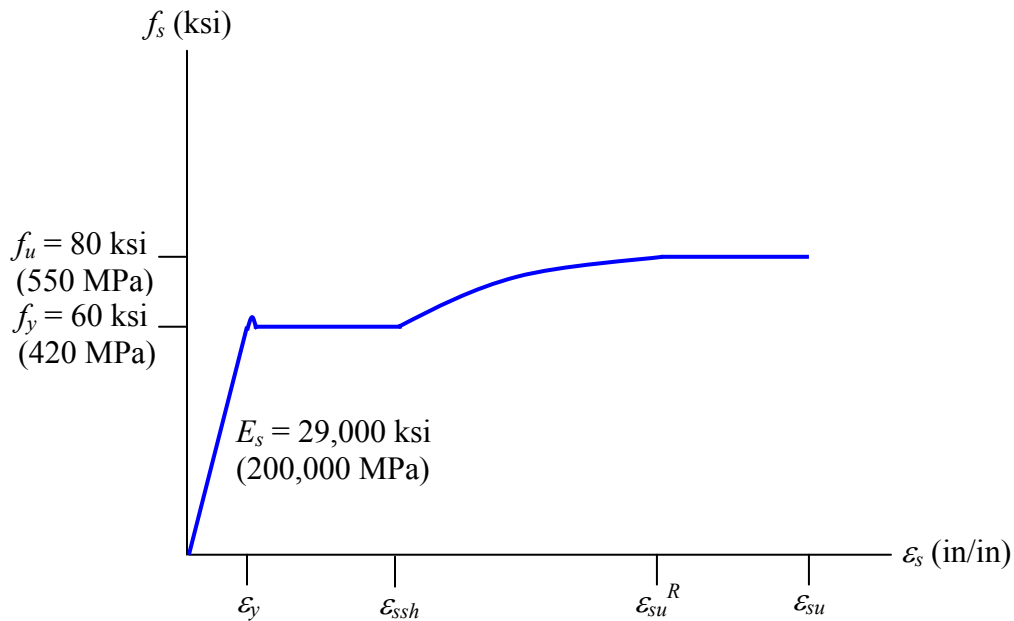


**Fig. 2.6 – Stress/strain curve of ASTM A706 Grade 60 rebar (CALTRANS 1999).**

In this study, the steel stress/strain curve and the properties shown in Fig. 2.7 are used. The average values of the properties of the Grade 60 steel were calculated and applied for all sizes of reinforcing bars. These properties are the ultimate tensile strain, reduced ultimate tensile strain, and the onset of strain hardening and the average values of these properties are shown in Fig. 2.7. The nonlinear strain hardening range of the actual relationship in Fig. 2.6 is substituted with a straight line approximation in Fig. 2.7.

Ultimate tensile strain\*  $\epsilon_{su(avg)} = 0.1050$

Reduced ultimate tensile strain\*  $\epsilon_{su}^R (avg) = 0.0750$

Onset of strain hardening\*  $\epsilon_{ssh(avg)} = 0.0052$

\* Note: Derived from values shown in Fig. 2.5

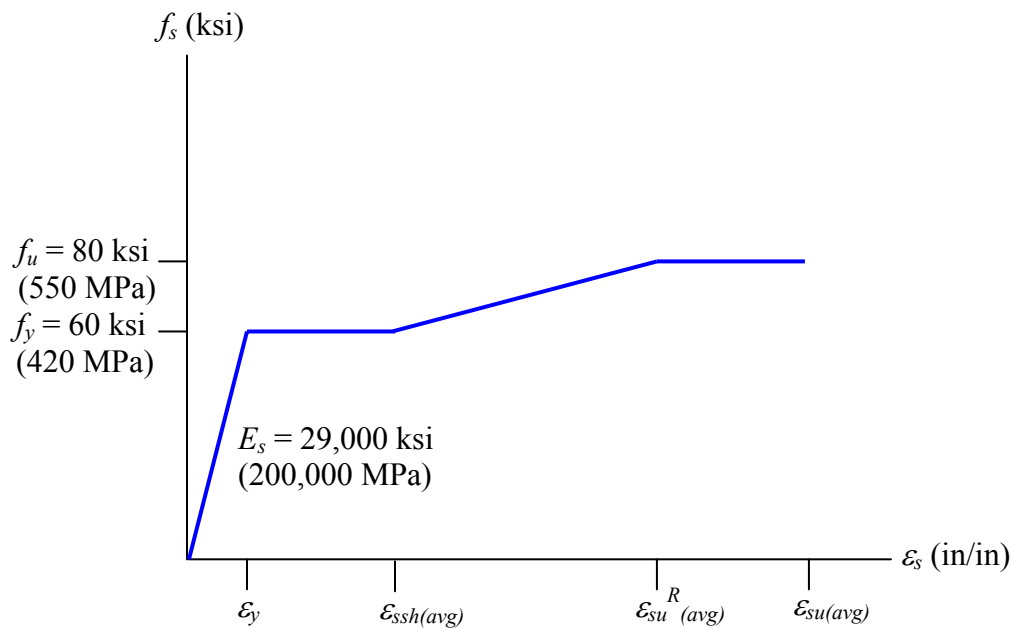


Fig. 2.7 – Modified stress/strain model for Grade 60 steel.

## 2.4 Prestressing Steel

The mechanical properties of commonly used prestressing strands or tendons will be introduced herein. Prestressing strands can be modeled with an idealized nonlinear stress/strain model shown in Fig. 2.8.

The relationships that describe the stress/strain relationships for 2 types of 7-wire low relaxation prestressing strands are as follows (PCI 1999):

*250-Type Strand:*

$$f_{ps} = E_{ps} \times \varepsilon_{ps} \text{ (ksi) } [ f_{ps} = E_{ps} \times \varepsilon_{ps} \text{ (MPa) } ], \varepsilon_{ps} < 0.0076 \quad (2.10.a-b)$$

$$f_{ps} = 250 - \frac{0.25}{\varepsilon_{ps}} \text{ (ksi) } [ f_{ps} = 1725 - \frac{1.72}{\varepsilon_{ps}} \text{ (MPa) } ], \varepsilon_{ps} \geq 0.0076 \quad (2.11.a-b)$$

*270-Type Strand:*

$$f_{ps} = E_{ps} \times \varepsilon_{ps} \text{ (ksi) } [ f_{ps} = E_{ps} \times \varepsilon_{ps} \text{ (MPa) } ], \varepsilon_{ps} < 0.0086 \quad (2.12.a-b)$$

$$f_{ps} = 270 - \frac{0.04}{\varepsilon_{ps} - 0.007} \text{ (ksi) } [ f_{ps} = 1860 - \frac{0.276}{\varepsilon_{ps} - 0.007} \text{ (MPa) } ], \varepsilon_{ps} \geq 0.0086 \quad (2.13.a-b)$$

The modulus of elasticity,  $E_{ps}$ , in Eqs. 2.10 and 2.12 is 28,500 ksi (196,500 MPa).

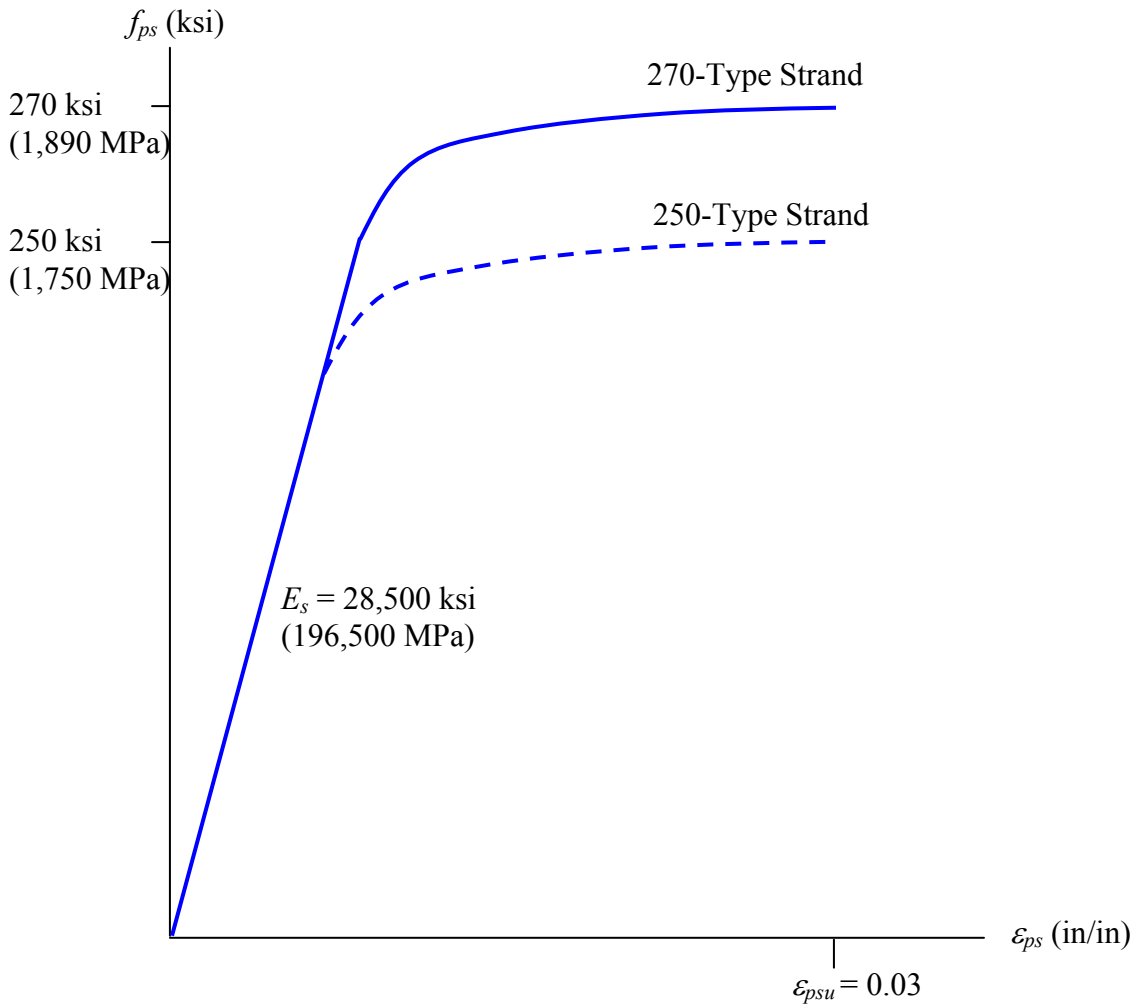


**Fig. 2.8 – Stress/strain curves of 7-wire low relaxation prestressing steel strands (PCI 1999).**

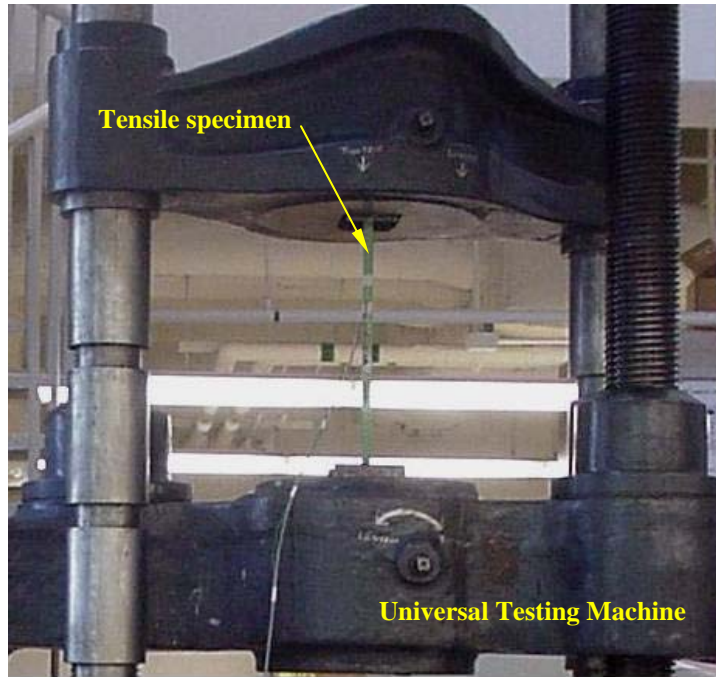
## 2.5 Fiber Reinforced Polymer (FRP) Composites

As described in the introductory chapter, fiber reinforced polymer (FRP) composites have many attractive attributes. They are non-corrosive, non-conductive and non-magnetic, and lightweight. The latter, for instance, could ease handling and lower transportation costs. Although FRP reinforcing bars can be manufactured in such a way that they have physical appearances and sizes comparable to conventional steel reinforcing bars, they can be many times lighter than steel rebars. Typically, the density or the mass density of FRP composites is on average five times lighter than steel (Table 2.2).

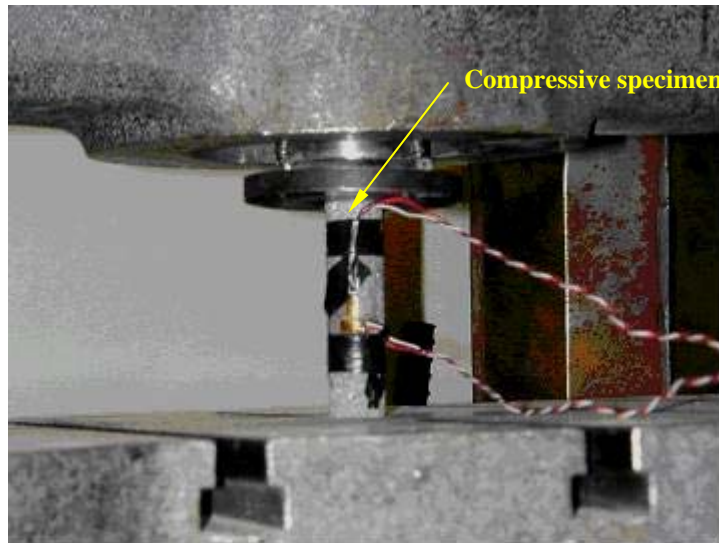
**Table 2.2** – Typical densities of FRP and steel bars, lb/ft<sup>3</sup> (kg/m<sup>3</sup>) (ACI 440 2001)

Material	Steel	AFRP	CFRP	GFRP
Density	492.5 (7900)	77.8–88.1 (1250–1400)	93.3–100.2 (1500–1600)	77.8–131.3 (1250–2100)

The mechanical properties (e.g. tensile and compression strengths, tensile and compression moduli of elasticity, bond strengths, etc.) of FRP reinforcing bars can be determined through different experimental tests. To be used in place of steel reinforcing bars or prestressing tendons in concrete, the properties of FRP reinforcing bars, i.e. tensile, compressive, etc., must first be validated. The tensile properties, mainly the tensile strength, elastic modulus in tension, and ultimate elongation or ultimate strain in tension, of a FRP rebar can be determined using the procedure described in the *Guide Test Methods for Fiber Reinforced Polymer (FRP) Rods and Sheets* prepared by ACI Subcommittee 440K (2002). Note that the same *Guide*, however, does not provide a test method to determining the compressive properties of FRP rebars. The compressive properties of FRP reinforcing bars, however, can be determined according to ASTM D695-02a (2003) for plastic materials. Compressive properties of interest are the compressive strength, elastic modulus in compression, and ultimate contraction or ultimate strain in compression. Typical tensile and compressive test set-ups are shown in Fig. 2.9.



**(a) Tensile Test Setup (University of Kentucky)**



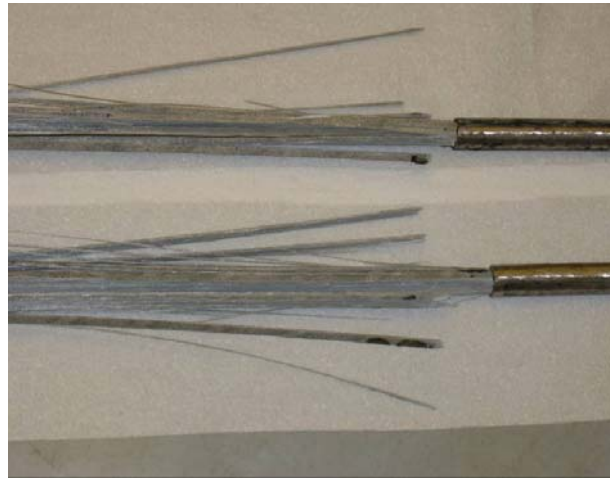
**(b) Compressive Test Setup (Laoubi 2002)**

**Fig. 2.9 – Typical tensile and compressive test setups.**

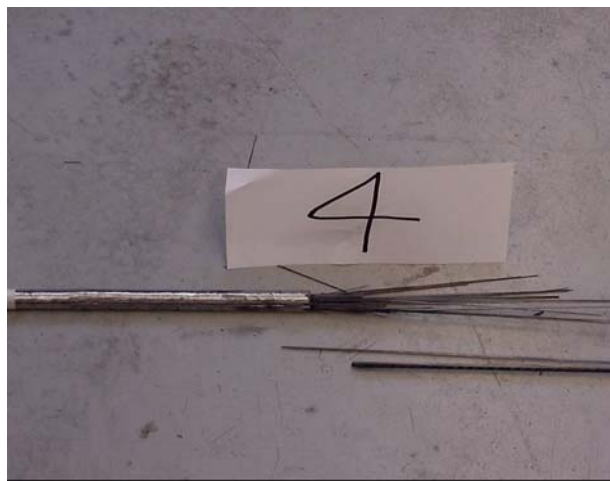


### 2.5.1 Tensile Properties of FRP Rebars

FRP reinforcing bars (e.g. AFRPs, CFRPs, and GFRPs) in tension typically exhibit linear elastic behavior until failure in contrast to steel which has a definite yielding plateau. As a result, FRP rebars exhibit brittle behavior, which if used in a concrete system, would give no warning of structural failure. Typical tensile failure mode of FRP reinforcing bars tested at the University of Kentucky is shown in Fig. 2.10. For comparison, tensile failure of ECS reinforcing bars exhibiting *necking effect* is shown in Fig. 2.11.



(a) Glass FRP rebar



(b) Carbon FRP rebar

**Fig. 2.10 – Typical tensile failure mode of FRP rebars.**

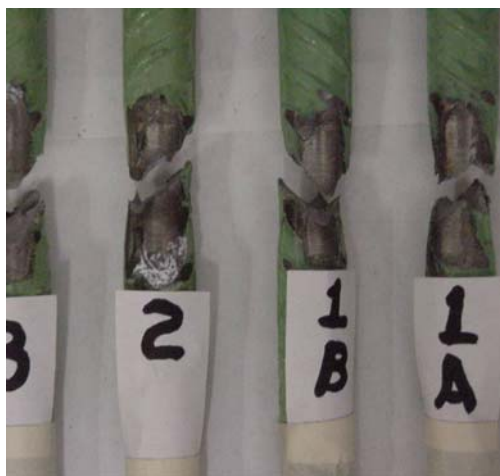


**Fig. 2.11 – Tensile failure mode of ECS rebars.**

FRP rebars can be designed and manufactured to tailor specific designs by selecting the volume and type of fibers (e.g. glass, carbon, or aramid) and resins (e.g. epoxy, polyester, or vinylester), fiber orientation, etc. These variations, hence, result in different properties for various types of FRP rebars (i.e. aramid, carbon, and glass FRP rebars). Table 2.3 provides one such example. As a result, a FRP design is typically dependent on the properties provided by the FRP manufacturer or fabricator known as the design or guaranteed values.

**Table 2.3 – Tensile properties of FRP bars (ACI 440 2001)**

Tensile Properties	Rebar Types		
	AFRP	CFRP	GFRP
Yield Strength $f_{yt}$ ksi (MPa)	Not applicable	Not applicable	Not applicable
Ultimate Strength $f_{ut}$ ksi (MPa)	145–203 (1000–1400)	87–420 (600–2900)	70–150 (483–1035)
Elastic Modulus $E_{ft}$ $\times 10^3$ ksi (GPa)	8.7–12.6 (60–87)	17.4–43.5 (120–300)	5.1–6.5 (35–45)
Rupture Strain $\epsilon_{ut}$ %	1.4–1.9	0.5–1.7	1.2–2.7

The linearly-elastic-until-failure behavior of CFRP bars in tension is shown in the experimental stress/strain curves of Fig. 2.12 (Hill et al. 2003):

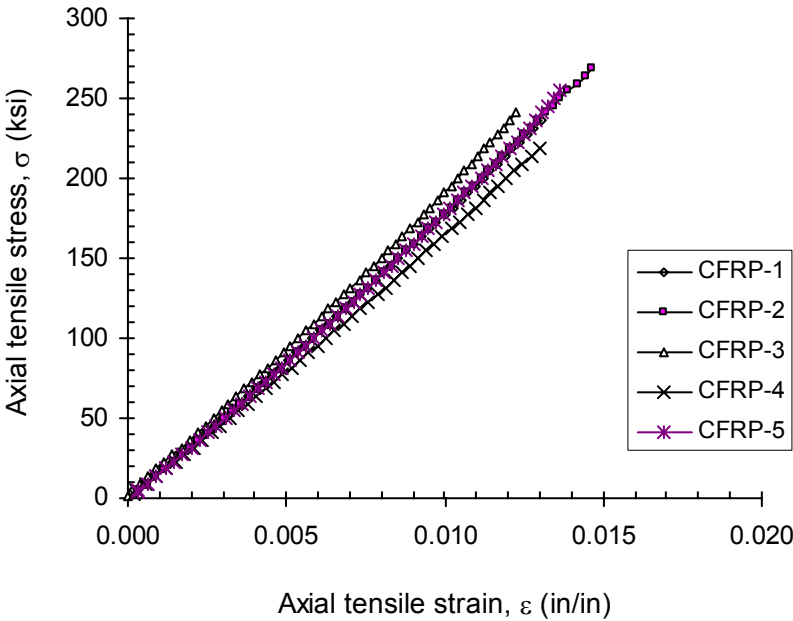


**Fig. 2.12 – Tensile stress/strain curves of CFRP rebars (Hill et al. 2003).**

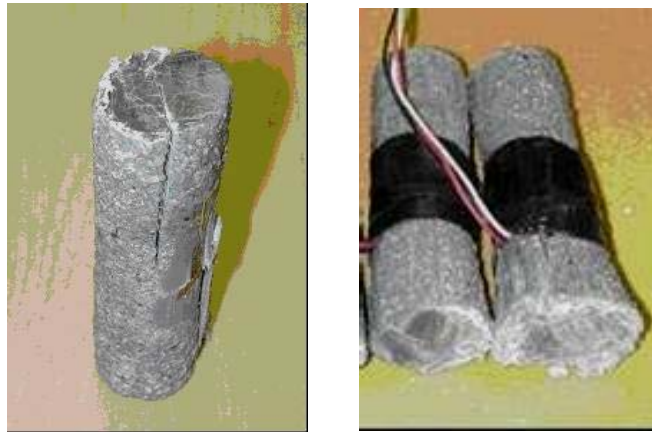
### 2.5.2 Compressive Properties of FRP Rebars

There has been very little interest in the compressive properties of FRP reinforcing bars. This is due to the following reasons:

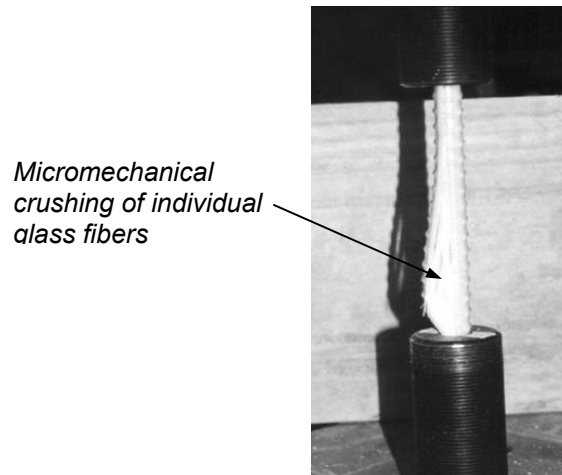
- In practical design applications, the direct effect of compression reinforcement on the ultimate bending strength of concrete flexural members is negligible; hence compression reinforcement is often ignored.
- Difficulties in effectively performing compression test; issues such as gripping and aligning procedures. In addition, stability of fibers in compression complicates testing and often results in inaccurate prediction of the compression properties of FRP rebars.

For FRP reinforcing bars to be accepted into the concrete community as compression reinforcement, a number of compressive properties must be validated. This is particularly important in applications where sophisticated analyses are required to understand and predict the behavior of FRP reinforced concrete members.

In concrete members where compression reinforcing bars were surrounded by concrete cover and core and confinement reinforcement (i.e. ties or spiral columns), the individual rebar behaves essentially like a short compression member – strength is independent of slenderness ratio. Under this circumstance, compression stress/strain behavior of FRP reinforcing bars can be characterized as linear elastic until failure (similar behavior exhibited by FRP rebars in tension). At crushing failure, the fibers separated from the resin matrix and buckled individually – termed as a micromechanical failure (Deitz et al. 2003) – as shown in Fig. 2.13. Note that steel specimen fails in a different manner in compression where it gets squashed as shown in Fig. 2.14. Note that buckling failure and combination of crushing and buckling failure for slender FRP specimens had also been identified (Deitz et al. 2003). Experimental compression stress/strain curves for GFRP rebars tested by Deitz et al. (2003) is shown in Fig. 2.15.



(a) Crushing of # 6 glass bars (Laoubi 2002)



(b) Crushing of 15mm-Ø glass bars (Deitz et al. 2003)

Fig. 2.13 – Typical compression failure of short FRP specimens.



Fig. 2.14 – Compression failure of short steel specimens (El-Hacha and Rizkalla 2002).

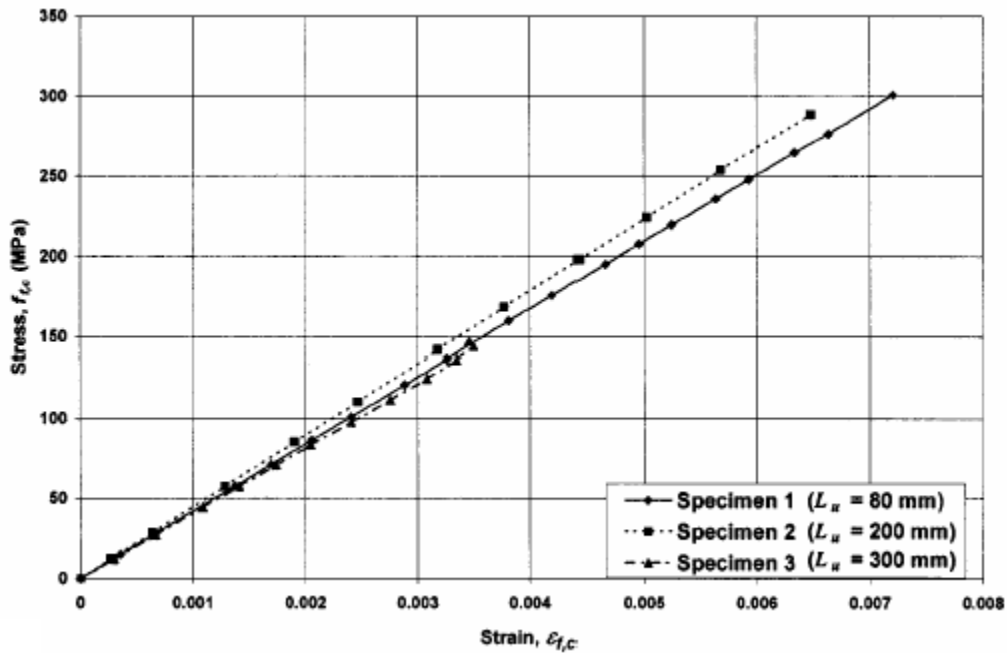


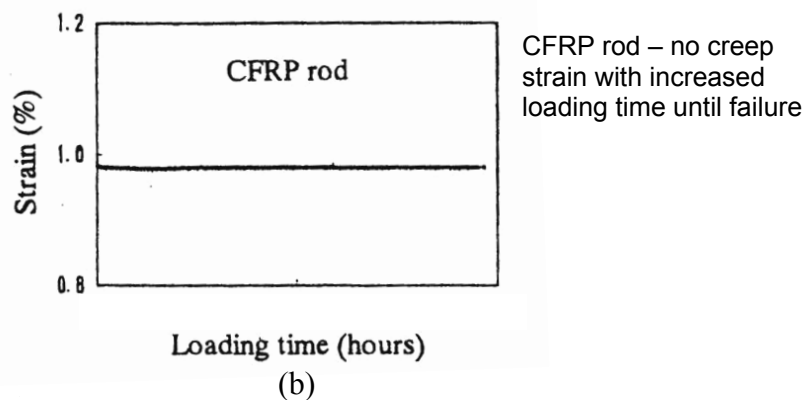
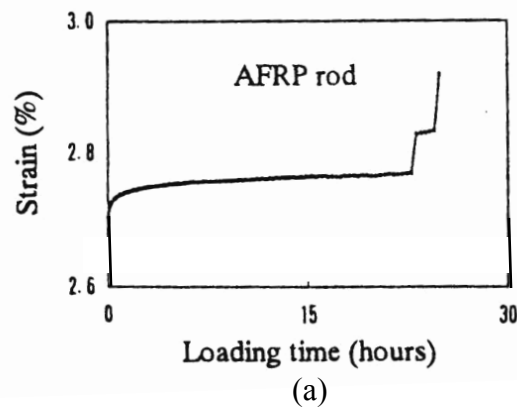
**Fig. 2.15 – Compression stress/strain curves of GFRP rebars (Deitz et al. 2003).**

There is a consensus that FRP rebars have lower compression strength ( $f_{uc}$ ) compared to their strength in tension ( $f_{ut}$ ). Deitz et al. (2003) reported that the ratio of experimental compression ultimate strength to experimental ultimate tension strength was approximately 0.5 (50%) for #15 (15 mm) GFRP bars produced by the Marshall Industries Composites that failed in crushing. Ratios of 0.55, 0.78, and 0.20 have been reported in ACI 440 (2001) for GFRP, CFRP, and AFRP rebars, respectively.

The compression elastic modulus ( $E_{fc}$ ) may sometimes be lower than the tensile elastic modulus ( $E_{ft}$ ) for a FRP rebar. Deitz et al. (2003) indicated that the elastic modulus of the GFRP bars tested was approximately the same in compression and tension. ACI 440 (2001) reported the compression elastic moduli were approximately 80%, 85%, and 100% to that of tensile elastic moduli for GFRP, CFRP, and AFRP, respectively. Note that the combination of lower ultimate strength and elastic modulus of FRP rebars in compression will result in lower ultimate strain ( $\epsilon_{fuc}$ ) – an important factor to be considered in design and analysis of FRP concrete members.

### 2.5.3 Long Term Properties of FRP Rebars

In addition to short term properties, i.e. static tensile and compressive properties, long term durability of FRP reinforcing bars must be ascertained as well. One important long term behavior of interest is the creep behavior of FRP rebars. FRP rebars when kept under a sustained tensile stress for a long duration, a creep rupture may likely to occur and the type of creep rupture failures largely depends on the type of continuous fibers. Different creep behaviors of AFRP, CFRP, and GFRP rods can be observed and explained with the aid of Fig. 2.16, and their characteristics are as follows (Yamaguchi et al. 1997): AFRP rods – gradual increase in creep strain with increased loading time until failure (Fig. 2.16.a); CFRP rods – no creep strain with increased loading time until failure (Fig. 2.16.b); and GFRP rods – step by step increase of creep strain occurred at different time intervals until failure. Note that Yamaguchi et al. (1997) performed these creep tests at the sustained stress levels at 60 to 90%, with 5% increments.



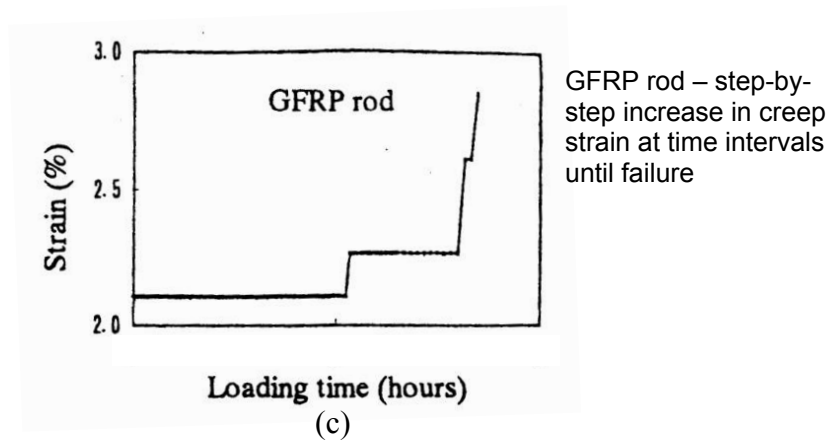


**Fig. 2.16 – Creep behaviors of (a) AFRP rod; (b) CFRP rod; and (c) GFRP rod (Yamaguchi et al. 1997).**

One useful parameter needed for a design criterion is the creep rupture time – time of rupture of a specific sustained load. The creep rupture time is generally evaluated and defined within the context of its eventual application. For instance, the creep rupture time of a FRP rebar at one hundred service year [or one-million hour ( $\approx 110$  years)]. Long term studies on creep property of FRP rebars are summarized as follows:

- Zou (2003) conducted long term tests on AFRP (Arapree) and CFRP (Leadline) prestressing rods of 7.8 and 8 mm diameters, respectively. The predicted 100 year creep coefficients – ratio of creep strain to elastic strain under a constant sustained stress – of AFRP and CFRP rods were 16.5 and 0 percents, respectively. Note that the predicted creep coefficient of CFRP in Zou’s study is consistent with the finding obtained in Yamaguchi et al. (1997) which concluded zero creep strain for CFRP bars. Zou (2003) also reported that stresses that can be maintained in AFRP (Arapree) and CFRP (Leadline) rods up to 100 years without failure were 52 and 79 percents of their guaranteed tensile strengths, respectively.
- Seki et al. (1997) tested GFRP rods made of E-glass fibers and concluded that the one million creep-rupture ratio of load was 53.1 percent. However, they noted that creep strains of GFRP rods were extremely small before creep rupture.



- Ando et al. (1997) conducted creep rupture tests on CFRP and AFRP tendons and predicted that the load ratio were approximately 79 and 63 percents, respectively, for one million hour.

**CHAPTER 3**  
**FRP REINFORCED CONCRETE COLUMNS:**  
**COLUMN CROSS-SECTIONAL (SHORT COLUMN) STRENGTH**

**3.1 Introduction**

In this chapter, the mechanical characteristics (e.g. stress/strain relationships, long term properties, etc) of concrete and reinforcing materials presented in Chapter 2 will be used together with the principles of mechanics to evaluate the axial load ( $P$ ) and moment ( $M$ ) interaction of a column cross-section. Additionally, this chapter presents the basic assumptions and equations pertinent in the analysis of a reinforced concrete column cross-section. Numerical analyses will be performed, and the results of these analyses will also be presented in subsequent sections.

**3.2 Basic Assumptions**

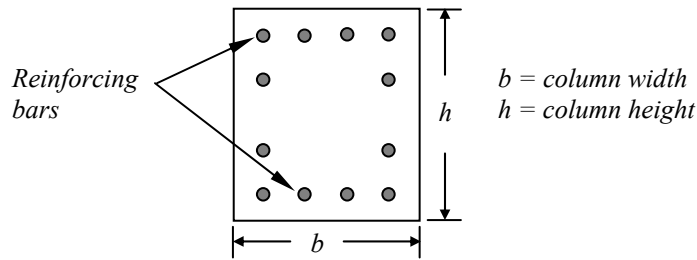
The axial load-moment ( $P$ - $M$ ) interaction strength of a reinforced concrete column cross-section is evaluated on the basis of the following assumptions:

- Plane sections remain plane under bending. Thus, the strain in the concrete and reinforcement are proportional to the distance from the neutral axis.
- Perfect bond exists between the reinforcement and concrete.
- The tensile strength of concrete can be neglected.
- The maximum strain,  $\varepsilon_c$ , in concrete nowhere exceeds an assumed ultimate concrete compressive strain,  $\varepsilon_{cu}$  – an Ultimate strength design assumption.
- The area of the concrete displaced by reinforcement in compression will be subtracted.

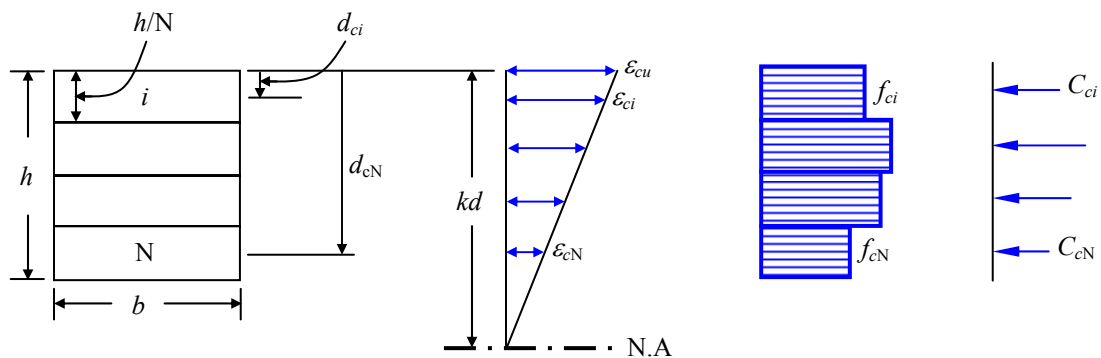
Note that the investigation of reinforced concrete columns in this dissertation is limited to columns with rectangular cross sections reinforced symmetrically.

### 3.3 Reinforced Concrete Column Cross Sectional Strength

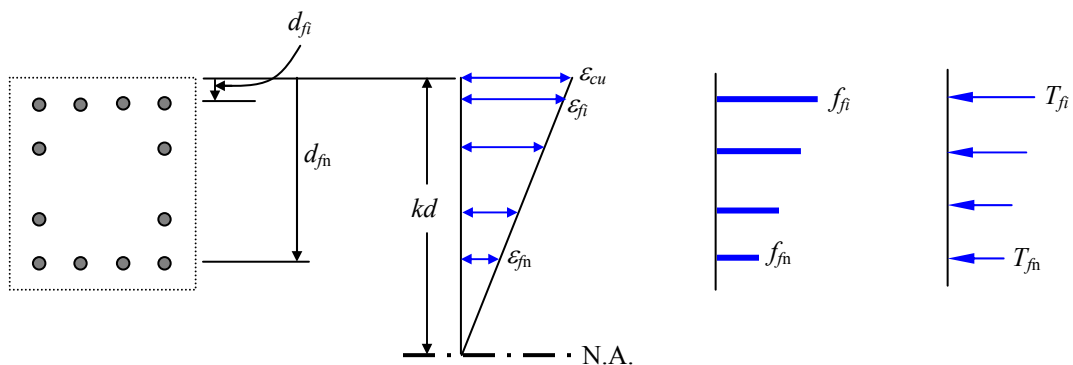
In this section the equations pertain to generating the  $P$ - $M$  points on an interaction diagram are derived. Equations for a rectangular cross-section column are developed and explained with the help of Fig. 3.1 (Note that the entire section shown in Fig. 3.1 is in compression).



(a) Rectangular column cross-section



(b) Concrete strips, strain distributions, stresses, and forces



(c) Reinforcement layouts, strain distributions, stresses, and forces

**Fig. 3.1 – Typical rectangular concrete column cross section.**

The column cross sectional strength is the accumulative strengths of its individual constituents; namely concrete and reinforcing elements. Hence, the contribution of these individuals can be computed separately as follows:

### 3.3.1 Concrete Compression Forces

As shown in Fig. 3.1.b, concrete compression force is to be calculated for each individual strip which has been divided in the compression zone into  $N$  equal-height concrete strips. To do that, the concrete compression strain ( $\varepsilon_{ci}$ ) must first be computed at mid-height of any concrete strip  $i$ , where distance  $d_{ci}$  is measured from the outermost compression fiber having an ultimate concrete compression strain ( $\varepsilon_{cu}$ ) to the mid-height of strip  $i$

$$\varepsilon_{ci} = \varepsilon_{cu} \left( \frac{kd - d_{ci}}{kd} \right) \quad (3.1)$$

And concrete compression force ( $C_{ci}$ ) in strip  $i$  can be expressed as

$$C_{ci} = f_{ci} b \frac{h}{N} \text{ when } kd \geq h \text{ (where cross section is in compression entirely)} \quad (3.2.a)$$

Or

$$C_{ci} = f_{ci} b \frac{kd}{N} \text{ when } kd < h \text{ (where cross section is in compression partially)} \quad (3.2.b)$$

$b$  and  $h$  are the width and height of the column cross-section.  $f_{ci}$  is the concrete stress and is a function of the concrete strain ( $\varepsilon_{ci}$ ) for strip  $i$ . Given  $\varepsilon_{ci}$ , concrete stress ( $f_{ci}$ ) can then be determined from the concrete stress/strain models presented previously in Chapter 2.  $kd$  in Eq. 3.2.b is the distance from the neutral axis to the extreme compression fiber of concrete. Eq. 3.2.b is used when only a portion of column cross section is in compression (or neutral axis is located in the column cross section). For consistency, the compression strain, stress, and force in this dissertation assume positive signs.

Additionally, the moment of individual concrete strips can also be computed about the centerline of the rectangular column cross-section which is located at the mid-height ( $h/2$ ) of a symmetrical section. For concrete strip  $i$ , this moment is

$$M_{ci} = C_{ci} \left( \frac{h}{2} - d_{ci} \right) \quad (3.3)$$

### 3.3.2 Reinforcement Tension and Compression Forces

For an assumed neutral axis ( $kd$ ) location, the reinforcement strain ( $\varepsilon_{fi}$ ) at the reinforcement layer  $i$  as shown in Fig. 3.1.c can be computed as

$$\varepsilon_{fi} = \varepsilon_{cu} \left( \frac{kd - d_{fi}}{kd} \right) \quad (3.4)$$

$d_{fi}$  in Eq. 3.4 is measured from the extreme concrete compression fiber to the center of the reinforcement in layer  $i$ . Note that when the computed  $\varepsilon_{fi}$  is positive the reinforcement is in compression and vice versa.

The reinforcement stress ( $f_{fi}$ ) in layer  $i$  can be determined once the reinforcement strain ( $\varepsilon_{fi}$ ) is known based on the reinforcement's stress/strain characteristic (see Chapter 2).

The tension or compression force ( $F_{fi}$ ) and moment ( $M_{fi}$ ) of the reinforcement at layer  $i$  can be computed using the following equations:

$$F_{fi} = A_{fi} f_{fi} \quad (3.5)$$

$$M_{fi} = F_{fi} \left( \frac{h}{2} - d_{fi} \right) \quad (3.6)$$

$A_{fi}$  in Eq. 3.5 is the reinforcement area of layer  $i$ . Similar to concrete moment of Eq. 3.3, the moment of Eq. 3.6 is also computed about the centerline ( $h/2$ ) of a symmetrical rectangular column cross-section.

### 3.3.3 Concrete Compressive Force Displaced by Reinforcement

Concrete areas displaced by reinforcements must be accounted for to avoid overestimation of column strength. This is especially true when large amount of reinforcement is involved. Hence, the concrete force and moment at displaced areas must be subtracted.

The concrete strain at layer  $i$  of reinforcement in the compression zone can be computed using Eq. 3.4 defined in previous section and shown here again as

$$\varepsilon_c = \varepsilon_{fi} = \varepsilon_{cu} \left( \frac{kd - d_{fi}}{kd} \right) \quad (3.4)$$

Once the corresponding concrete strain in Eq. 3.4 has been computed, the concrete stress at layer  $i$  of reinforcement can be determined based on the appropriate concrete stress/strain models presented in Chapter 2. The concrete force ( $C_{cfi}$ ) and moment ( $M_{cfi}$ ) at layer  $i$  of reinforcement having a reinforcement area of  $A_{fi}$  can be expressed as

$$C_{cfi} = A_{fi} f_{ci} \quad (3.8)$$

$$M_{cfi} = C_{cfi} \left( \frac{h}{2} - d_{fi} \right) \quad (3.9)$$

It should be emphasized that the concrete force and moment (Eqs. 3.7 and 3.8) due to the displaced areas only apply to concrete in the compression zone only. Note Eq. 3.9 is again calculated at the mid-height ( $h/2$ ) of a symmetrical rectangular column cross-section.

### 3.3.4 Reinforced Concrete Column Cross-Sectional ( $P$ - $M$ ) Strength

Keeping in mind that the cross sectional strength ( $P$ - $M$ ) of a reinforced concrete column is the sum of the individual strengths, the following equations can be developed. The resultant force ( $P$ ) and moment ( $M$ ) in a symmetrical reinforced concrete column cross-section can be expressed as

$$P = \sum_{i=1}^N C_{ci} + \sum_{i=1}^n F_{fi} - \sum_{i=1}^m C_{cfi} \quad (3.10)$$

$$M = \sum_{i=1}^N C_{ci} \left( \frac{h}{2} - d_{ci} \right) + \sum_{i=1}^n F_{fi} \left( \frac{h}{2} - d_{fi} \right) - \sum_{i=1}^m C_{cfi} \left( \frac{h}{2} - d_{fi} \right) \quad (3.11)$$

It can be shown that Eq. 3.10 is the sum of Eqs. 3.2, 3.5 and 3.8, whereas Eq. 3.11 represents the sum of Eqs. 3.3, 3.6 and 3.9. A series of computations (i.e. Eqs. 3.10 and 3.11) can be performed for a number of assumed locations of neutral axis to obtain the overall column strength curve ( $P$ - $M$  strength interaction). The  $P$ - $M$  strength curve represents the capacity of reinforced concrete sections to resist combination of axial and bending loads (e.g. failure of a reinforced concrete section is assumed when a combination of axial and bending forces falls on or outside of a  $P$ - $M$  curve).

The magnitude of curvature corresponding to a specific axial load level for a section can also be determined as

$$\phi = \frac{\varepsilon_{cu}}{kd} \quad (3.12)$$

The moment-curvature ( $M$ - $\phi$ ) relationship for a specific axial load level can be derived and used for deflection computation (Chapter 4).

### 3.4 Strength Interaction of Reinforced Concrete Column Cross Sections

Using the equations derived in previous sections coupled with material properties presented in Chapter 2, strength ( $P$ - $M$ ) interaction of concrete columns reinforced with specific reinforcement type can be generated. Before any examination of FRP reinforced concrete columns, the following schematic  $P$ - $M$  interaction diagram of a typical steel reinforced concrete column cross section is presented in Fig. 3.2.

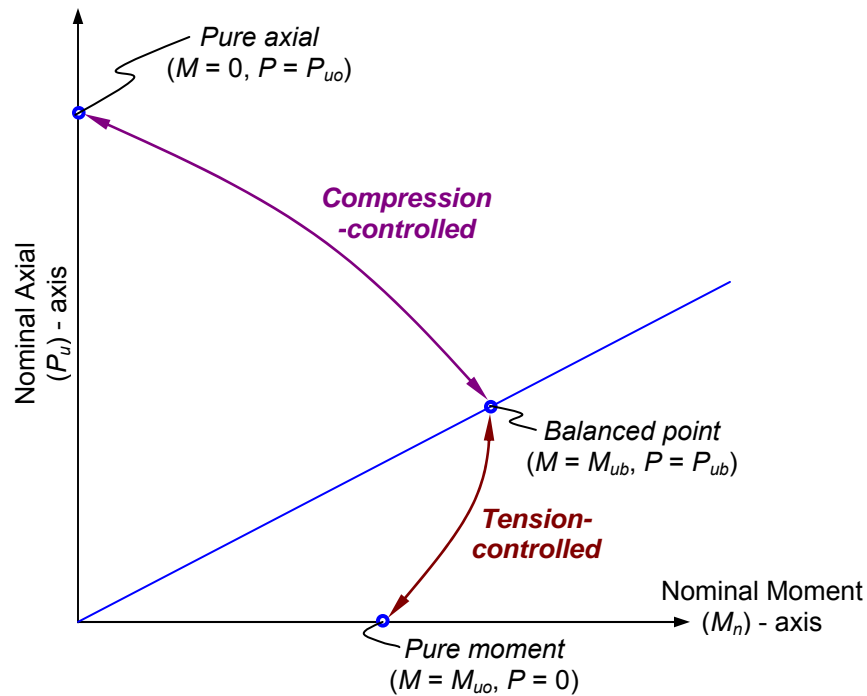


**Fig. 3.2 – Typical strength ( $P_u$ - $M_u$ ) interaction of steel reinforced column cross sections.**

The strength interaction diagram shown in the schematic is derived when the extreme concrete compression fiber reaches the predetermined ultimate concrete strain ( $\epsilon_{cu}$ ) – hence ultimate strength interaction diagram. Recall one of the ultimate concrete strains is the ACI usable strain of 0.003 – this is known also as the short term ultimate strain in this dissertation. Three distinct points (points of pure axial, balanced, and pure moment) depicted in the diagram can be identified and determined analytically for any column cross section.



The regions, as normally defined in ACI or in other publications, between these points are: (1) Compression controlled region – where strain in the compression fiber reaches its predetermined ultimate strain before tension steel reaches yield strain ( $\epsilon_s < \epsilon_y$ ), and (2) tension controlled section – where steel has yielded ( $\epsilon_s \geq \epsilon_y$ ) when compression strain in concrete reaches its predetermined strain. The dividing point between the compression controlled and tension controlled regions is the *balanced* point. This is a point where concrete strain in the compression fiber reaches its predetermined ultimate ( $\epsilon_c = \epsilon_{cu}$ ) and steel in the outermost tension layer reaches its yield strength ( $\epsilon_s = \epsilon_y$ ) simultaneously.

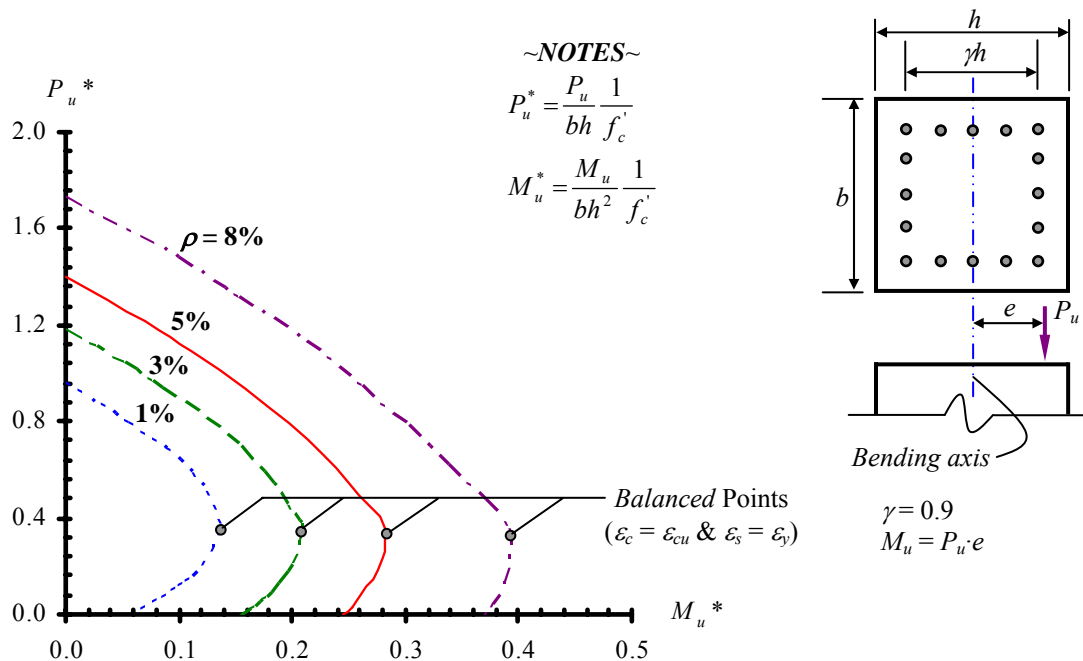


**Fig. 3.3 – Short term non-dimensional interaction diagram of Grade 60 steel reinforced concrete column cross sections.**

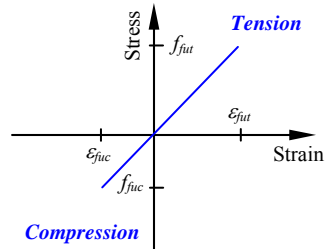
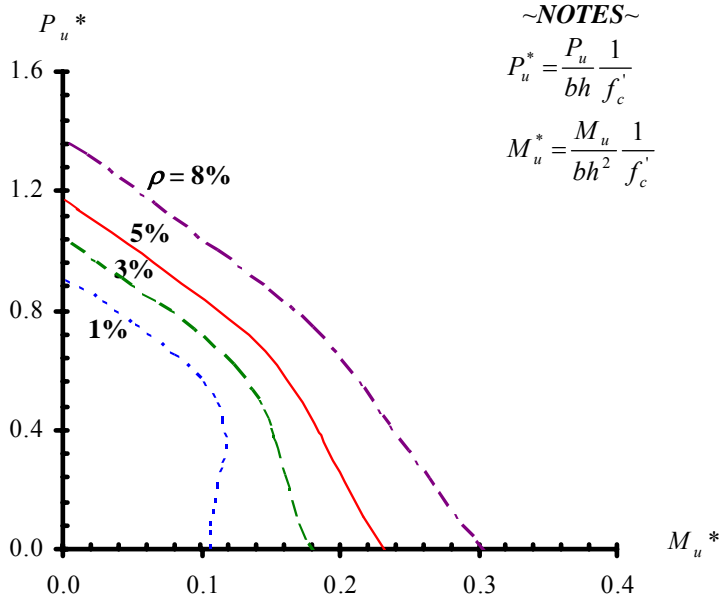
Short term non-dimensional interaction diagram for a rectangular (or square) column cross section reinforced symmetrically with Grade 60 steels is shown in Fig. 3.3. Recall the short term (ST) ultimate concrete compression strain is the ACI usable strain of 0.003. Stress/strain relations of concrete and Grade 60 steel are those shown in Figs. 2.1 and 2.6. Individual interaction curves in Fig. 3.3 were generated based on the ACI limits (ACI 318 2002)

for reinforcement of compression members:  $0.01A_g \leq A_s \leq 0.08A_g$ , where  $A_g$  and  $A_s$  are the gross column cross sectional area and area of steel reinforcement, respectively.

The upper reinforcement limit ( $\rho = A_s/bh = 8\%$ ) was established based on practicality as concrete columns are usually reinforced with reinforcement ratios no greater than 0.06 to prevent rebar congestion. The lower reinforcement limit (1%) set in 1933 by ACI Committee 105 (1933) to prevent steel reinforcement from reaching the yield level under sustained service loads as creep and shrinkage in concrete transfer load from the concrete to the reinforcement. This lower limit, however, might be low as most of the steel reinforcement employed in current engineering practice have higher grade (Grade 60 or higher) than what had been used in the past. A study conducted by Lin and Furlong (1995) concluded that longitudinal steel rebar in concrete columns did not yield even with reinforcement ratio as low as 0.25%. They also indicated that the ACI-318 lower reinforcement ratio of 1% is high, but reasonable for reinforced concrete columns sized 12" to 24" (305 mm to 610 mm) in buildings.

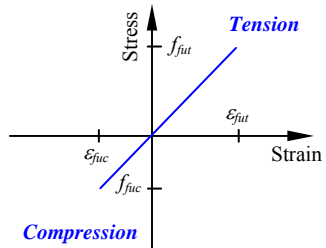
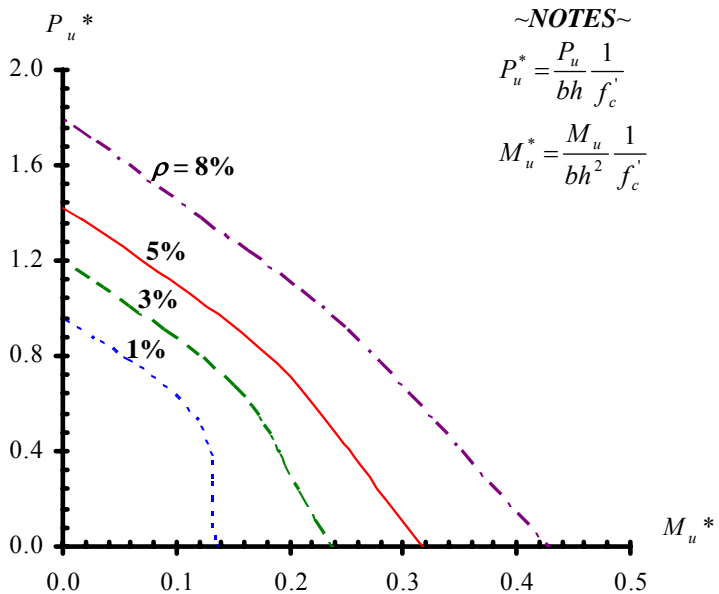
Typically, the strength interaction of steel reinforced concrete column cross sections has the following characteristic (see Fig. 3.3): a reduction of axial load is accompanied by increases in moment strength from pure axial condition to the *balanced* points. It is then followed by simultaneous reduction of axial load and moment strength from the *balanced* point to the condition of pure flexure. The *balanced* points, points where concrete compression strain reaches its predetermined ultimate strain ( $\epsilon_{cu}$ ) at the same time steel reaches its yield strain ( $\epsilon_y$ ), can be determined mathematically and are easily identified from the interaction curves.

Theoretical short term interaction diagrams of concrete column cross sections reinforced with FRP reinforcement (Figs. 3.4 – 3.6) have also been generated based on assumptions and equations presented previously. Types of FRP reinforcements and their mechanical properties are presented in the accompanied interaction diagrams. In generating Figs. 3.4 – 3.6, mechanical properties assumed were consistent and conservative with what had been reported in the literatures. The layout of FRP reinforcement is similar to the steel RC cross section shown in Fig. 3.3.



Aramid (AFRP) mechanical properties for interaction diagram of Fig. 3.4:  
 $f_{fut} = E_{ft} \cdot \epsilon_{fut}$  &  $f_{fuc} = E_{fc} \cdot \epsilon_{fuc}$ ;  
 $E_{ft} = 12,600$  ksi (87 MPa);  
 $E_{fc} = E_{ft}$ ;  
 $\epsilon_{fut} = 2.4\%$ ; &  
 $\epsilon_{fuc} / \epsilon_{fut} = 0.5$

**Fig. 3.4 – Short term non-dimensional interaction diagram of aramid (AFRP) reinforced concrete column cross sections.**



Carbon (CFRP) mechanical properties for interaction diagram of Fig. 3.5:  
 $f_{fut} = E_{ft} \cdot \epsilon_{fut}$  &  $f_{fuc} = E_{fc} \cdot \epsilon_{fuc}$ ;  
 $E_{ft} = 21,300$  ksi (147 MPa);  
 $E_{fc} = E_{ft}$ ;  
 $\epsilon_{fut} = 1.6\%$ ; &  
 $\epsilon_{fuc} / \epsilon_{fut} = 0.5$

**Fig. 3.5 – Short term non-dimensional interaction diagram of carbon (CFRP) reinforced concrete column cross sections.**

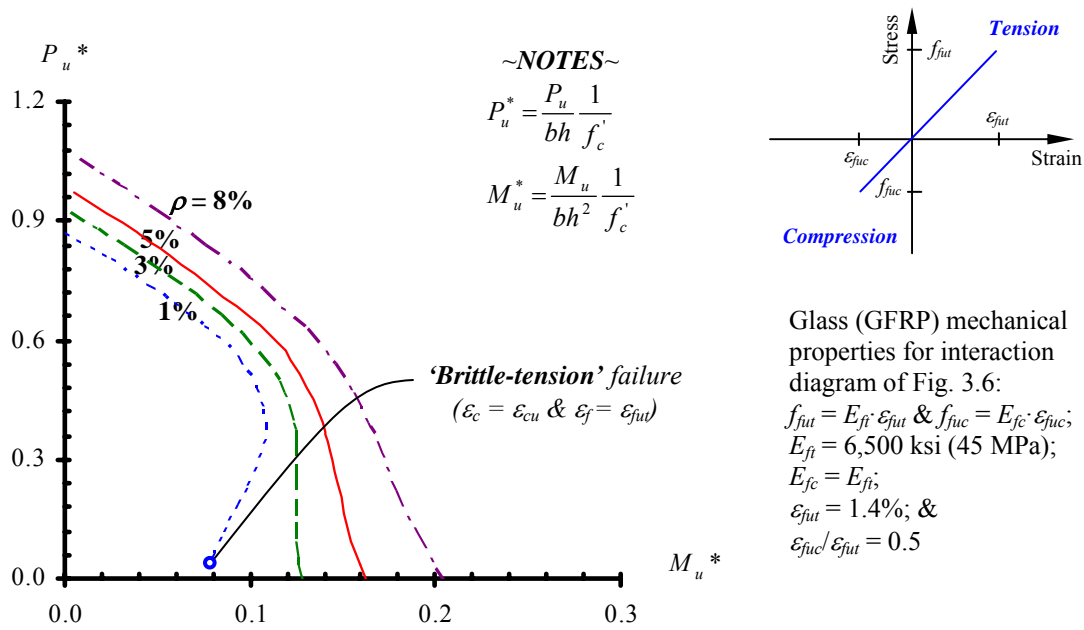


**Fig. 3.6 – Short term non-dimensional interaction diagram of glass (GFRP) reinforced concrete column cross sections.**

Based on Figs. 3.4 – 3.6, the following observations can be made for concrete column cross sections reinforced with FRP rebars:

- Unlike steel RC column cross sections, there is no definite strength interaction pattern. Steel RC column cross sections typically exhibit a reduction of axial load accompanied by increases in moment forces from pure axial to *balanced* conditions, and then reduction of both axial and moment forces from *balanced* to pure bending (see Fig. 3.3). FRP RC column cross sections, however, in some cases show an increase in moment resistance as axial load decreases from pure axial to pure bending condition. The scenario is especially apparent with the greater reinforcement ratio ( $\rho \geq 3\%$ ) coupled with higher FRP modulus of elasticity.
- Strength interaction of steel and FRP RC column cross sections is derived based on and dictated by the concrete's ultimate compression strength and strain. Unlike steel RC, FRP strength interaction will not exhibit *balanced* point indicative of FRP's linearly-elastic stress/strain characteristic.

- Though FRP rebar has strength many times higher than conventional steel rebar, it has ultimate strain that is likely to be many times lower compared to that of steel. Therefore, the likelihood that FRP rebar failed in tension at or before concrete reaches its ultimate in compression exists. This failure is termed ‘*brittle-tension*’ failure. One such example is shown in Fig. 3.6 where reinforcement ratio of 1% was considered in generating the strength interaction of GFRP RC column cross section.

It is worth to examine the effect of the compression elastic modulus of FRP reinforcement on the strength interaction as this property is generally and consistently varied from its counterpart in tension (see Section 2.3.2). Short term interaction diagrams, with  $\rho = 3\%$ , considering three different hypothetical ratios of elastic compression moduli to tension moduli of 1.0, 0.5, and 0.1, respectively, were derived and presented in Fig. 3.7:

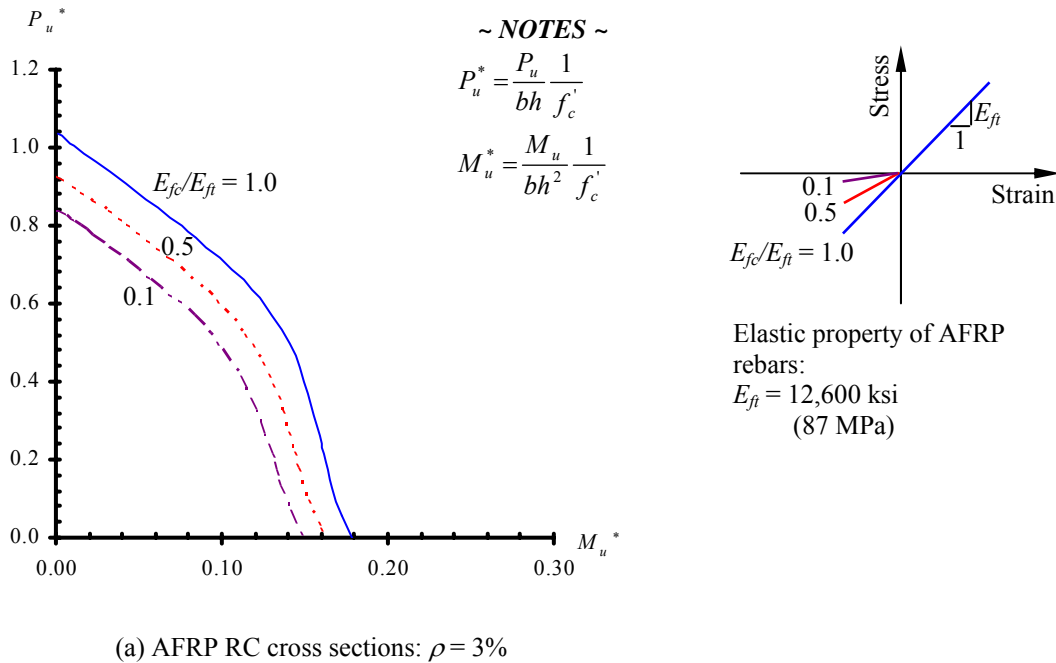
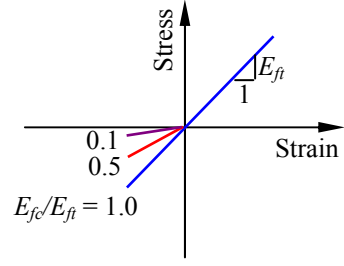
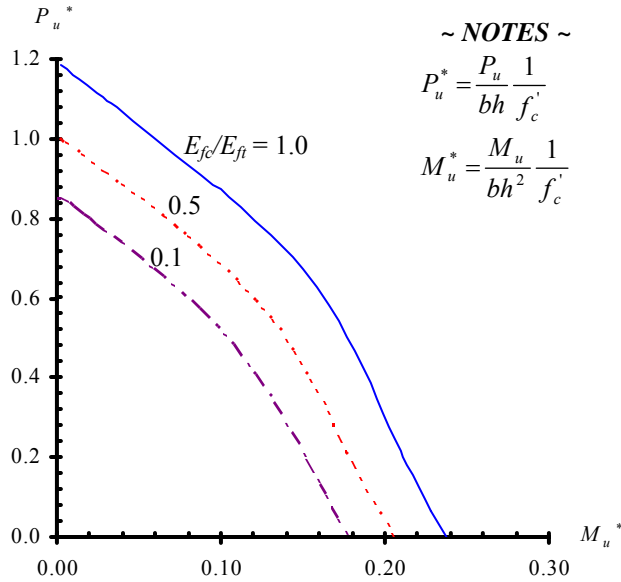
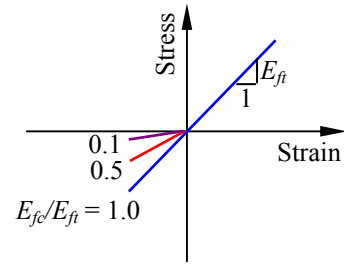
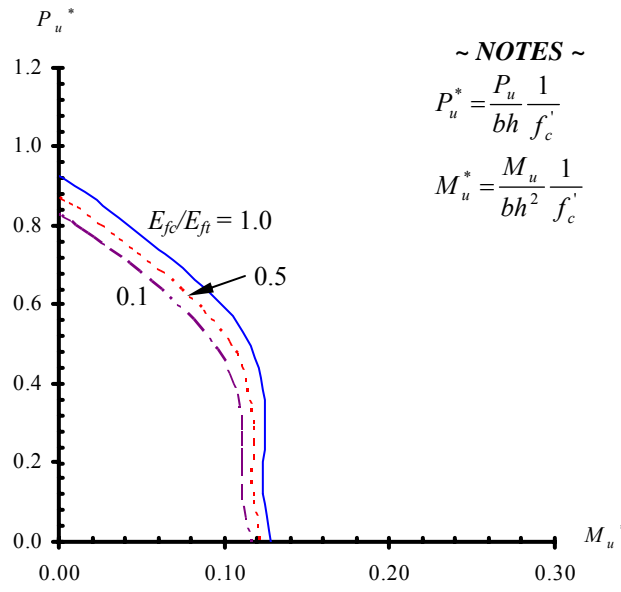


**Fig. 3.7 – The effect of reduced elastic compression modulus on FRP RC column cross sectional strength.**



Elastic property of CFRP rebar:  
 $E_{ft} = 21,300 \text{ ksi}$   
 $(147 \text{ MPa})$

(b) CFRP RC cross sections:  $\rho = 3\%$



Elastic property of GFRP rebar:  
 $E_{ft} = 6,500 \text{ ksi}$   
 $(45 \text{ MPa})$

(c) GFRP RC cross sections:  $\rho = 3\%$

**Fig. 3.7 (Cont.) – The effect of reduced elastic compression modulus on FRP RC column cross sectional strength.**

It should be noted that the interaction curves of the individual RC column cross sections reinforced FRP rebar shown in Fig. 3.7 were plotted on identical scales of  $x$ - and  $y$ - axes for comparative purposes. Since individual FRPs have significantly different properties, Fig. 3.7 offers these findings:

- Overall strength reduction was observed, as expected, when elastic compression modulus of the individual FRP reinforcement was lowered, respectively.
- Greater strength reduction was observed for RC column cross sections reinforced with FRP rebar that had higher stiffness and vice versa.

One may argue that ignoring or excluding the strength contribution of FRP rebar in the compression zone would likely yield a more conservative strength interaction, this is commonly done in flexural design in concrete practices, especially when compression properties of FRP rebar are not readily available. However, as indicated in Fig. 3.7.b, the exclusion of compression FRP rebar (or  $E_{fc}/E_{ft} = 0$ ) in strength prediction will lead to underestimation and inaccurate prediction of strength interaction. It should also be noted that the underestimation of strength interaction will increase when larger reinforcement ratio was considered.

To confidently use FRP rebars as potential alternative reinforcement to steel, long term effects need to be considered. Long term concrete stress/strain curves [i.e. typical long term (TLT) and realistic long term (RLT) stress/strain curves] have been presented in Chapter 2. How these curves contrast with the short term (ST) concrete stress/strain curve are shown in Fig. 3.8.

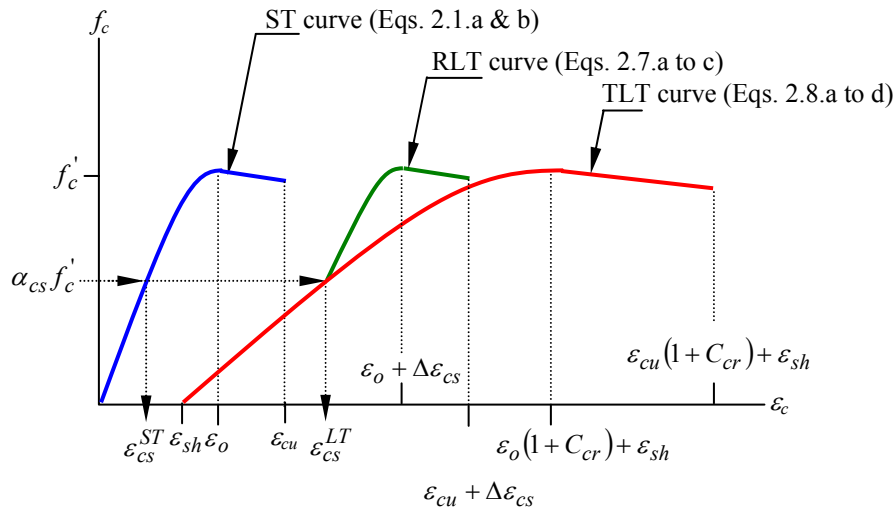


**Fig. 3.8 – A composite of the short and long term concrete loadings (A reproduction of Fig. 2.5).**

As discussed in Chapter 2, limiting ultimate concrete compression strain of long term stress/strain models is a function of its concrete compression strength ( $f'_c$ ), assumed concrete shrinkage strain ( $\epsilon_{sh}$ ), service stress/load factor ( $\alpha_{cs}$ ), etc. For illustrative purposes, the strength interaction diagrams (Figs. 3.8 – 3.11) were derived based on the following parameter values:  $f'_c = 5,000$  psi (35 MPa),  $\alpha_{sc} = 0.45$ , and  $\epsilon_{sh} = 0.0006$ . The resulting creep coefficient,  $C_{cr}$ , was 2.67, and the ultimate limiting concrete compression strains increased from the ACI usable strain of 0.003 (ST concrete model) to 0.00524 and 0.0116 for realistic (RLT) and typical (TLT) long term concrete stress/strain models, respectively. As indicated in Fig. 3.9, the change in concrete strain or increase in ultimate concrete strain did not lead to change in ultimate concrete stress.



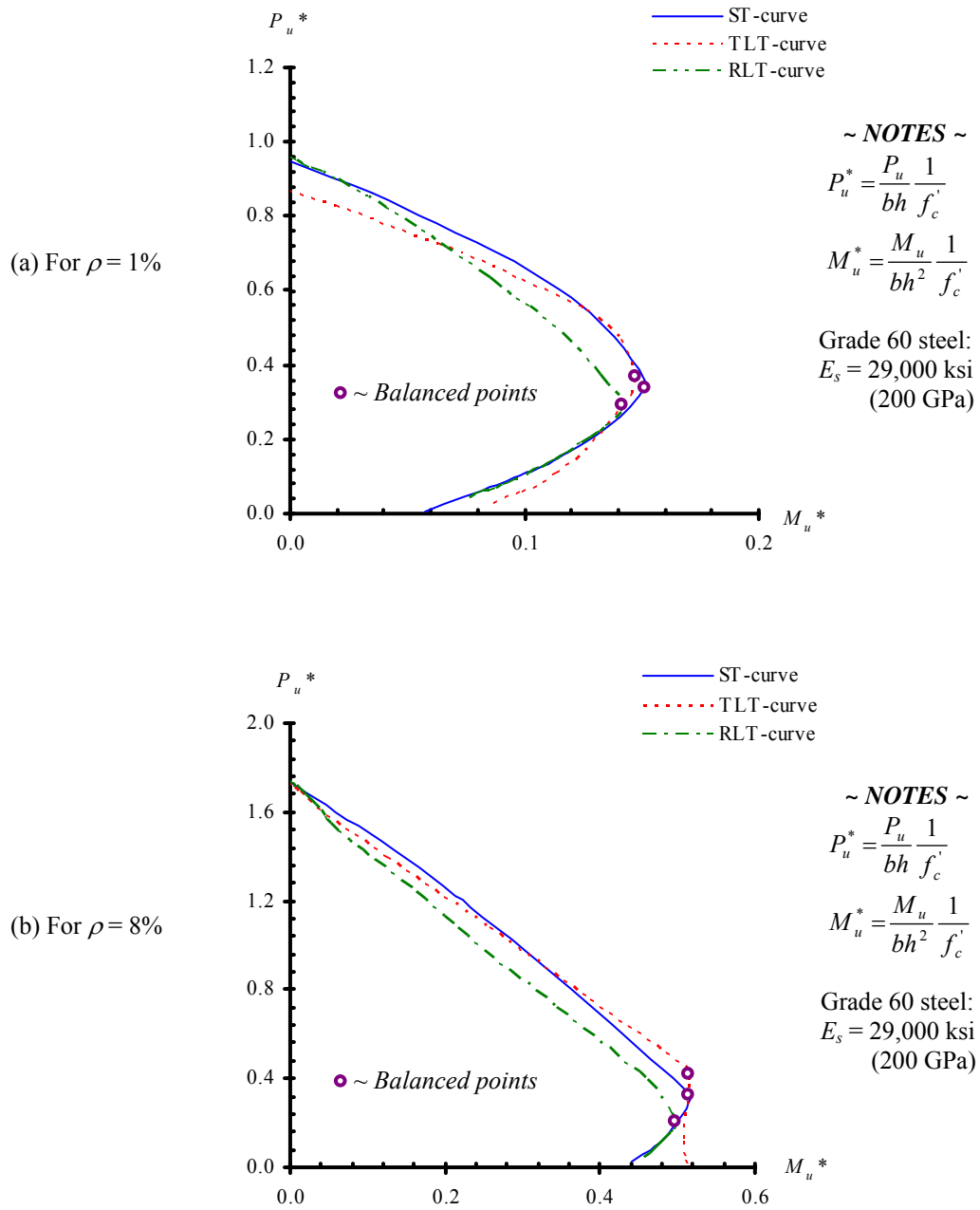


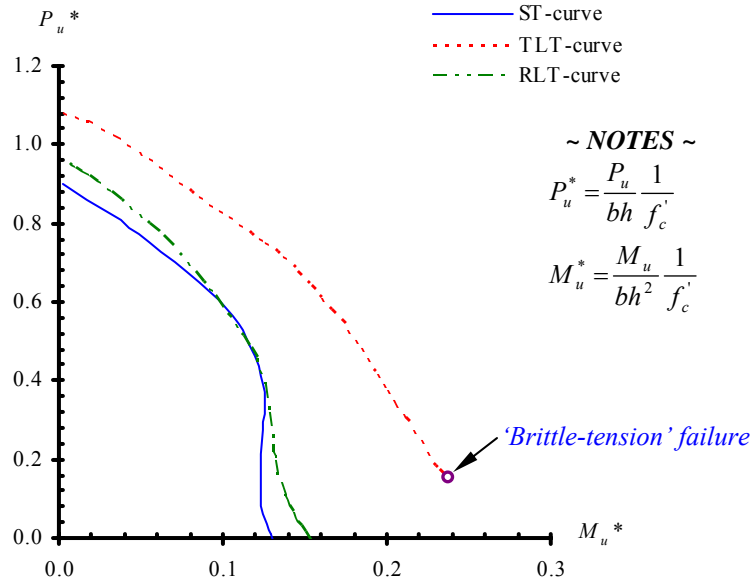
**Fig. 3.9 – Long term strength interaction diagrams of steel reinforced concrete column cross sections.**

Long term strength interactions for concrete column cross section reinforced with Grade 60 steel have been generated, and the following can be observed (Choo et al. 2003):

- The increase of the long term ultimate concrete compression strain of the TLT curve resulted in inconsequential change in column ultimate strength for  $\rho$  of 1%, while a relative increase in moment strength was noted for  $\rho$  of 8% at low axial loads. This increase in moment strength can be ascribed to the increase in steel strains and stresses into the strain hardening region (see Fig. 2.6).
- Significant reductions in strength can be observed above the balanced points when the RLT relationship was used. The reduction can be explained by the fact that much of the concrete in the compression region is at lower stress than with the ST relationship, but the steel strain did not reach strain hardening.

Choo et al. (2003) concluded that the RLT relationship was a more realistic long term model for concrete, and indicated that the ACI and other models were somewhat unconservative. Theoretical long term strength interactions of concrete column cross section reinforced with different FRP types have been derived using similar long term concrete models (see Sections 2.2.2. and 2.2.3) and are presented in Figs. 3.10 – 3.12.

(a) For  $\rho = 1\%$   
 AFRP (ST):  
 $E_{ft} = 12,600 \text{ ksi (187 GPa)}$   
 $\varepsilon_{fut} = 2.4\%$   
 $E_{fc} = E_{ft}$   
 $\varepsilon_{fuc} / \varepsilon_{fut} = 0.5$



(b) For  $\rho = 8\%$   
 AFRP (ST):  
 $E_{ft} = 12,600 \text{ ksi (187 GPa)}$   
 $\varepsilon_{fut} = 2.4\%$   
 $E_{fc} = E_{ft}$   
 $\varepsilon_{fuc} / \varepsilon_{fut} = 0.5$

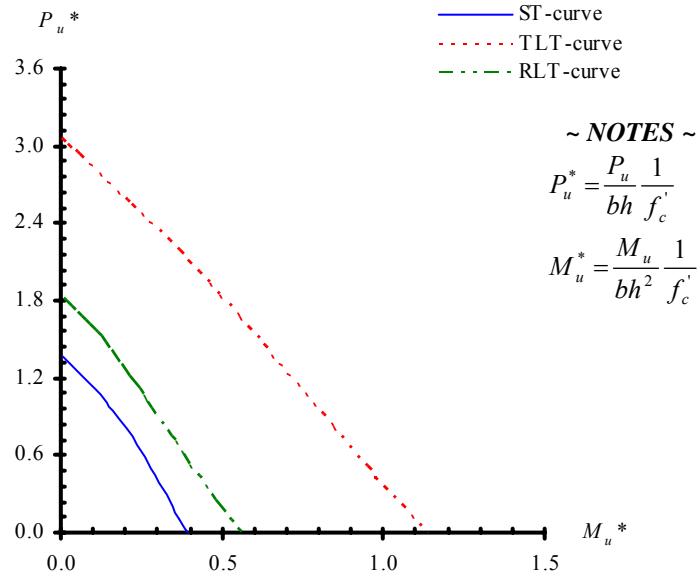
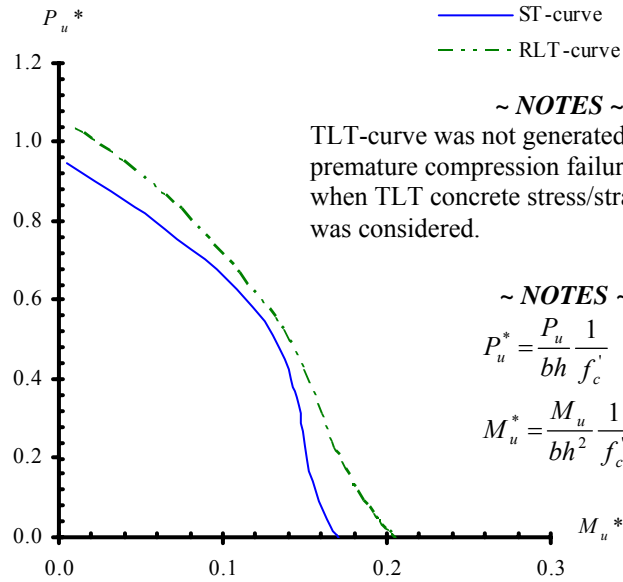


**Fig. 3.10 – Long term strength interaction diagrams of AFRP reinforced concrete column cross sections.**

(a) For  $\rho = 1\%$

CFRP (ST):  
 $E_{ft} = 21,300$  ksi (147 GPa)  
 $\varepsilon_{fut} = 1.6\%$   
 $E_{fc} = E_{ft}$   
 $\varepsilon_{fuc}/\varepsilon_{fut} = 0.5$



(b) For  $\rho = 8\%$

CFRP (ST):  
 $E_{ft} = 21,300$  ksi (147 GPa)  
 $\varepsilon_{fut} = 1.6\%$   
 $E_{fc} = E_{ft}$   
 $\varepsilon_{fuc}/\varepsilon_{fut} = 0.5$

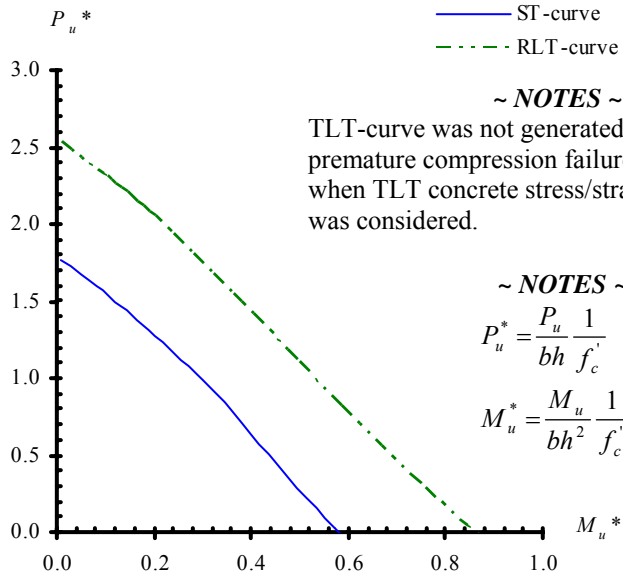
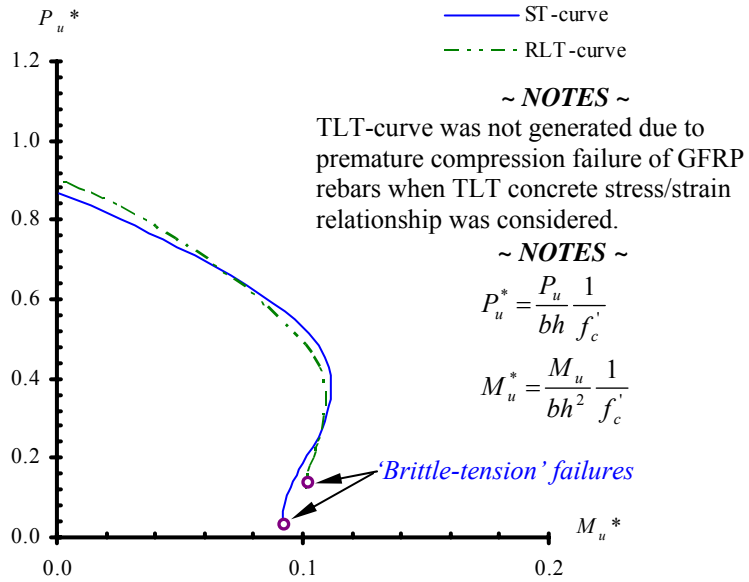


**Fig. 3.11 – Long term strength interaction diagrams of CFRP reinforced concrete column cross sections.**

(a) For  $\rho = 1\%$   
 GFRP (ST):  
 $E_{ft} = 6,500 \text{ ksi (45 GPa)}$   
 $\varepsilon_{fut} = 1.4\%$   
 $E_{fc} = E_{ft}$   
 $\varepsilon_{fuc} / \varepsilon_{fut} = 0.5$



(b) For  $\rho = 8\%$   
 GFRP (ST):  
 $E_{ft} = 6,500 \text{ ksi (45 GPa)}$   
 $\varepsilon_{fut} = 1.4\%$   
 $E_{fc} = E_{ft}$   
 $\varepsilon_{fuc} / \varepsilon_{fut} = 0.5$

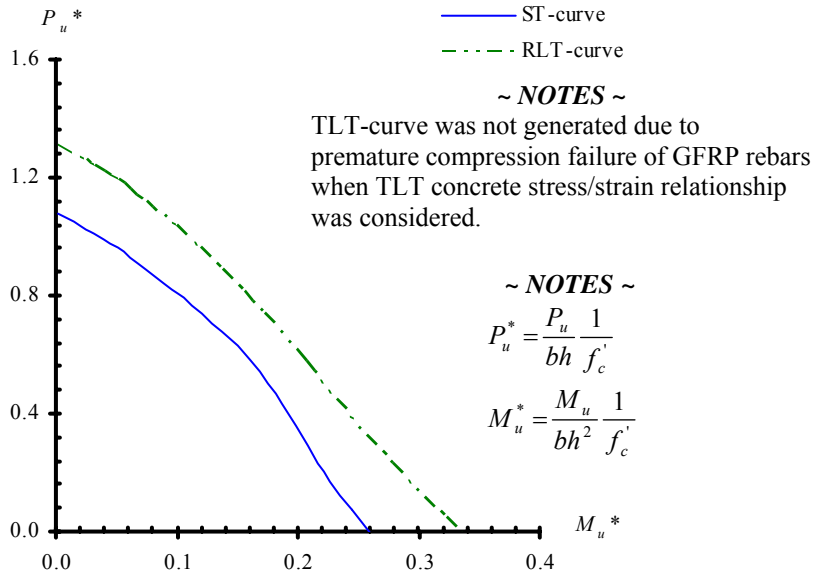


**Fig. 3.12 – Long term strength interaction diagrams of GFRP reinforced concrete column cross sections.**

The increase of ultimate limiting concrete compression strains, e.g. TLT and RLT concrete stress/strain models, due to concrete creep ( $\epsilon_{cr}$ ) and shrinkage ( $\epsilon_{sh}$ ) coupled with reduction (assumed 55% –lower bound of what had been reported in the literature) in ultimate tensile strains in FRP has the following effects on concrete column cross sections reinforced with FRP reinforcements:

- The possibility of *brittle-tension* failure may occur when long term concrete effects were considered, even when no such failure occurred during the initial short term analysis. One such example is shown in Fig. 3.9.a where AFRP RC column cross section with reinforcement ratio of 1% experienced *brittle-tension* failure when TLT concrete model was used. One other scenario is shown in Fig. 3.11.a where *brittle-tension* failure occurred at much earlier stage of strength interaction [strength interaction curve in this dissertation is generated starting from pure axial to balanced (for steel RC) to pure bending conditions] or at a higher axial load level when RLT and ST curves were compared. To overcome this problem, reinforcement ratio of FRP RC column cross sections may have to be increased as FRP reinforcement in such column cross sections will not be strained or stressed as high as approaching or exceeding FRP's ultimate strain ( $\epsilon_{fult}$ ) in tension (see Fig. 3.9.b).
- In addition to *brittle-tension* failure, *premature compression* failure of FRP reinforcement in compression may occur when long term concrete effects were considered. Such examples are depicted in Figs. 3.10.a & b, and Figs. 3.11. a & b. In these Figures, it can be seen that the limiting ultimate concrete strain of TLT concrete model has exceeded the ultimate compression strains ( $\epsilon_{fuc}$ ) of CFRP and GFRP rebars assumed in these theoretical examples. Note that TLT curves in these figures were not generated on purpose. If plotted, it should also be noted that the compression strength of the TLT strength interaction curves was contributed only by concrete, and was rather insignificant when reinforcement ratio increased.
- In the absence of both *brittle-tension* and *premature compression* failures, FRP RC column cross sectional strength will generally gain, in some cases significant increase can be expected, with time. Recall that strength interaction of steel RC column cross sections experienced no such drastic difference when long term effects were considered.

Comparing the strength interactions of the ST curves to the RLT curves, in which a more realistic load path was considered for the RLT concrete model, the magnitude of strength increase can be attributed to two main factors: increase in reinforcement ratio ( $\rho$ ) and elastic moduli ( $E_{ft}$  or  $E_{fc}$ ). Examples of strength increase are shown in Figs. 3.9.a & b, 3.10.a & b, and 3.11.b.

- The change in concrete shrinkage strain ( $\varepsilon_{sh}$ ) which typically ranges between  $2 \times 10^{-4}$  to  $12 \times 10^{-4}$ , though not presented here, caused no significant gain or loss in strength in all (steel and FRP) RC column cross sections. The increase in concrete shrinkage strain which directly resulted in increase (or rightward shift of stress/strain curve) in the ultimate limiting concrete compression strain would have triggered brittle-tension failure at an earlier stage in strength interaction diagram or at a higher axial load level, however, its effect was not discernible.

### 3.5 Concluding Remarks

Short and long term strength evaluations of FRP reinforced concrete columns of rectangular shapes under uni-axial bending were based on equilibrium conditions, strain compatibility, and material constitutive laws, and assumptions pertinent to steel reinforced concrete columns (i.e. ACI 318-02). The following are observations and findings related to strength interaction of FRP RC columns:

- Unlike steel RC column cross sections which strength interaction has well-defined compression- and tension-controlled regions with *balanced* points as a transitional point, FRP RC column cross sections do not exhibit such a pattern due to FRP's linearly-elastic material characteristic. In some instances, as a result, FRP RC column cross section may exhibit increase in moment resistance as axial load decreases.
- It is known that compression elastic modulus of FRP rebar is invariably lower than its tension elastic modulus, the reduced stiffness in compression may significantly lower the overall strength, especially in concrete column cross sections reinforced with relatively stiff FRP rebar.

- Though the exclusion of compression reinforcement during strength calculation is a common practice in flexural design of concrete members, ignoring the FRP compression reinforcement in column strength may lead to greatly underestimation and inaccurate prediction of column strength interaction.
- Short and long term ultimate strength evaluation – in which strength interaction was derived based on predetermined ultimate limiting strain of concrete in compression – of FRP RC column cross sections revealed the potential of such columns failed either *prematurely* in compression or *brittle* failure in tension. The former signifies that only concrete, in the absence of reinforcement, will assume load bearing responsibility, and the latter indicates that columns fail in an explosive manner without prior warning.
- The strength evaluation also revealed the importance of performing long term analysis by considering creep and shrinkage of concrete and long term effects of FRP rebar on FRP reinforced concrete columns as the aforementioned failures may or may not be revealed during short term analysis.
- In the absence of *premature compression* and *brittle tension* failures, FRP RC columns exhibit in most cases increase in strength interaction whereas steel RC columns show no significant gain or loss in strength.

In light of these findings, a design procedure taking multitude of factors into account is devised and presented in Chapter 6 to overcome failure of FRP rebar in RC columns, particular the ones that deal with *brittle tension* failure. Details derivation of the procedure will be presented in Chapter 6.



## CHAPTER 4

### FRP REINFORCED CONCRETE COLUMNS: SLENDER COLUMN STRENGTH

#### 4.1 Introduction

In the treatment of compression members in Chapter 3, the assumption was made that the effects of buckling and lateral deflection on strength were small enough to be ignored, hence the analyses and results in Chapter 3 represent the cross section (short column) strength of a typical reinforced concrete column. Short columns are columns that have a low slenderness ratio  $L/r$  ( $L$  = column height and  $r$  = radius of gyration =  $\sqrt{I/A}$ ) are also commonly referred to as column segments, 'zero' length columns, or columns with sufficient lateral bracing (Harik and Gesund 1986). The failure of short columns can be associated with the failure of their constituent materials prior to reaching a buckling mode of failure. For example, short concrete columns reinforced with steel reinforcement can fail by crushing of the concrete on the compression side. In the case of FRP reinforced concrete columns, failure can either be initiated by crushing of concrete in compression, crushing of FRP rebar prematurely in compression, or brittle-tensile rupture of FRP rebar as demonstrated in previous chapter.

Adoption of higher strength steel and concrete has led to the increased use of slender concrete compression members. Hence, the effects of secondary bending moments caused by the coupling of the axial load and lateral deflection must be considered when the strength of a column is to be determined. As an illustration, Fig. 4.1 shows an eccentrically loaded column deforming laterally and developing additional moment due to the lateral deflection,  $\Delta$ . For *short* columns, the lateral deflection will be insignificant ( $\Delta \approx 0$ ) and can be ignored, and hence the load-moment ( $P$ - $M$ ) interaction will be almost linear (line  $O$ - $A$  in Fig. 4.1.c). The maximum axial load for such columns will be  $P_o$  (Point  $A$ ) with a column moment,  $P_o \cdot e$ .

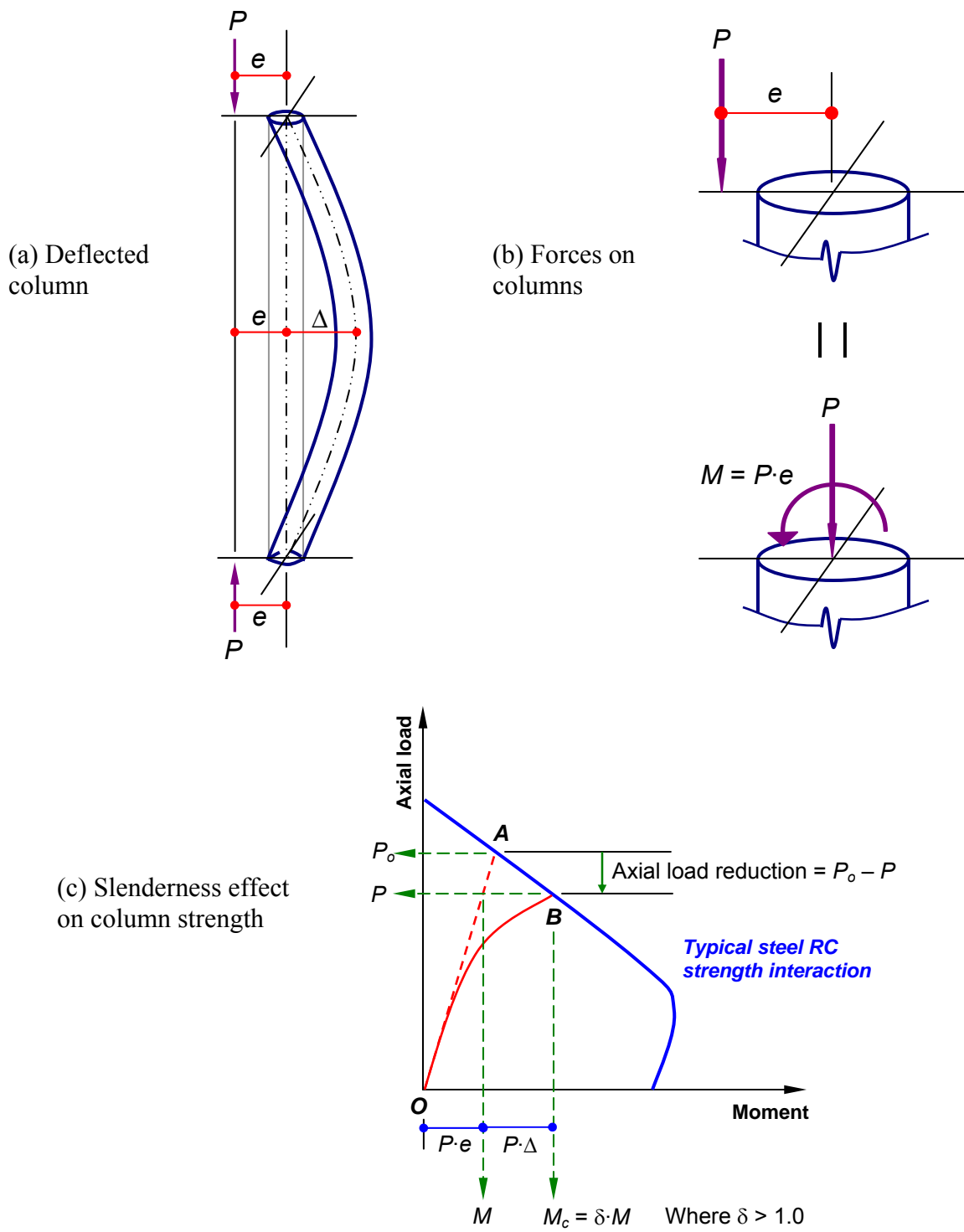


**Fig. 4.1 – Column strength due to slenderness effect.**

However, when the column becomes increasing slender or longer, the product of axial load,  $P$ , and lateral deflection,  $\Delta$ , becomes increasingly large and significant. The lateral deflection,  $\Delta$ , which increases nonlinearly, will produce a secondary moment,  $P \cdot \Delta$ , in addition to  $P \cdot e$ . The load-moment interaction of such columns is shown as line  $O-B$  in Fig. 4.1.c. Due to the added moment, the axial load of the column will be reduced from  $P_o$  to  $P$  (or from Point  $A$  to Point  $B$ ) with a corresponding column moment,  $M_c$ , of  $P \cdot (e + \Delta)$ . Such reduction in axial load capacity is referred to as *slenderness effect* (MacGregor 1997).

#### 4.2 Review of ACI 318-02: Moment Magnification Method in Non-sway Frames

In this section, the ACI moment magnification method treating a compression member in a non-sway frame will be reviewed. The ACI 318 (2002) permits the slenderness effects in a non-sway frame to be ignored if

$$\frac{kL_u}{r} \leq 34 - 12 \left( \frac{M_1}{M_2} \right) \quad (\text{ACI Eq. 10-8})$$

$k$  is the effective length factor (or equivalent pin-end length) for a compression member. As shown in Fig. 4.2, factor  $k$  must be determined for various rotational and translational end restraint conditions (Wang and Salmon 1998).

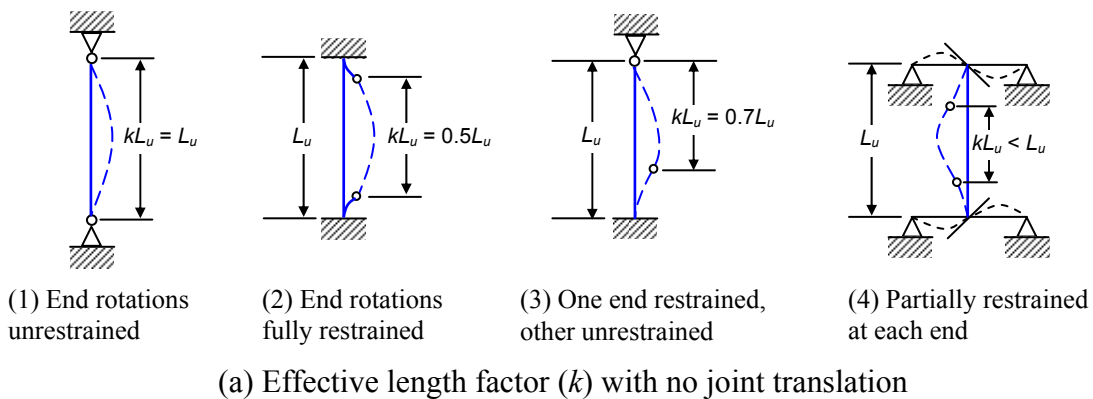
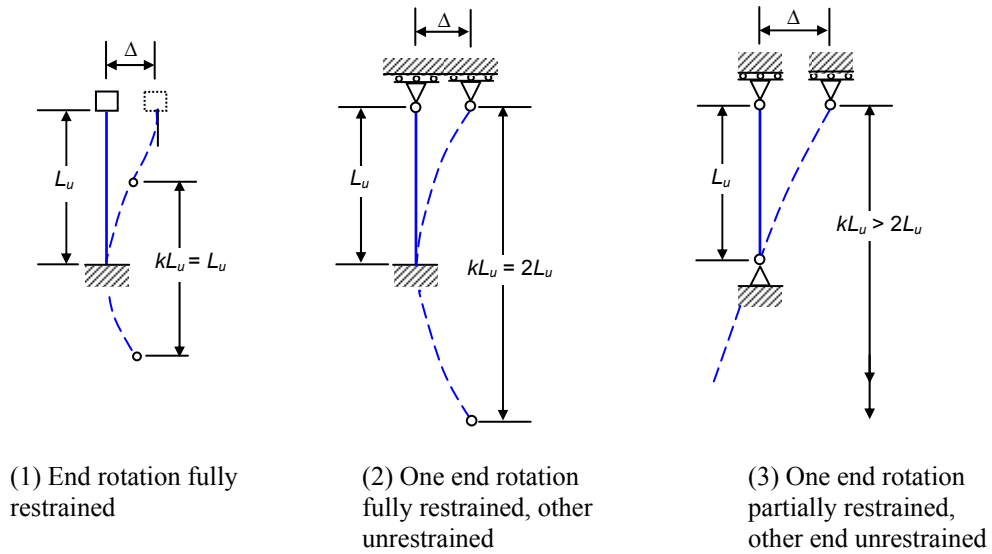
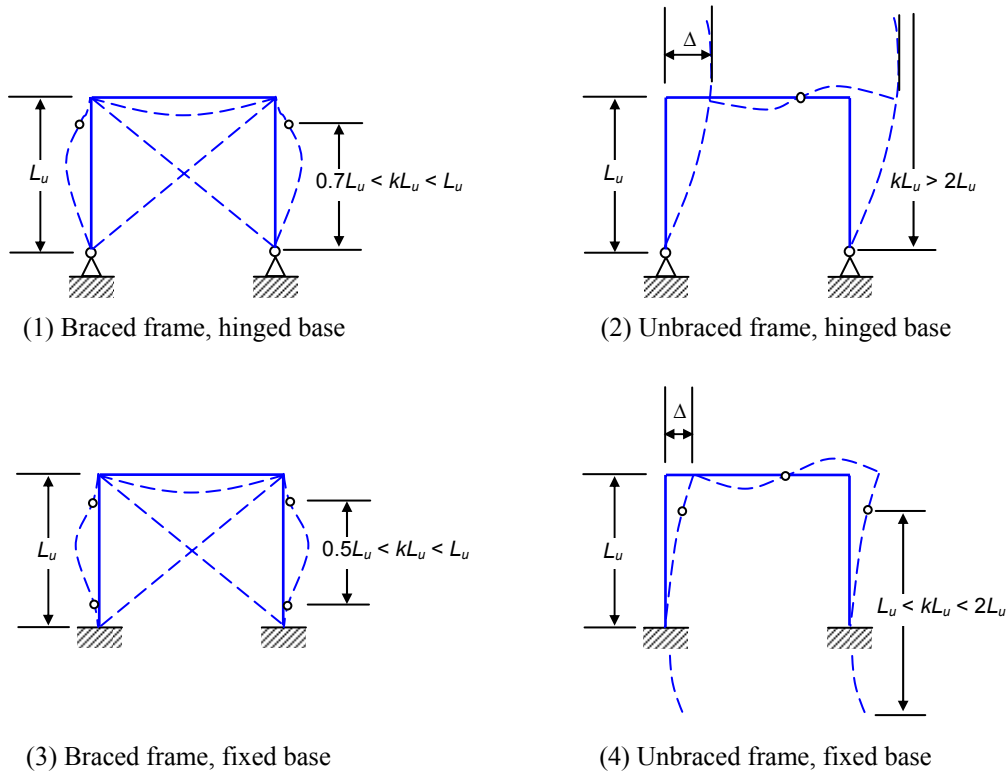


**Fig. 4.2 – Effective length factor ( $k$ ) of columns.**



(b) Effective length factor ( $k$ ) with possible joint translation



(c) Effective length factor ( $k$ ) for frames

**Fig. 4.2 (Cont.) – Effective length factor ( $k$ ) of columns.**

$L_u$  is the laterally unsupported length of a compression member, and  $r$  is the radius of gyration of the cross section.  $M_1$  and  $M_2$  are column ends moments where  $M_1/M_2$  in the equation is not taken less than -0.5.  $M_2$  is the lesser of the two end moments. The term  $M_1/M_2$  is positive when the column is bent in single curvature and negative in double curvature.

In addition, the compression members shall be designed for the factored axial load  $P_u$  and the magnified factored moment  $M_c$ , where  $M_c$  is expressed as follows:

$$M_c = \delta_{ns} M_2 \quad (\text{ACI Eq. 10-9})$$

Eq. 10-9 of ACI predicts  $M_c$  by multiplying  $M_2$  by a moment magnification factor  $\delta_{ns}$  (subscript  $ns$  denotes non-sway) which can be determined as follows

$$\delta_{ns} = \frac{C_m}{1 - \frac{P_u}{0.75P_c}} \geq 1.0 \quad (\text{ACI Eq. 10-10})$$

$P_c$  in the ACI Code is defined as the critical load and is expressed as

$$P_c = \frac{\pi^2 EI}{(kl_u)^2} \quad (\text{ACI Eq. 10-11})$$

The column stiffness,  $EI$ , can be taken as

$$EI = \frac{(0.2E_c I_g + E_s I_s)}{1 + \beta_d} \quad (\text{ACI Eq. 10-12})$$

or conservatively as,  $EI = \frac{0.4E_c I_g}{1 + \beta_d}$  (ACI Eq. 10-13)

where  $E_c$  and  $E_s$  are the moduli and elasticity of concrete and reinforcement, respectively, and  $I_g$  and  $I_s$  are the moments of inertia of gross concrete section and reinforcement about the centroidal axis of member cross section.

The column stiffness in Eq. 10-12 of ACI was derived for small eccentricity ratios and high levels of axial load where the slenderness effects are most pronounced (ACI 318-99 Section R10.12.3). Eqs. 10-12 and 13 are divided by  $(1 + \beta_d)$  due to sustained load in which  $\beta_d$  is defined by ACI as the ratio of maximum factored axial dead load to the total factored load in a non-sway frame. To simplify, ACI also permits the use of  $\beta_d$  equal 0.6, hence Eq. 10-13 can become  $EI = 0.25E_cI_g$ .

For members without transverse loads between supports, ACI requires that  $C_m$  to be taken as

$$C_m = 0.6 + 0.4 \frac{M_1}{M_2} \geq 0.4 \quad (\text{ACI Eq. 10-14})$$

The minimum  $M_2$  allowed in the ACI Code is

$$M_{2,\min} = P_u(0.6 + 0.03h), \text{ where } h \text{ is in inches}$$

$$\text{Or } M_{2,\min} = P_u(15 + 0.03h), \text{ where } h \text{ is in millimeters} \quad (\text{ACI Eq. 10-15})$$

The calculation of critical load,  $P_c$ , in ACI Eq. 10-11 involves the use of the column stiffness,  $EI$ , which is the slope of the relationship between moment and curvature. The nonlinear stress/strain responses of concrete and steel have long been recognized. The combination of concrete and reinforcement results in nonlinear moment-curvature responses of a typical concrete reinforced member. As a result, the value of  $EI$  chosen for a given column section, axial load level, and slenderness must approximate the  $EI$  of the column at failure load taking cracking, creep, and the non-linearity of the concrete and reinforcement stress/strain curves into consideration (MacGregor 1997, Rodriguez-Gutierrez and Aristizabal-Ochoa 2001). The approximate expression for  $EI$  in ACI 318-02 will clearly not accurately predict the real

load-deflection or therefore the real axial load-moment response of a reinforced concrete column. Hence, in order to determine the inelastic behavior of reinforced concrete columns, the complete axial load-moment-curvature relationship must be generated and used.

### 4.3 Deflection Method for Reinforced Concrete Columns

It appears that the effect of secondary bending moments ( $P \cdot \Delta$ ) for a column caused by the axial load ( $P$ ) and lateral deflections ( $\Delta$ ) can be accounted for once the column lateral deflections along its length have been determined. Subsequently, the added bending moment ( $P \cdot \Delta$ ) can be determined based on the deformed geometry of a column as depicted in Fig. 4.3.

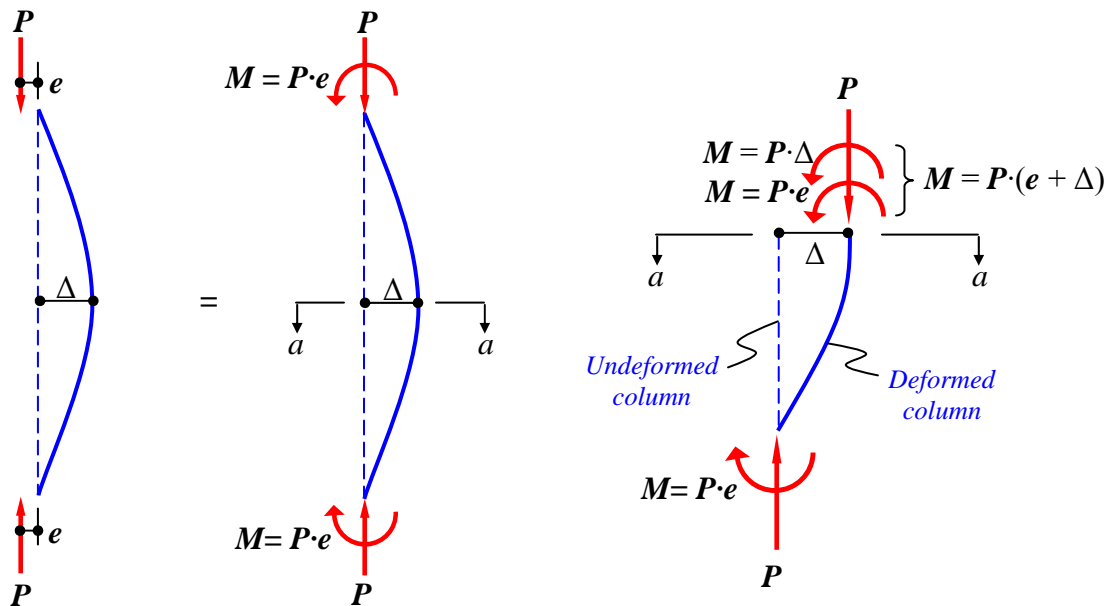


**Fig. 4.3 – Secondary moment due to the lateral deflection of a column subjected to a constant eccentricity ( $e$ ).**

In this dissertation, the study of slenderness effect in concrete columns with FRP bars will be limited to pin-ended columns subjected to a constant eccentricity at both ends as shown in Fig. 4.3. In general, a governing differential equation for all columns with any boundary conditions is defined as (Chen and Lui 1987)

$$EI \frac{d^4 y}{dx^4} + P \frac{d^2 y}{dx^2} = 0 \quad (4.1)$$

$y$  is the lateral deflection varies along the column axis (or  $x$ -axis).  $P$  is the applied axial force at the support, and  $EI$  is the column stiffness. For a column with a constant  $EI$ , Eq. 4.1 can be expressed as (Chen and Lui 1987)

$$\frac{d^4 y}{dx^4} + k^2 \frac{d^2 y}{dx^2} = 0 \quad (4.2)$$

and

$$k^2 = \frac{P}{EI} \quad (4.3)$$

If a direct analytical solution such as a deflection function,  $y = f(x)$ , can be obtained for Eq. 4.2, then the other physical responses such as slope and curvature can be calculated by appropriately differentiating the deflection function. The internal force such as moment can then be calculated from the equilibrium of the deformed column. For concrete columns, which are generally in-elastic, the column stiffness,  $EI$ , varies as compared to elastic members which have a simple form of moment-curvature relation ( $M = EI \cdot \phi$ ).

In this investigation, an alternative solution procedure which uses a numerical integration procedure presented by Chen and Atsuta (1976) will be used. The use of the numerical integration scheme requires first the moment-curvature relations to be developed. Therefore, in the investigation of concrete columns, the tasks are: (1) development of the axial load-moment-curvature ( $P$ - $M$ - $\phi$ ) responses, and (2) determination of column lateral deflection using the numerical scheme. In summary, the method accounts for geometrical nonlinearity by introducing the secondary moment ( $P \cdot \Delta$ ) into the calculation, and the material nonlinearity based



on the derived nonlinear  $P$ - $M$ - $\phi$  relations (Chen and Lui 1987). The details of the overall scheme are as follows.

#### 4.3.1 Development of Axial Load-Moment-Curvature ( $P$ - $M$ - $\phi$ ) Relationship

The basic assumptions presented for reinforced column cross-sections and equations developed in Chapter 3 can be used here to generate the axial load-moment-curvature ( $P$ - $M$ - $\phi$ ) relationships of a concrete column at any desired location. The procedure is summarized in the following steps:

1. Divide the column cross section into  $N$  number of strips and assume the location of a neutral axis.
2. Select a small value for the concrete strain,  $\epsilon_c$ , at the outermost concrete fiber in compression.
3. From linear strain distribution, determine the strains at the center of all concrete strips in compression and the strains in all reinforcing bars.
4. Using concrete and reinforcement stress-strain relations, determine the stresses, and consequently forces, in tension or compression in each reinforcing bar, and in each strip of concrete in the compression zone.
5. The resultant axial load,  $P$ , and the bending moment,  $M$ , that the cross section will resist for the assumed strain distribution and curvature can be determined by summing the vertical forces, and the moments about the centroid of the cross section. The associated curvature,  $\phi$ , is equal to the strain,  $\epsilon_c$ , in step 2 divided by the distance  $kd$ , from the outermost fiber in compression to the neutral axis.
6.  $\epsilon_c$  is increased by a small amount  $\Delta\epsilon_c$ , and the procedure from step 4 above is repeated. Steps 4 and 6 are repeated until a predetermined limiting compression strain  $\epsilon_{cu}$  is reached. For instance, the  $\epsilon_{cu}$  of the ST-curve will be the ACI-318 ultimate concrete compression strain of 0.003. After the ultimate compression strain has been used, a new location of the neutral axis is selected and the procedure is repeated from step 2. A table of axial load-moment-curvature is created from the results.

Examples of the axial load-moment-curvature relations will be presented graphically later in the following sections. It should be noted that *ultimate* strength interaction relations of concrete columns presented in previous chapter were based on an ultimate concrete compression strain,  $\epsilon_{cu}$ . Here, however, the strength interactions are generated by incrementally varying the concrete compression strain until an ultimate is reached (see Step 6 above).

### 4.3.2 Numerical Computation of Column Deflection

The numerical procedure used to obtain lateral displacements of a column is described with the aid of Fig. 4.4. The lateral displacements  $\Delta_i$ , and slopes  $\theta_i$  at points  $x_i$  of a column are successively calculated for an assumed initial slope  $\theta_0$  at  $x_0$  for a given combination of  $P$  and  $M$  at  $x_0$ . Chen and Atsuta (1976) pointed out that the deflections calculated using this numerical scheme required no prior assumption of deflected column shape (e.g. deflected shape in sine or cosine wave).

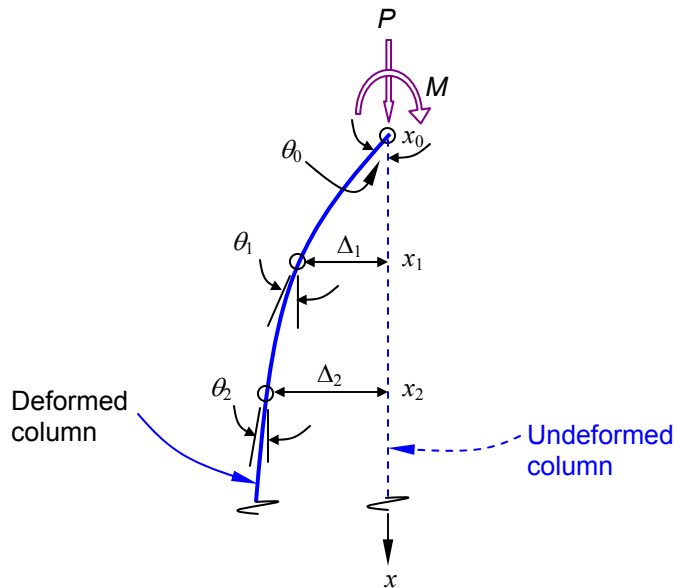


Fig. 4.4 – Numerical integration for column deflection.

The discrete points,  $x_1$ ,  $x_2$ , and so on, are chosen with small intervals so that the displacement and the slope at any point  $i$  may be approximated by the following numerical integration equations (Chen and Atsuta 1976)

$$\Delta_i = \Delta_{i-1} + \theta_{i-1}(x_i - x_{i-1}) - \frac{1}{2}\phi_{i-1}(x_i - x_{i-1})^2 \quad (4.4)$$

$$\theta_i = \theta_{i-1} - \phi_i(x_i - x_{i-1}) \quad (4.5)$$

Using the  $P$ - $M$ - $\phi$  relationships (see section 4.3.1) developed for the column cross section, the curvature at point  $i$  is computed as functions of the axial load and moment

$$\phi_i = f(M_i, P) \quad (4.4)$$

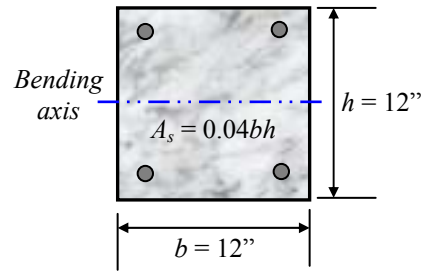
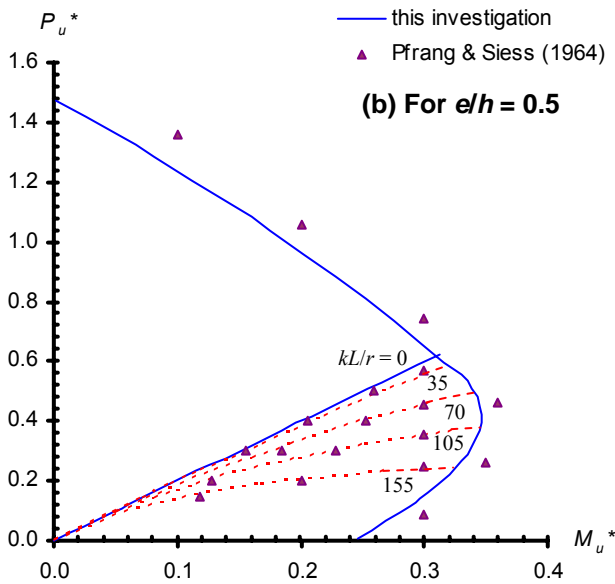
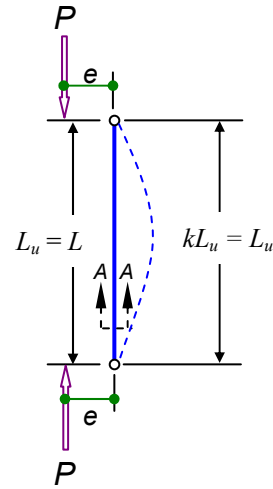
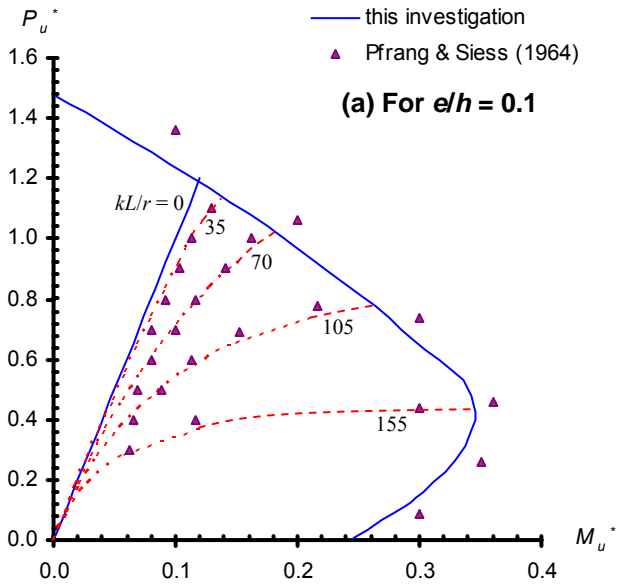
Harik and Gesund (1986) recommended use of ten and twenty segments for column bending in single and double-curvature, respectively. This recommendation is followed herein.

The procedure is repeated by changing  $\theta_0$  until the correct displacement is obtained. The correct displacements are those for which the slope at mid-height equals zero for symmetrical end conditions, or for which the displacement equals zero at the end of a column subjected to an axial load ( $P$ ) with unequal moments at the ends. The moments along the column, including the maximum moment, can be determined from the lateral displacements.

Repeating the above procedure for increasing values of  $P$ , the corresponding lateral displacements along the column can be computed. The column responses such as the axial force-lateral displacement and the axial force-maximum moment resistance can be generated.

#### 4.4 Slender Reinforced Concrete Column Strength

To verify the adequacy and accuracy of the method described in previous section, the results of concrete columns reinforced with steel rebar generated by Pfrang and Siess (1964) were used for comparison. As shown in Fig. 4.5, the Pfrang and Siess's column was a pin-end column loaded eccentrically at column ends to simulate a column that bends in single curvature. Fig. 4.5 also shows the reinforcement layout of the column cross section, which was maintained throughout the entire column. The ST concrete curve presented in Chapter 2 will be used with Pfrang and Siess's specified concrete compression strength ( $f'_c$ ) of 3,000 psi (21 MPa). Matching the steel properties assumed in Pfrang and Siess's column, a linearly-elastic and plastic steel stress/strain response was used with a specified yield strength ( $f_y$ ) of 45,000 psi (310 MPa) and elasticity modulus ( $E_s$ ) of 29,000,000 psi (200 GPa). The dimensionless axial load-moment responses of various slenderness ratios ( $kL/r$ ) and the strength interactions of the column are plotted for two different eccentricities ( $e$ ) as depicted in Fig. 4.5.



**Section A - A**

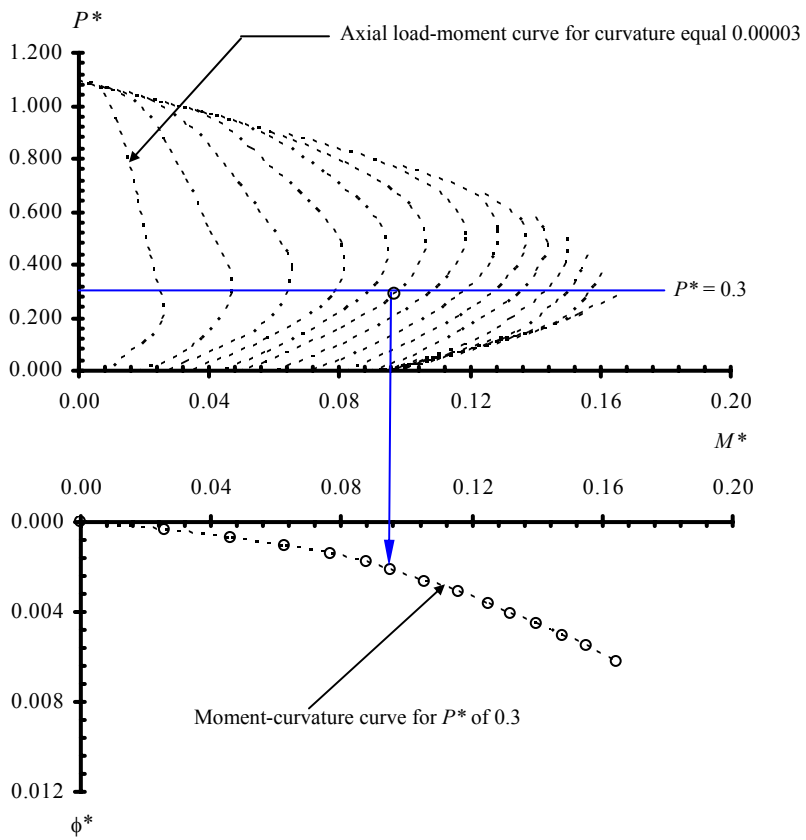
**Note:** see notations in previous chapter for  $P_u^*$  and  $M_u^*$

**Fig. 4.5 – The axial load-moment interaction curves of Pfrang and Siess (1964) for steel reinforced concrete slender columns bent in single curvature.**

It is clearly shown for concrete columns reinforced with steel rebar how the increase of slenderness ratios impacted the axial load-moment responses – greater column moment as a result of greater deflection due to increase slenderness. The use of the integration procedure coupled with axial load-moment-curvature responses (not shown) generated with the column section produced the theoretical axial load-moment curves (dotted red lines in the figure) that are in good agreement with the Pfrang and Siess’s curves (filled triangles in the figure). Note that the strength interaction ( $P_u^* - M_u^*$ ) – shown in solid blue line – generated using current procedure was slightly lower than those generated by Pfrang and Siess’s. This may be attributed to the fact that the displaced area of concrete by the reinforcing bars was accounted for in the calculation.

With above justification, the procedure was then used to study the slender column behavior of reinforced concrete column reinforced with steel and FRP rebars. Fig. 4.6 shows how the axial load ( $P$ ), moment ( $M$ ), and curvature ( $\phi$ ) of a concrete column cross section reinforced with Grade 60 steel (stress/strain relationship of Grade 60 steel is presented in Section 2.4) are related. For the sample steel reinforced concrete columns of Fig. 4.6, the following parameters were used: cross section of 12-in by 12-in (305 mm x 305 mm); typical concrete cover ( $C_c$ ) of 1½-in (40 mm); and four #8 rebars ( $\rho = 2.2\%$ ) placed at each corner of the cross section. The columns were assumed to be properly confined, and that local buckling of reinforcement would not occur. Figs. 4.7 – 4.9 are various responses of concrete columns reinforced with FRP rebars: aramind (A), carbon (C), and glass (G) FRP rebars. The FRP reinforced concrete columns in Figs. 4.7 – 4.9 assumed the same configuration described for Grade 60 steel reinforced concrete columns of Fig. 4.6. FRP rebars assumed the same properties given in previous examples presented in Chapter 3.

It should be noted that the reinforcement ratio ( $\rho$ ) of 2.2% was selected in these examples to specifically preclude FRP rebars’ rupture either in tension or compression. One such example is shown in Fig. 3.6 of Chapter 3 where reinforced concrete column cross sections reinforced with GFRP rebars endured *brittle-tension* failure for  $\rho$  of 1%, though not occurring at higher  $\rho$  ratios. Hence, the selection of  $\rho$  equals 2.2%, after rigorous numerical computations, was to ensure either *premature-compression* or *brittle-tension* failure would not occur in the types of FRP reinforced concrete columns selected as examples.



$$P^* = \frac{P}{bh f'_c}$$

$$M^* = \frac{M}{bh^2 f'_c}$$

$$\phi^* = \phi h$$

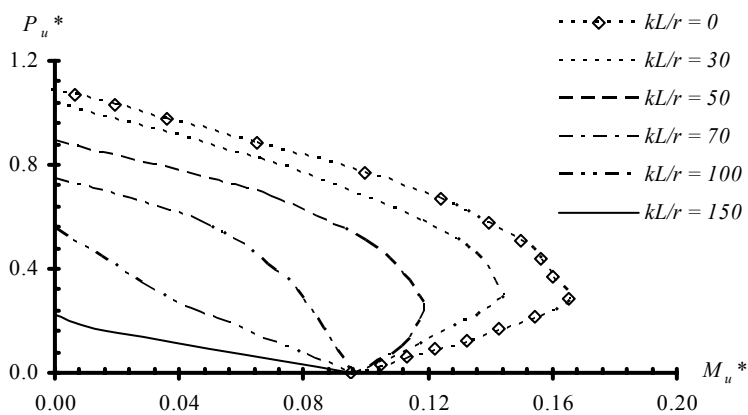
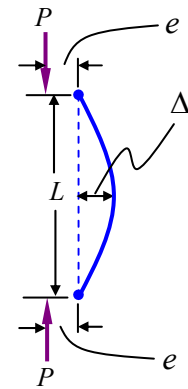
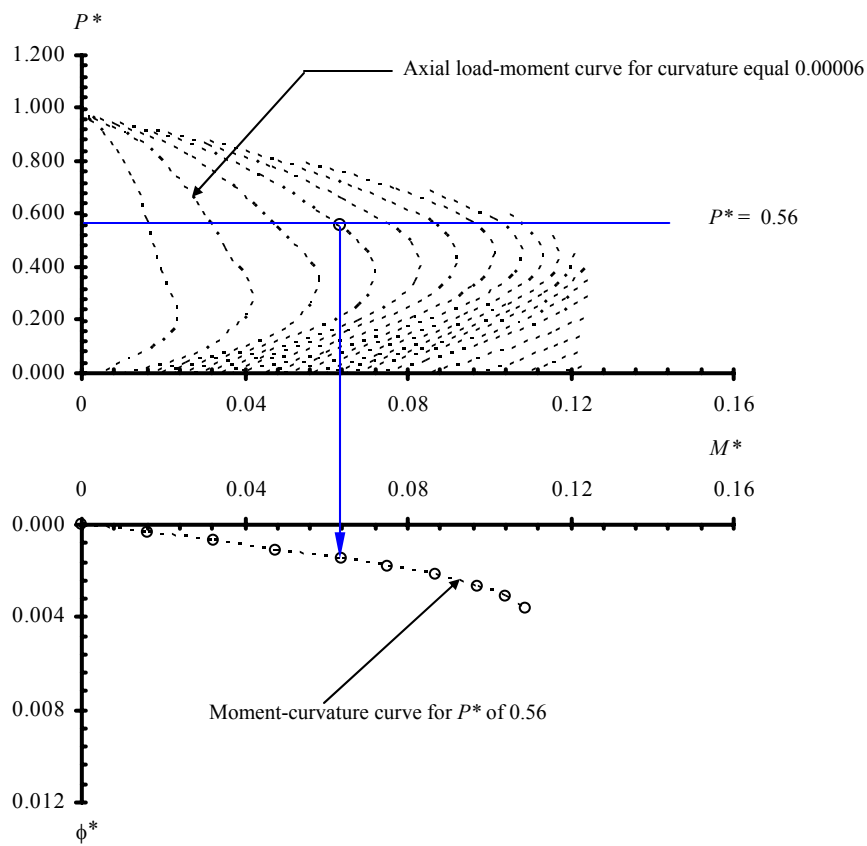


**Fig. 4.6 – Short term interaction responses of the axial load-moment and moment-curvature relationships ( $P^*-M^*-\phi^*$ ), and the ultimate axial load-moment ( $P_u^*-M_u^*$ ) relationships of Grade-60 steel RC concrete columns.**



$$P^* = \frac{P}{bh} \frac{1}{f'_c}$$

$$M^* = \frac{M}{bh^2} \frac{1}{f'_c}$$

$$\phi^* = \phi h$$

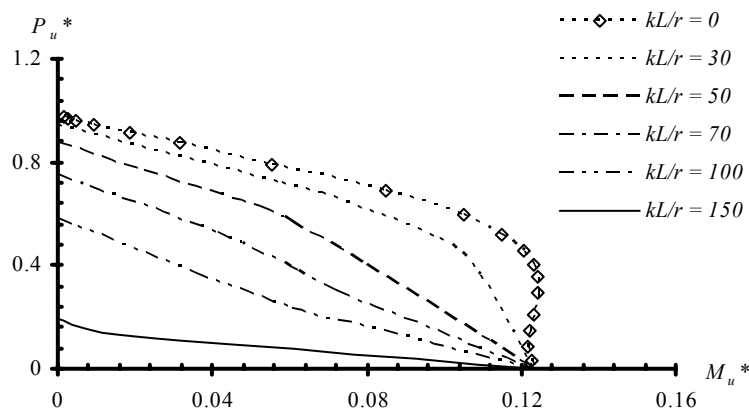
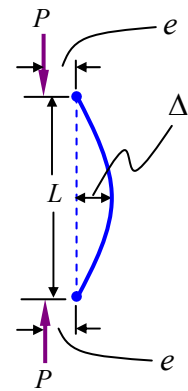
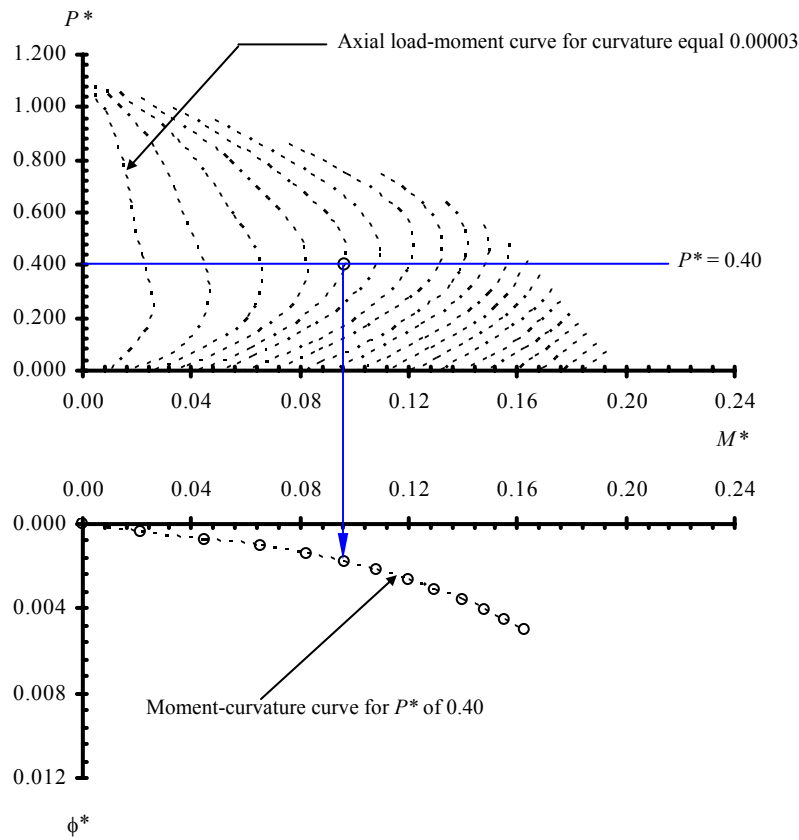


**Fig. 4.7 – Short term interaction responses of the axial load-moment and moment-curvature relationships ( $P^* - M^* - \phi^*$ ), and the ultimate axial load-moment ( $P_u^* - M_u^*$ ) relationships of AFRP RC concrete columns.**





$$P^* = \frac{P}{bh f'_c}$$

$$M^* = \frac{M}{bh^2 f'_c}$$

$$\phi^* = \phi h$$

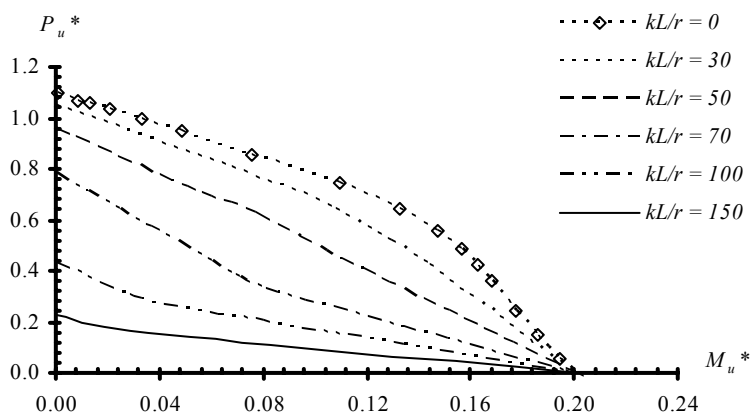
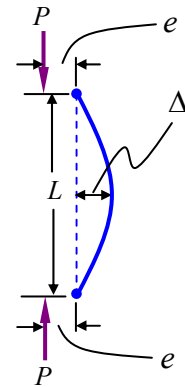
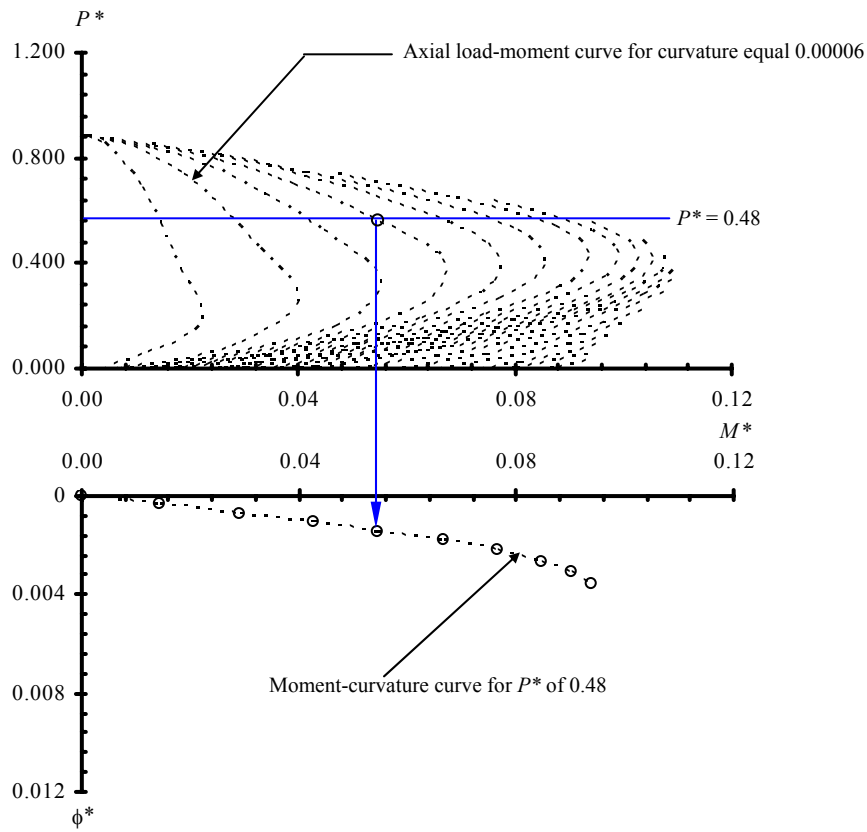


**Fig. 4.8 – Short term interaction responses of the axial load-moment and moment-curvature relationships ( $P^* - M^* - \phi^*$ ), and the ultimate axial load-moment ( $P_u^* - M_u^*$ ) relationships of CFRP RC concrete columns.**



$$P^* = \frac{P}{bh f'_c}$$

$$M^* = \frac{M}{bh^2 f'_c}$$

$$\phi^* = \phi h$$

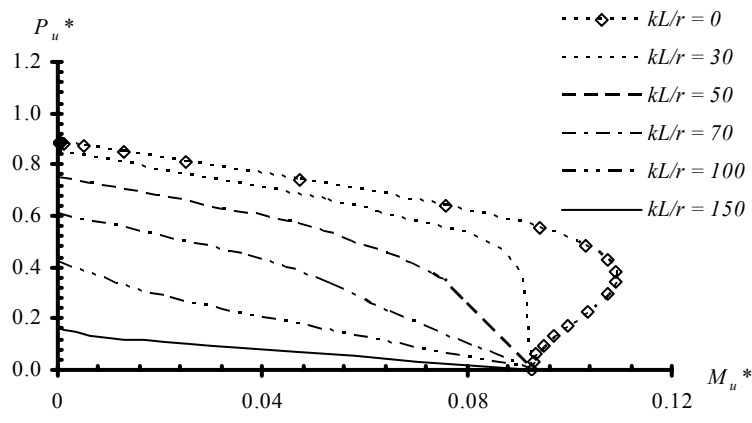
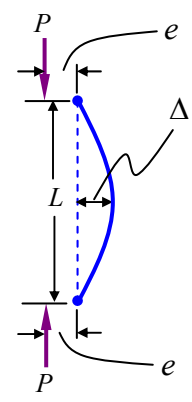


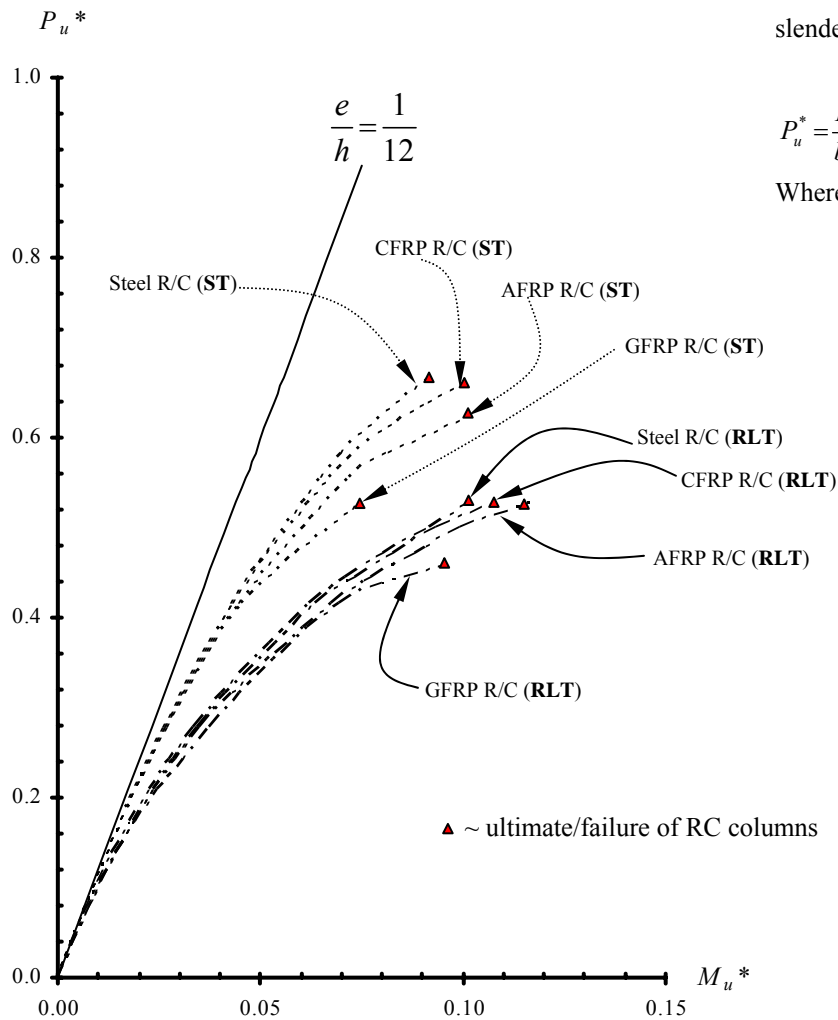
**Fig. 4.9 – Short term interaction responses of the axial load-moment and moment-curvature relationships ( $P^* - M^* - \phi^*$ ), and the ultimate axial load-moment ( $P_u^* - M_u^*$ ) relationships of CFRP RC concrete columns.**

The numerical approach was used successful in predicting the slender concrete columns responses with steel and FRP rebars. Based on the results, the following observations can be made:

- All concrete columns, with different types of longitudinal reinforcement, exhibit non-linear moment-curvature ( $M-\phi$ ) responses;
- Increase in column length has significant impact on overall strength interaction – strength interaction reduction was observed as slenderness ratio ( $kL/r$ ) was increased regardless the type of reinforced concrete columns.

The effects of the difference in longitudinal reinforcement properties (e.g. steel, AFRP, CFRP, & GFRP) and long term loading in concrete were examined in Fig. 4.10:

- Though FRP rebars have lower elastic moduli [e.g. Young's modulus ( $E$ ) of GFRP used in this example is almost 5 times lower than that of steel], the columns produced very similar axial load-moment responses in early stages of axial loading (throughout service loading range). A more distinct difference, however, was observed nearing the ultimate or failure load stage where reinforced concrete columns reinforced with FRP longitudinal rebars generally produced greater deflection as a result of lower column stiffness ( $EI$ );
- Long term (RLT) effect weakened the reinforced concrete columns by also reducing their column stiffness ( $EI$ ) resulting in greater deflection and hence producing greater secondary moment. The reduction of column stiffness is a result of increased curvature due to increased in concrete compression strain.



Column bents in single-curvature with slenderness ratio,  $\frac{kL}{r} = 50$ .

$$P_u^* = \frac{P_u}{bh f_c'} \frac{1}{f_c'}, \text{ and } M_u^* = \frac{P_u(e + \Delta)}{bh f_c'} \frac{1}{f_c'}$$

Where  $P_u$  is the applied axial load.

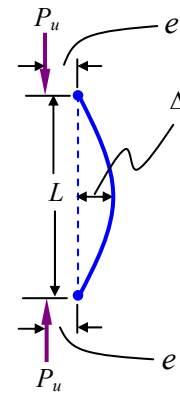


**Fig. 4.10 – Slender axial load-moment responses of various RC columns due to long term concrete loading.**

## CHAPTER 5

### PRESTRESSED CONCRETE (PC) COLUMNS WITH FRP COMPOSITES

#### 5.1 Introduction – Prestressing Concrete Columns with Steel Tendons

It may seem illogical, at first glance, to introduce initial stress (or prestress) into compression members, its presence, however, does offer some benefits (Harik and Whitney 1988, & Naaman 1982):

- Prestressing in a concrete column with steel strands/tendons generally leads to a reduction in its resistance to compression but improves its capacity in resisting bending as shown in the schematic of Fig. 5.1. This can be beneficial for compression members subjected to substantial bending.

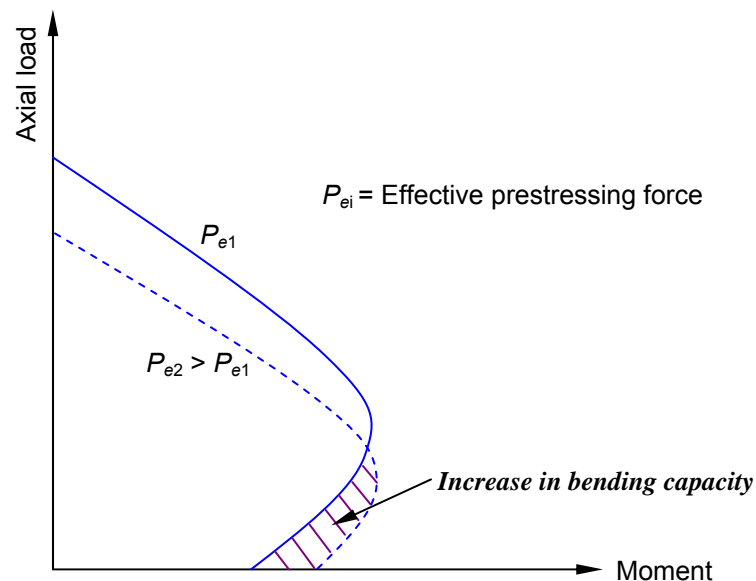


**Fig. 5.1 – Effect of prestressing on the column strength interaction.**

- The use of prestressing increases the concrete columns' resistance to first cracking. Consequently, the column's deflection in the 'uncracked' state is greatly reduced and its performance in service is improved.

- Since a column's capacity is directly proportional to the concrete strength ( $f_c'$ ), hence the use of high-strength prestressing reinforcement permits the use of high-strength concrete in column design. Typical effect of concrete strength on column strength interaction is shown in Fig. 5.2 – the use of higher strength concrete provides substantial improvement in compression strength and smaller improvement in bending strength.
- Prestressed members are usually precast. As a result, precast prestressed concrete elements eliminate the need of construction forms. In addition, precasting allows the production of concrete elements in a controlled environment.

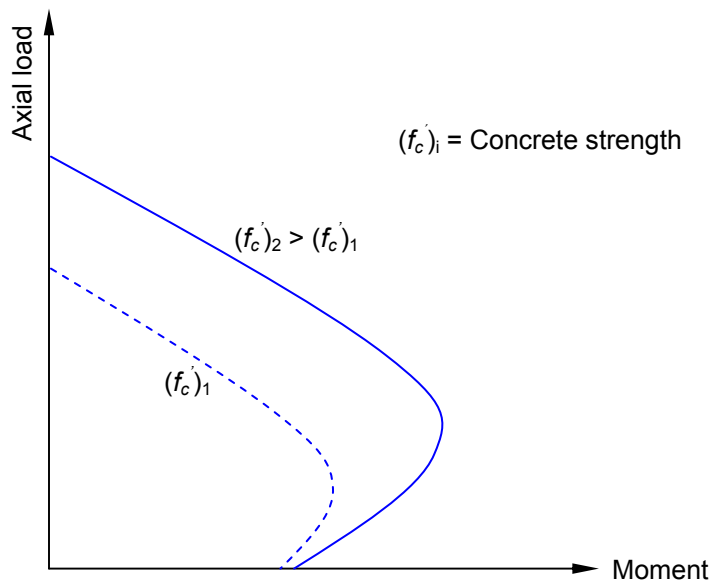


**Fig. 5.2 – Effect of concrete strength on the column strength interaction.**

## 5.2 Prestressing Concrete Columns with FRP tendons

Similar in reinforced concrete application, one of the principal advantages of FRP reinforcement for prestressing is the ability to configure the reinforcement to meet specific performance and design objectives. As a result, FRP composites have been proposed for use as prestressing reinforcements in concrete structures. In the United States, full-size prestressed concrete piles using FRP tendons/cables in several demonstration projects have been

documented (Iyer 1995; Iyer et al. 1996; Arockiasamy and Amer 1998; & Schiebel and Nanni 2000). The principal conclusions from the demonstration studies are as follows:

- The performance of FRP prestressed and steel prestressed piles during driving of piles were similar;
- FRP ties performed satisfactory based on the absence of damage following the driving operation – the tie spacing used was identical to that in comparable steel prestressed piles;
- The results indicated that there were no inherent problems in driving FRP prestressed piles and their performance was comparable to that of steel prestressed piles.

Like FRP reinforced concrete columns of Chapters 3 and 4, prestressed concrete compression members with FRP composites can be analyzed similar to steel prestressed concrete columns. Basic assumptions such as the ones presented in Chapter 3 for reinforced concrete columns can be used. The subsequent section presents equations for deriving the strength interaction relation of prestressed concrete columns with FRP reinforcement. It should be noted that the equations are derived for concrete columns contain only prestressing reinforcement (Partially prestressed concrete columns containing non-prestressing reinforcement are not addressed) in bonded applications.

### **5.3 Derivation of the Strength Interaction Relation of Prestressed Concrete Columns in Bonded Applications**

The strength interaction ( $P$ - $M$ ) of a prestressed concrete column is comprised of the accumulative strengths of its individual constituents: concrete and prestressing reinforcement. As a result, the contribution of these individuals can be computed separately and combined as follows:

#### **5.3.1 Concrete Compression Forces**

Concrete compression forces and concrete forces displaced by prestressing reinforcement can be computed using equations presented in sections 3.3.1 and 3.3.3. These equations are repeated herein as:

$$C_{ci} = f_{ci} b \frac{h}{N} \text{ when } kd \geq h \text{ (where cross section is in compression entirely)} \quad (3.2.a)$$

Or

$$C_{ci} = f_{ci} b \frac{kd}{N} \text{ when } kd < h \text{ (where cross section is in compression partially)} \quad (3.2.b)$$

$$M_{ci} = C_{ci} \left( \frac{h}{2} - d_{ci} \right) \quad (3.3)$$

The concrete compression force and moment displaced by prestressing reinforcement in the compression zone are:

$$C_{cfi} = A_{pfi} f_{ci} \quad (3.8)$$

$$M_{cfi} = C_{cfi} \left( \frac{h}{2} - d_{fi} \right) \quad (3.9)$$

Where  $A_{pfi}$  is the area of FRP prestressing reinforcement at layer  $i$ . All other notations are defined previously in Chapter 3.

### 5.3.2 Prestressing Reinforcement Forces

The strain, stress, axial force, and moment of FRP prestressing reinforcements in a concrete column are determined for a rectangular column cross section shown in Fig. 5.3 as follows:



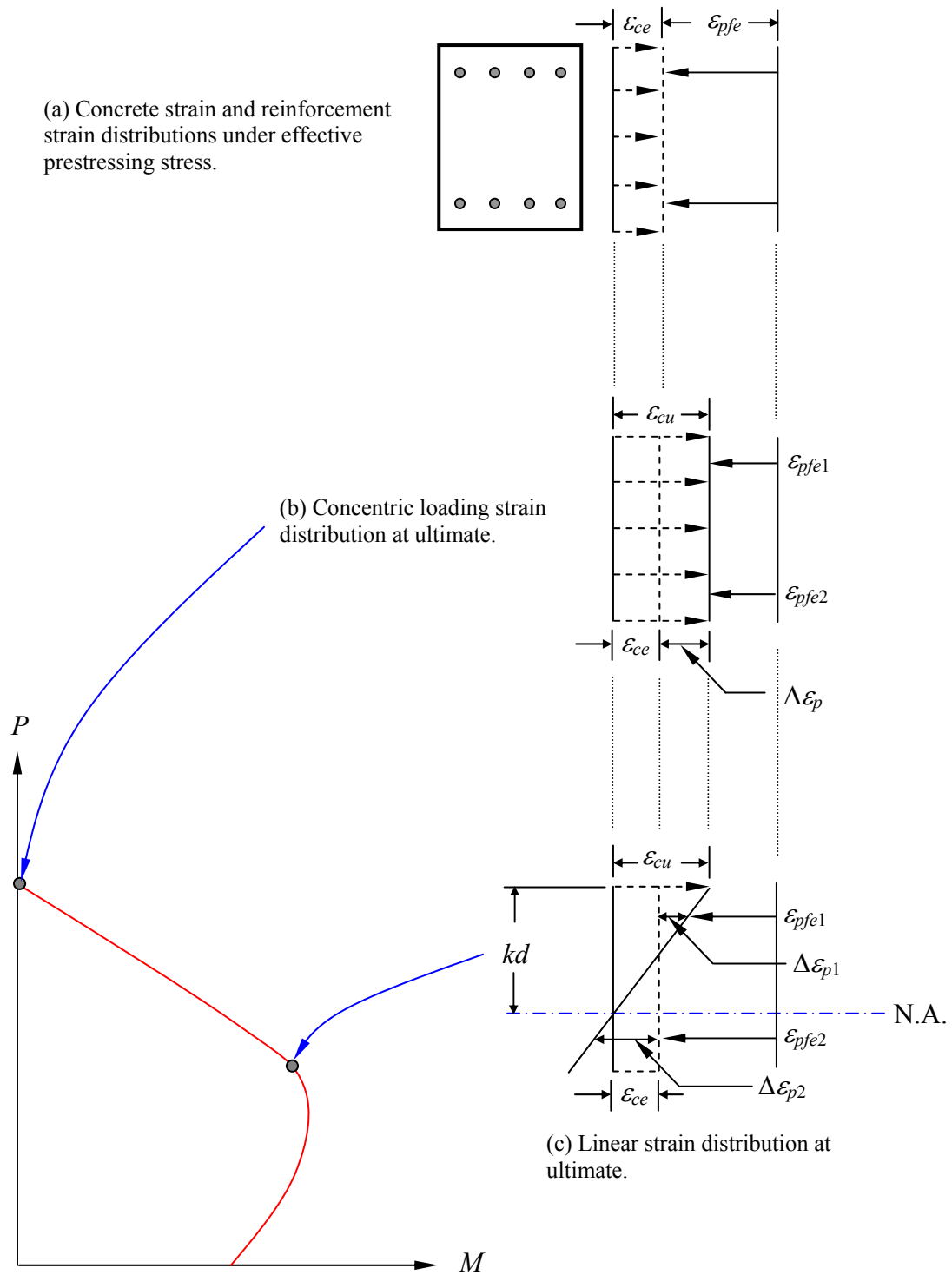


**Figure 5.3** – Typical strength interaction of a steel prestressed concrete column.

Under the action of effective prestressing force ( $P_{fe} = A_{pf}f_{fe}$ ), a uniform concrete strain ( $\epsilon_{ce}$ ) will presumably be developed as a result of concrete cross section stressed uniformly under the prestressing force (all prestressing reinforcements are distributed symmetrically and stressed equally, as shown in Fig. 5.3.a). The effective prestressing force ( $P_{fe}$ ) is the tensile force in prestressing reinforcement that will remain for the lifespan of the member after *all* the losses have been accounted for such as the ones due to the elastic shortening of concrete, relaxation of stressed tendons, creep and shrinkage of concrete, etc. The uniform concrete strain is expressed as

$$\epsilon_{ce} = \frac{A_{pf} f_{fe}}{(A_g - A_{pf})E_c} \quad (5.1)$$

$A_{pf}$  is the area of all prestressing reinforcements ( $\sum A_{pfi}$ , where  $A_{pfi}$  is the area of a prestressing tendons at layer  $i$ , and  $i = 1, 2, \dots, n$ ), and  $A_g$  is the gross area of the column cross-section.  $E_c$  is the elastic modulus of concrete, and  $f_{fe}$  is the effective prestressing stress (ksi or MPa) after all losses.

The corresponding effective reinforcement strain ( $\epsilon_{pfe}$ ) as shown in Fig. 5.3.a can be obtained through Hooke's Law for material having linear-elastic stress/strain relationship, where  $E_f$  is the elastic modulus of FRP reinforcement:

$$\epsilon_{pfe} = \frac{f_{fe}}{E_{pf}} \quad (5.2)$$

The axial force ( $F_{pfi}$ ) and moment ( $M_{pfi}$ ) produced by the prestressing reinforcement in layer  $i$  determined about the centerline of a symmetrical column cross section can be expressed as follows:

$$F_{pfi} = A_{pfi}E_{pfi}\epsilon_{pfi} \quad (5.3)$$

$$M_{pfi} = F_{pfi} \left( \frac{h}{2} - d_{pfi} \right) \quad (5.4)$$

$d_{pfi}$  is a known quantity and is the distance from the extreme concrete compression fiber to the center of the prestressing reinforcement of layer  $i$ .  $\varepsilon_{pfi}$  in Eq. 5.3 is the reinforcement strain of layer  $i$ , and is dependent on the effective reinforcement strain,  $\varepsilon_{pfe}$  (Eq. 5.2) as shown in Fig. 5.3.c:

$$\varepsilon_{pfi} = \varepsilon_{pfe} + \Delta\varepsilon_{pi} \quad (5.5)$$

where  $\Delta\varepsilon_{pi}$  can be computed when the location of neutral axis or  $kd$  is known:

$$\Delta\varepsilon_{pi} = \varepsilon_{cu} \left( \frac{kd - d_{pfi}}{kd} \right) + \varepsilon_{ce} \quad (5.6)$$

#### 5.4 Strength Interaction Relation of PC Columns with FRP Reinforcement

The resultant axial force and moment of a rectangular RC column cross section are the summation of axial forces and moments of concrete and prestressing reinforcement:

$$P = \sum_{i=1}^N C_{ci} + \sum_{i=1}^n F_{pfi} - \sum_{i=1}^m C_{cfi} \quad (5.8)$$

$$M = \sum_{i=1}^N C_{ci} \left( \frac{h}{2} - d_{ci} \right) + \sum_{i=1}^n F_{pfi} \left( \frac{h}{2} - d_{pfi} \right) - \sum_{i=1}^m C_{cfi} \left( \frac{h}{2} - d_{pfi} \right) \quad (5.9)$$

The complete strength interaction ( $P$ - $M$ ) relation can be computed using these equations and repeated for a series of assumed locations of the neutral axis.

The procedure was used to generate the strength interaction (Fig. 5.4) of a prestressed concrete column with 270K-steel prestressing strands (Nawy 1996) – stress/strain relation of 270K steel prestressing strand is shown in Fig. 2.7 of Chapter 2. The cross sectional dimensions and material properties used are included in Fig. 5.4. Based on the analytical results, the following observations can be made:

- The strength interaction calculated with this procedure based on nonlinear concrete stress/strain relation presented in Chapter 3, though slight less, is in good agreement with Nawy’s (see Fig. 5.4) who used equivalent concrete stress block and factor, and neglected the concrete areas occupied by prestressing strands; and
- At pure bending, Nawy (1996) neglected the effect of the steel in the compression region in his calculation, hence resulted in lower moment strength as compared to current investigation.

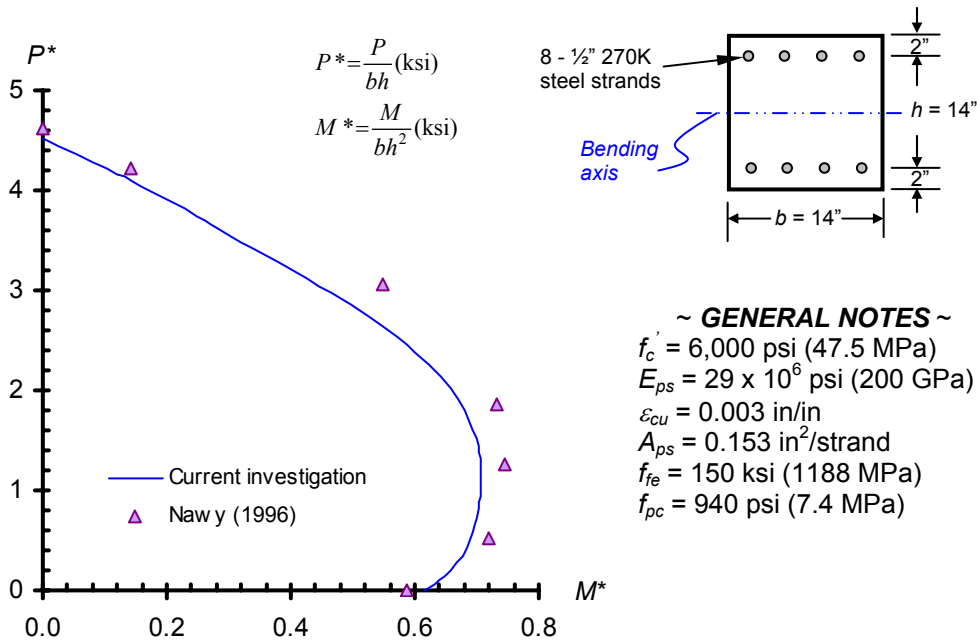


**Fig. 5.4 – Strength interaction diagram of steel PC column (Nawy 1996).**

Typical strength interactions of prestressed concrete column cross sections with various FRP tendons been generated (Figs. 5.5-5.7) using the approach in previous section. Several factors influencing strength interactions of prestressed concrete column cross sections were considered. They include the effective prestress force ( $P_{fe}$ ) in prestressing reinforcement, specified concrete strength ( $f'_c$ ), reinforcement ratio ( $\rho = A_{pf}/bh$ ), and long term effects of concrete:

#### **5.4.1 Influence of Effective Prestress Force on Strength Interaction**

Unlike reinforced concrete compression members, ACI-318 does not set a requirement for the amount of longitudinal reinforcement needed for prestressed concrete compression members. Instead, the code requires that concrete compression members to be prestressed with an average effective prestress in concrete ( $f_{pc} = P_{fe}/A_g$ ) of equal to or greater than 1.5 MPa (220 psi), or otherwise the concrete compression members be designed using similar provisions governed concrete compression members with non-prestressed reinforcement (e.g. minimum and maximum reinforcement ratios of 1 and 8%, respectively). In compliance with current code provisions, concrete sections prestressed with FRP tendons shown in Fig. 5.5 were stressed to have the following average effective prestresses ( $f_{pc}$ ) in concrete: 220, 550 (2.5 x 220), and 1,100 (5 x 220) psi [1.5, 3.75, and 7.5 MPa], respectively. Since glass fibers have poor resistance to creep and are more susceptible to alkaline degradation, in addition to having low transverse compressive strength, compared to carbon and aramid tendons, examples related to this specific fiber are omitted. Strength interactions shown in Fig. 5.5 were generated based on the cross sectional configuration shown in Fig. 5.4.

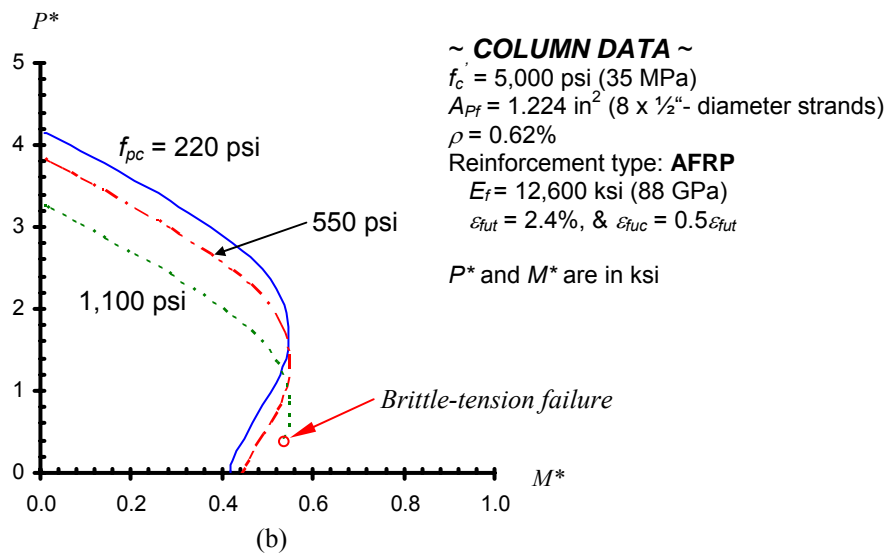
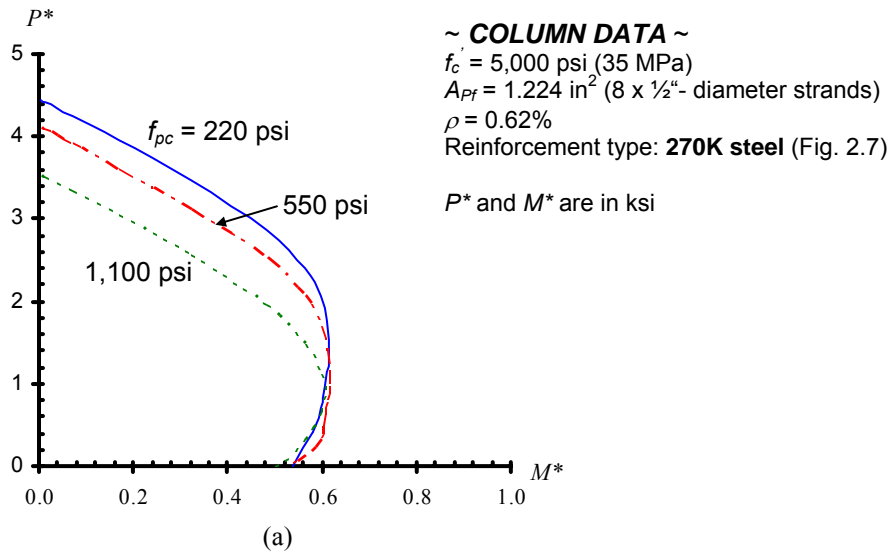


**Fig. 5.5 – Influence of effective prestresses ( $f_{pc}$ ) in concrete on strength interactions of FRP column cross sections.**

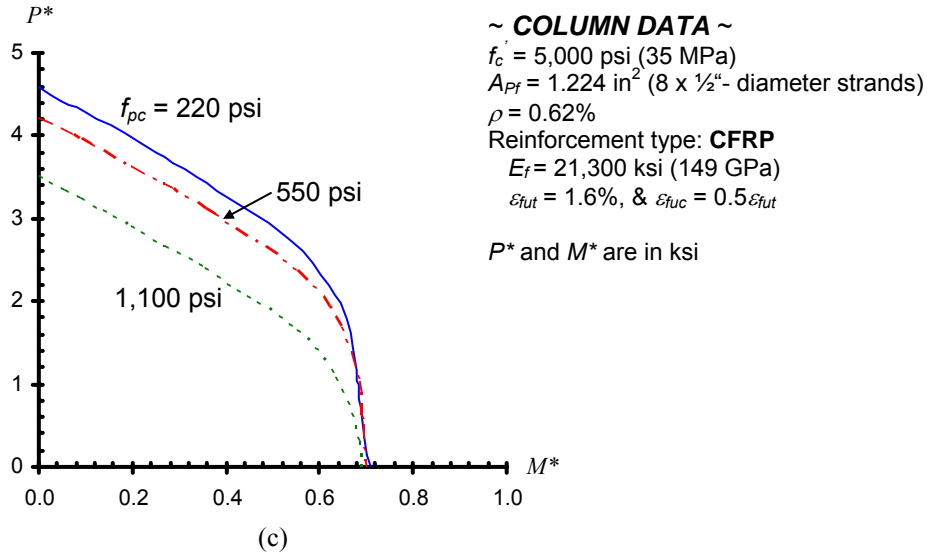


**Fig. 5.5 (Cont.) – Influence of effective prestresses ( $f_{pc}$ ) in concrete on strength interactions of FRP column cross sections.**

Based on the results shown in Fig. 5.5, the following observations can be made:

- The increase in effective prestresses ( $f_{pc}$ ) in concrete reduced the axial compression strength of all prestressed concrete compression members, while only slight increase in moment resistance was observed in the case of steel and AFRP prestressed concrete compression members when  $f_{pc}$  was increased from 220 psi to 550 psi (Figs. 5.5.a & b);
- The increase in  $f_{pc}$  resulted in the reduction of overall strength interaction of CFRP prestressed concrete compression members. No increase of moment resistance was observed (Fig. 5.5.c); and
- The increase of  $f_{pc}$  to 1,100 psi resulted in *brittle-tension* failure of AFRP prestressed concrete compression member (Fig. 5.5.b). The failure as previously defined in related to tension rupture of AFRP tendons. In the absence of brittle-tension failure, however, an increase of moment resistance can be anticipated.

### 5.4.2 Influence of Concrete Compression Strength on Strength Interaction

One of the advantages associated with the use of high-strength prestressing reinforcement is the use of high-strength concrete (Harik and Whitney 1988). Fig. 5.6 examines the effect of concrete compression strength ( $f'_c$ ) on strength interaction of prestressed concrete columns. Three different strengths of concrete were used to generate these strength interactions: 4,000 psi (28 MPa), 5,000 psi (35 MPa), and 6,000 psi (42 MPa), respectively.

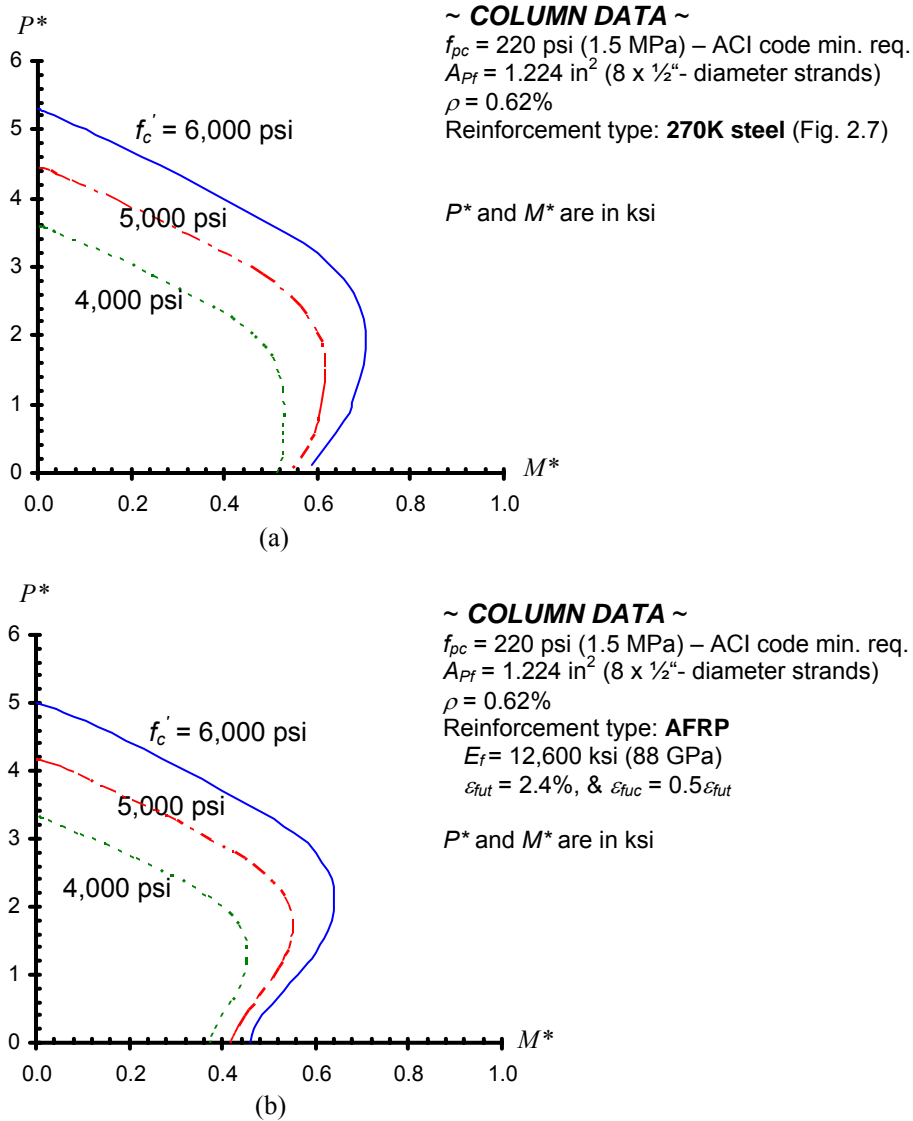


**Fig. 5.6 – Influence of concrete compression strength on strength interactions of FRP column cross sections.**



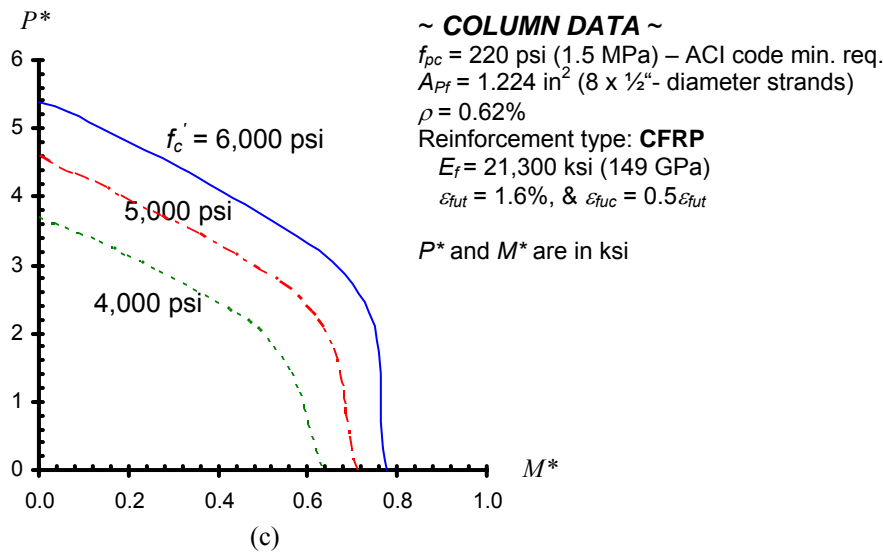


**Fig. 5.6 (Cont.) – Influence of concrete compression strength on strength interactions of FRP column cross sections.**

Based on the results, the following points can be concluded:

- With all other parameters remain constant, the increase of concrete compression strength (from 4,000 psi to 6,000 psi) increased the overall strength interaction of prestressed concrete columns as expected.
- CFRP prestressed concrete columns gained significant increase in axial compression strength and moment resistance. Similar significant increase in axial capacity was attained in AFRP prestressed concrete columns, however, only slight increase in moment resistance was observed. The amount increase in moment resistance is associated with the stiffness of prestressing tendons used.
- Prestressed concrete columns with 270K-steel prestressing stands have considerable increase in axial compression strength as concrete compression strength increases, however, only smaller increase only was observed in its moment resistance. This is due to the stress/strain relation of 270K-steel.

### 5.4.3 Influence of Reinforcement Ratio on Strength Interaction

Fig. 5.7 shows the effect of increasing reinforcement ratio on the strength interactions of prestressed concrete columns. In this cases, the effective concrete prestress ( $f_{pc}$ ) was kept at code required 220 psi (1.5 MPa). The original reinforcement ratio of 0.62 percent for cross section shown in Fig. 5.4 was doubled to 1.24 percent with concrete compression strength of 5,000 psi (35 MPa).

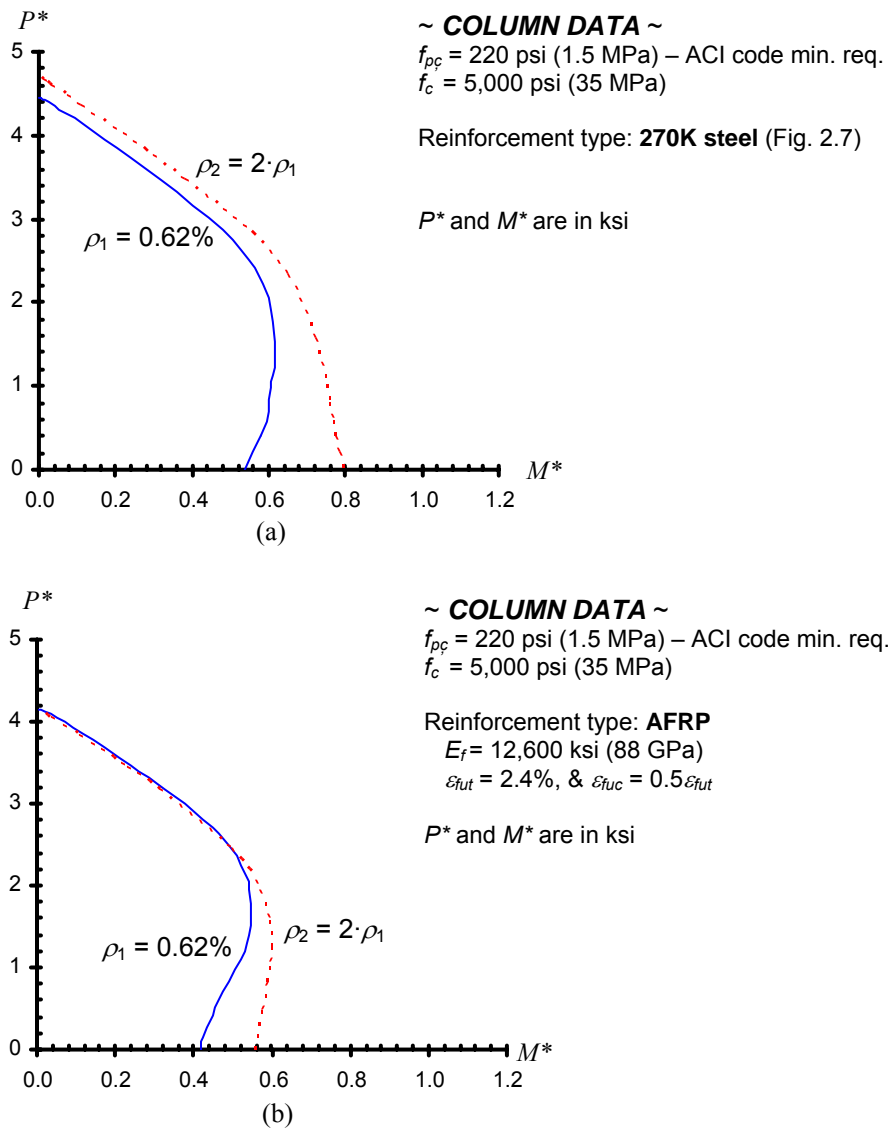


**Fig. 5.7 – Influence of reinforcement ratio on strength interactions of FRP column cross sections.**

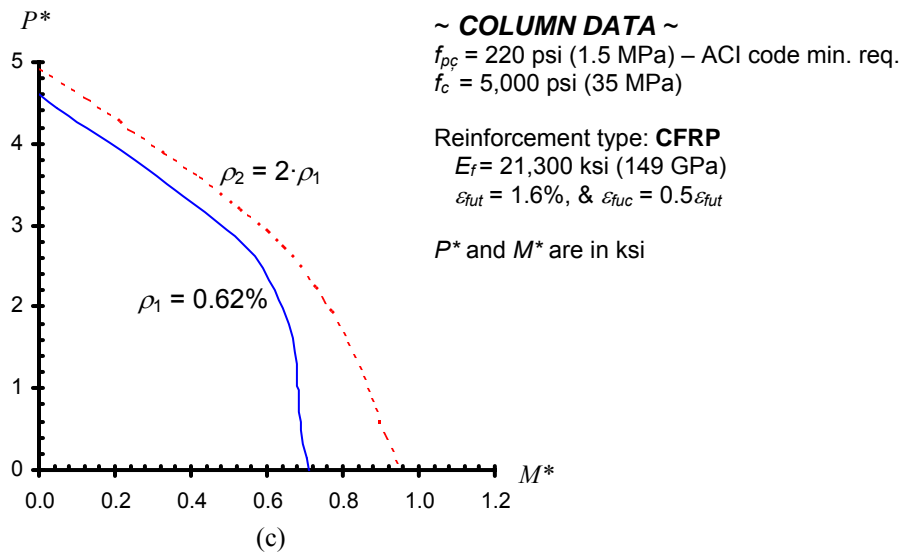


**Fig. 5.7 (Cont.) – Influence of reinforcement ratio on strength interactions of FRP column cross sections.**

Increasing reinforcement ratio has the following effects on strength interaction:

- In general, an increase in the amount of prestressing reinforcement leads to significant increase in bending or pure bending resistance; and
- Increasing the amount of prestressing reinforcement may or may not lead to reduction or increase of axial compression strength (i.e. prestressed columns with AFRP reinforcement which has low elastic modulus gained no pure axial strength when reinforcement ratio was doubled in this case; whereas prestress columns with CFRP whose modulus is almost three times that of AFRP, gained substantial axial strength in addition to moment strength).

#### **5.4.4 Influence of Concrete Long Term Loading on Strength Interaction**

Similar to reinforced concrete columns with FRP composites, the behavior of prestressed concrete columns with similar reinforcement needs to be ascertained, in order to effectively and confidently use in design applications. Fig. 5.8 shown a prestressed concrete column (Fig. 5.4)

with CFRP prestressing tendons analyzed with instantaneous (short term) and long term (TLT and RLT-curve) concrete stress/strain relations presented in Chapter 2.

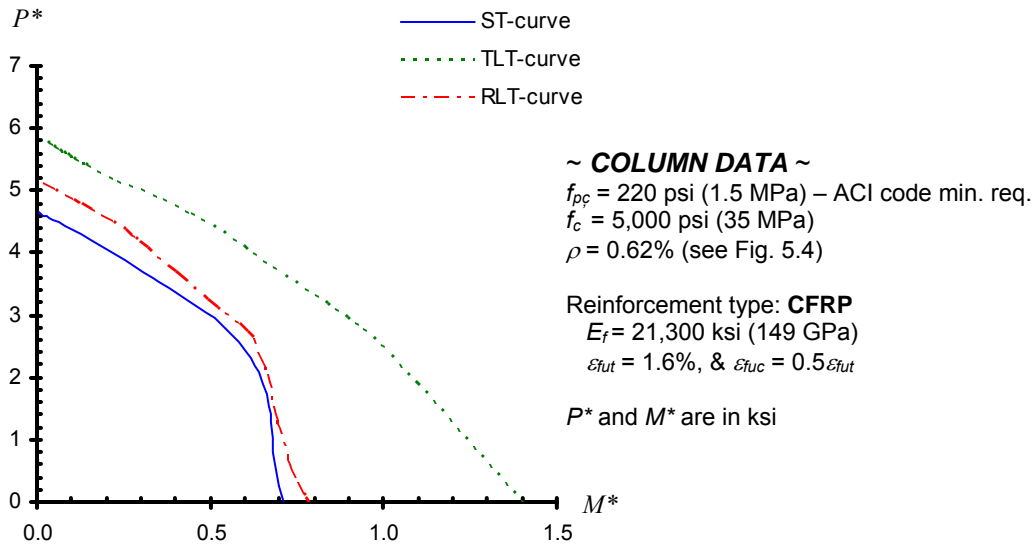


**Fig. 5.8 – Effect of long term concrete loadings on strength interactions of FRP column cross sections.**

Like typical reinforced concrete columns with FRP rebars (see Chapter 3), the prestressed concrete column with CFRP prestressing tendons shown in Fig. 5.8, in the absence of *premature compression* or *brittle-tension* failure, exhibited overall increase in strength interaction due to the fact that:

- The two long term (TLT and RLT) concrete loadings increased the ultimate concrete compression strain ( $\epsilon_{cu}$ ), and that led to the increase of strains developed in CFRP tendons in either tension or compression. The increase in tensile ( $\epsilon_{ft}$ ) or compression ( $\epsilon_{fc}$ ) strain, without exceeding the tendon's ultimate tensile ( $\epsilon_{fut}$ ) or compression ( $\epsilon_{fuc}$ ) strain, and the corresponding stresses, and resulted in overall increase in strength interaction.

Example given in Fig. 5.8 affirmed that this specific CFRP tendons is suited for use as prestressing tendon in concrete columns because of no tendon rupture occurring while gaining significant strength.

## 5.5 Slender Prestressed Concrete Columns with FRP Prestressing Reinforcement

Prestressing concrete piles are usually slender columns for which the effect of buckling (or lateral stability) is significant. For example, the documented demonstration projects (Iyer 1995; Iyer et al. 1996; Arockiasamy and Amer 1998; & Schiebel and Nanni 2000) have FRP prestressing concrete piles with lengths ranging from 25-ft to 60-ft (7.62 m to 18.3 m) with  $L/r$  ratio greater than 70. Due to slenderness effect, the columns' strength is less than that of their cross section and must be evaluated in function of their length, cross section dimensions, mechanical characteristics, restraint conditions at their ends, etc.

The numerical approach presented in Chapter 4 can be used to generate the axial load-moment-curvature responses and the ultimate strength interaction of prestressed concrete columns. Two such examples are shown in Figs. 5.9-5.11 where concrete columns are prestressed with AFRP and CFRP prestressing reinforcement. Figs. 5.9-5.10 show how the axial load, moment, and curvature are related. While the figures only show the nonlinear moment-curvature responses at a specific axial load levels, moment-curvature responses at other axial load levels can be generated in similar manner.

Shown in Fig. 5.11 are the ultimate strength interactions of the FRP prestressed concrete columns of different slenderness ratios ( $kL/r$ ) – columns were assumed to be pin-ended with effective column length factor of 1.0. As expected, the ultimate strength interaction is a function the column length; as the column length (or slenderness ratio) increases the overall ultimate strength interaction reduces.

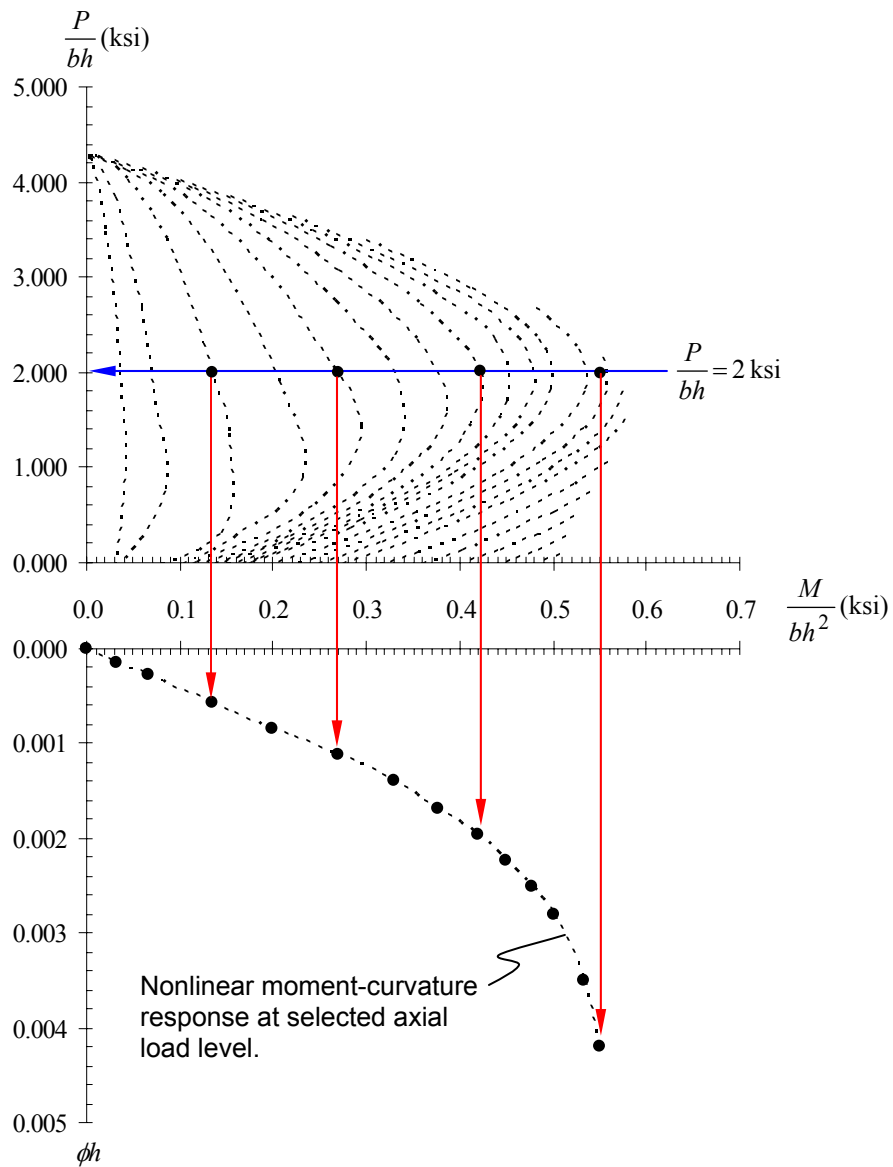


**Fig. 5.9 – Typical axial load-moment-curvature responses of prestressed concrete columns with AFRP as prestressing reinforcement.**

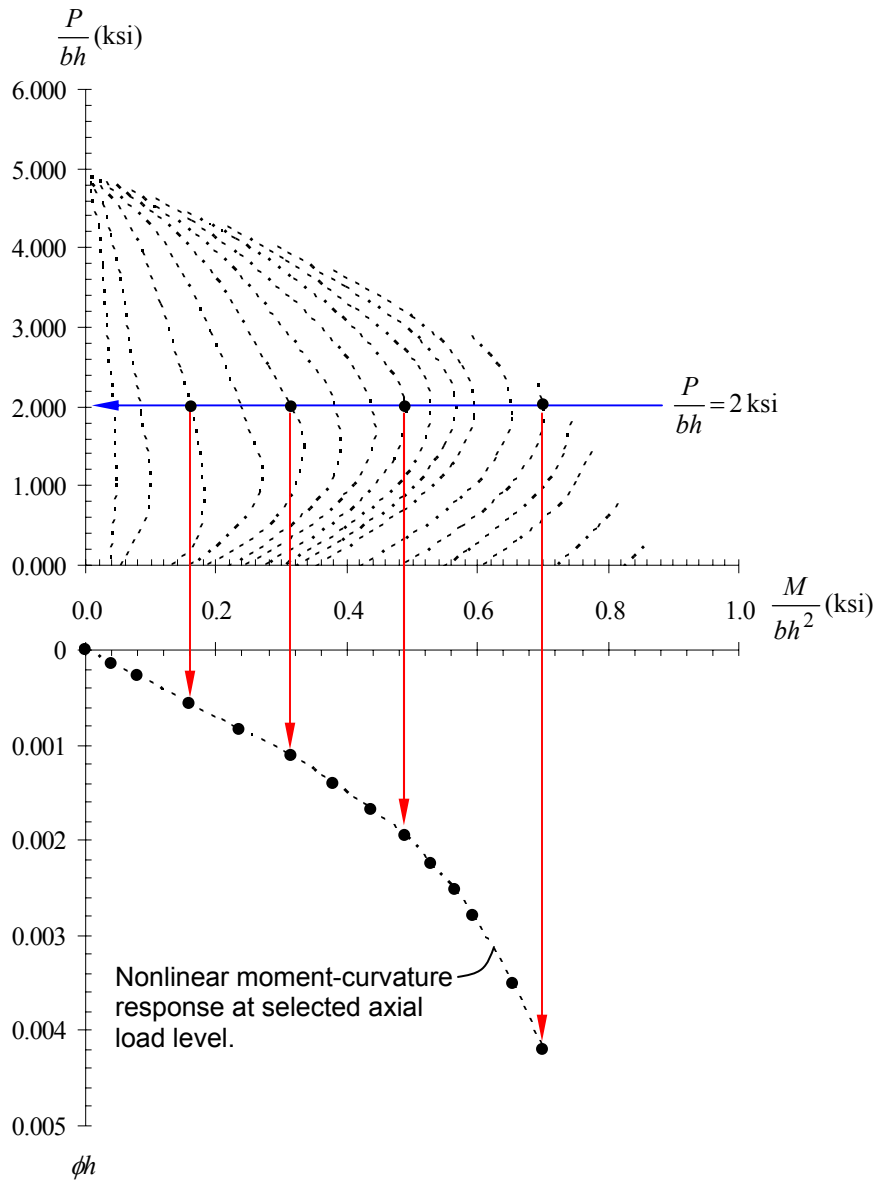


**Fig. 5.10 – Typical axial load-moment-curvature responses of prestressed concrete column with CFRP as prestressing reinforcement.**

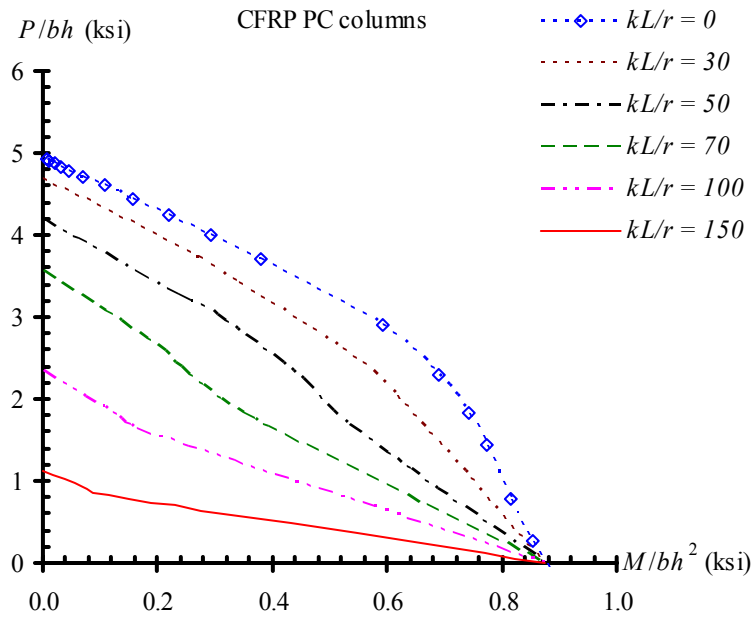
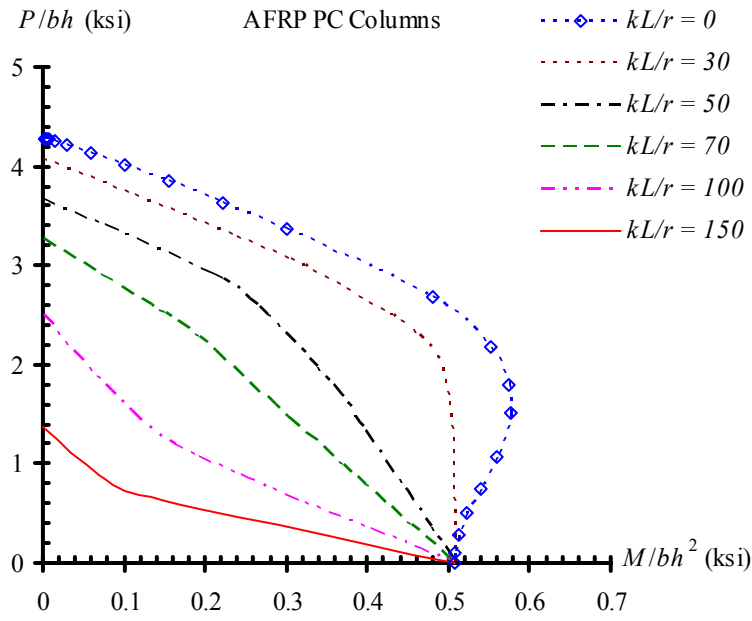


**Fig. 5.11 – Ultimate strength interaction diagrams of prestressed concrete columns with AFRP and CFRP as prestressing reinforcements.**



## 5.6 Concluding Remarks

The use of FRP composites in prestressing applications offers a viable alternative to conventional steel tendons/strands due to their strength which typically is many times greater than the conventional reinforcement's. In addition, FRP tendons are non-conducting and non-magnetic in nature, and their non-corrosive nature is particularly attractive. In this chapter, prestressed concrete columns with FRP tendons were analyzed using the same assumptions and principles pertaining for prestressed concrete columns with steel prestressing tendons/strands. The principal findings and conclusions related to rectangular prestressed concrete columns bonded with FRP tendons are as follows:

- Initial prestresses were introduced to concrete columns with high-strength steel (e.g. 250K and 270K steel strands) because of the gain in bending resistance while some amount of axial compression strength was sacrificed. This apparently can be beneficial for columns subjected to bending. For concrete columns prestressed with FRP tendons, similar conclusion may or may not be reached (For example, concrete columns in Fig. 5.5.b exhibit similar behavior observed in concrete columns with steel. However, prestressed concrete columns in Fig. 5.5.c have their overall strength reduced with increased prestressing). In some cases, introduction of prestresses may be detrimental from a standpoint that noticeable reduction in overall strength may be observed.
- Similar to concrete columns reinforced with FRP rebars, the use of FRP tendons as prestressing tendons for concrete columns required extra precaution as the tendons could potentially fail prematurely in compression or in tension prior to concrete reaching its ultimate strain and strength. Similar to reinforced concrete columns with FRP rebars, these failures can be characterized as premature-compression or brittle-tension failure.
- The use of higher strength concrete coupled with prestressing steel resulted in increase in axial load strength while only marginal increase in moment resistance was observed. Similar behavior has been observed for concrete columns prestressed with FRP tendons. In some cases, significant moment resistance was gained depending on the type of FRP tendons used.

- Regardless of the type of tendons used (e.g. steel or FRP), the increase in the amount of reinforcement (or increase in reinforcement ratio) used in concrete columns generally led to increase in overall strength interaction, particularly the moment resistance. This is consistently true since reinforcements in concrete columns are the primary contributor of tensile strength, and hence the increase in this quantity would lead to increase in bending resistance.
- Barring from premature compression or brittle-tension failure, the strength interaction of concrete columns prestressed with FRP tendons increased when long term effects such as creep and shrinkage of concrete were considered. Long term effects led to the increase in the ultimate concrete compression strain ( $\epsilon_{cu}$ ). That in turn led to greater development of strains and stresses in FRP tendons which translated into increase in overall strength interaction. Such phenomena was not observed in concrete columns prestressed with steel tendons because increase in steel strain led in minimal stress increase due to its stress/strain relation.
- The strength interaction of slender concrete columns prestressed with FRP tendons using similar methodology presented for slender reinforced concrete columns. As expected, the strength interaction of such columns are affected more by the column length rather than the reinforcement used.

## CHAPTER 6

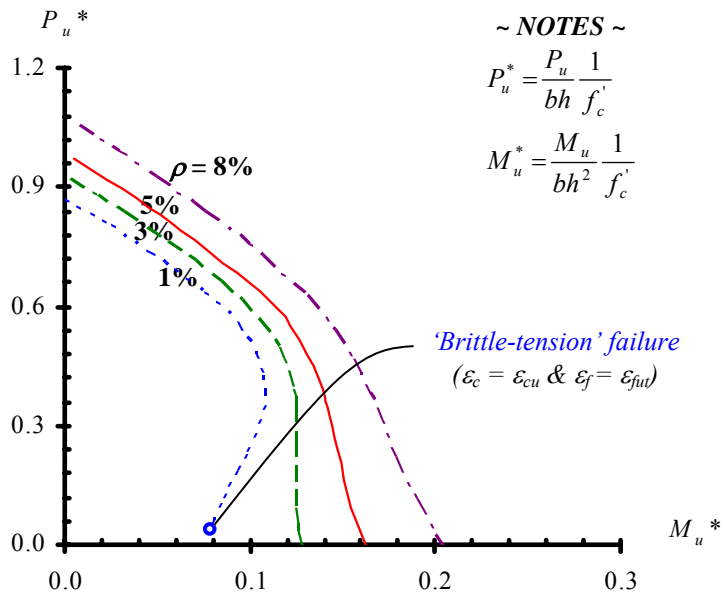
### A RATIONAL APPROACH TOWARDS THE DESIGN OF REINFORCED CONCRETE COMPRESSION MEMBERS WITH FRP REBAR

#### 6.1 Introduction

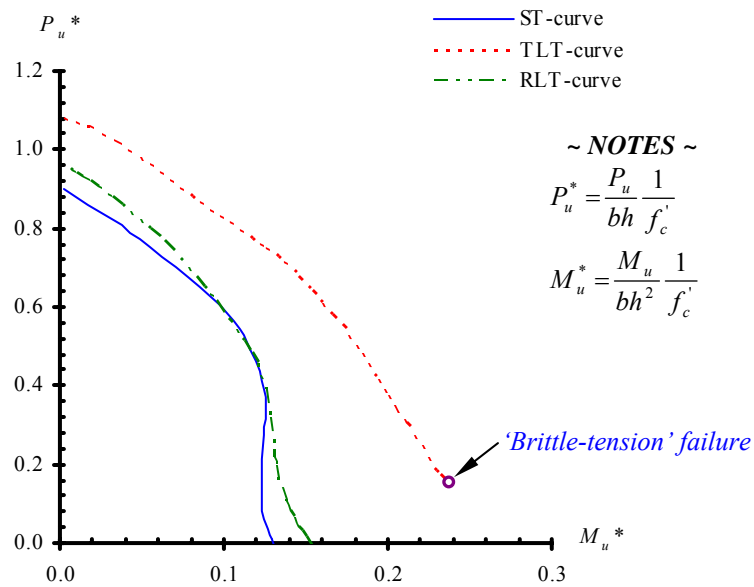
Column strength analyses performed on reinforced and prestressed concrete columns based on equilibrium condition, strain compatibility, and material constitutive laws (Chapters 3 – 5), indicated the possibility of the following failure modes occurring:

- *Premature-compression* failure. A failure mode that is defined as compression rupture of FRP rebars in concrete columns prior to concrete reaching its pre-defined limiting (or ultimate) strain; and
- *Brittle-tension* failure. A failure mode that is defined as tension rupture of FRP rebars in concrete columns prior to concrete reaching its pre-defined (or ultimate) strain.

Since, in both cases, concrete is not reaching its ultimate strain, it will presumably not realize its full strength in compression. The likelihood of *premature-compression* failure is presumably smaller than *brittle-tension* failure for concrete columns reinforced with FRP rebars, since the ultimate compression strain ( $\epsilon_{fuc}$ ) of FRP rebars is generally many times larger than the assumed ultimate concrete compression strain ( $\epsilon_{cu}$ ). For instance, ACI 318 assumes a short term ultimate concrete compression strain of 0.003. This is also true even when long term effects such as creep and shrinkage are considered (see Chapter 3). *Brittle-tension* failure, on the other hand, is more likely to occur since the tensile strain ( $\epsilon_{ft}$ ) can easily exceed the ultimate tensile strain ( $\epsilon_{fult}$ ) of FRP rebars. This is evident when concrete columns are subjected to bending. Additionally, the inclusion of long term effects would heighten the chances of *brittle-tension* failure occurring since creep and shrinkage would transfer much of the load carried by concrete to reinforcement, and hence result in increasing reinforcement strain and stress. Figs. 3.6 and 3.9.a are repeated in Fig. 6.1 to illustrate the *brittle-tension* failure of concrete columns reinforced with FRP rebars.



(a) Short term analysis of concrete columns with GFRP Rebar (Fig. 3.6)



(b) Long term analysis of concrete columns with AFRP Rebar (Fig. 3.9.a)

**Fig. 6.1 – Brittle-tension failures of concrete columns with FRP rebars.**

## 6.2 Strength Interaction (P-M) Analysis of Concrete Columns Reinforced with FRP Rebar

As previously indicated, the strength of a concrete column reinforced with FRP rebars can be presented in the form of axial load-bending moment ( $P$ - $M$ ) interaction relations. The interaction is derived based on equilibrium of stresses, Bernoulli linear strain compatibility, and material constitutive law (Chapters 3 – 5). The nominal interaction strength is obtained based upon concrete in the outmost compression fiber reaching its pre-defined limiting strain (ultimate strain,  $\varepsilon_c = \varepsilon_{cu}$ ). For instance, the ACI 318 (2002) assumes an instantaneous (short term) concrete limiting (or ultimate) strain of 0.003.

The nominal strength interaction ( $P$ - $M$ ) relation for a steel reinforced concrete column cross section is defined by the outmost concrete fiber in compression reaches the ultimate strain while the outermost steel layer in tension may or may not reach yield stress. The region of the interaction curve where the steel in the outermost tension layer is still in the elastic range is normally is termed *compression control region*, while *tension control region* indicates the region of the interaction curve where steel rebars have yielded. Serving as the transition between the two regions is a “*balance*” point. This point is defined as the outermost concrete fiber reaches its ultimate in compression and the outermost steel layer reaches the yield strain simultaneously.

A similar approach can be used to define the strength interaction of a concrete column reinforced with FRP rebars. Consider the schematic interaction diagrams of Fig. 6.2. The strength interaction curve **A** of a column cross section reinforced with FRP rebars is obtained based on an ultimate concrete strain of 0.003, and it illustrates *brittle-tension* failure as depicted. A pair of required strengths ( $M_n, P_n$ ) is also shown in Fig. 6.2. At first glance, it appears that the strength interaction curve **A** would have adequate strength to withstand the load combination as it falls inside an apparent extension of the strength envelope **A**. However, due to *brittle-tension* failure, the lower part of the nominal strength curve of the column cross section should have been obtained based upon the ultimate tensile strain ( $\varepsilon_{fut}$ ) of the FRP rebar. The lower part of the interaction diagram is therefore now shown as strength interaction curve **B**, and the continuation of strength interaction curve **A** with reduced  $\varepsilon_{cu}$ . Obviously the original load combination would have failed the column in this particular case. Because FRP rebar does not yield as defined by its

linearly-elastic-until-failure stress/strain relationship, the failure of the column is expected to be sudden and catastrophic as there would be no warning of impending tension rupture. It has been documented in various experimental programs that flexural members reinforced with FRP rebars failed due to concrete crushing exhibit a more progressive, less catastrophic, and a higher deformability behavior (Nanni 1993; Jaeger et al. 1997; Theriault and Benmokrane 1998).

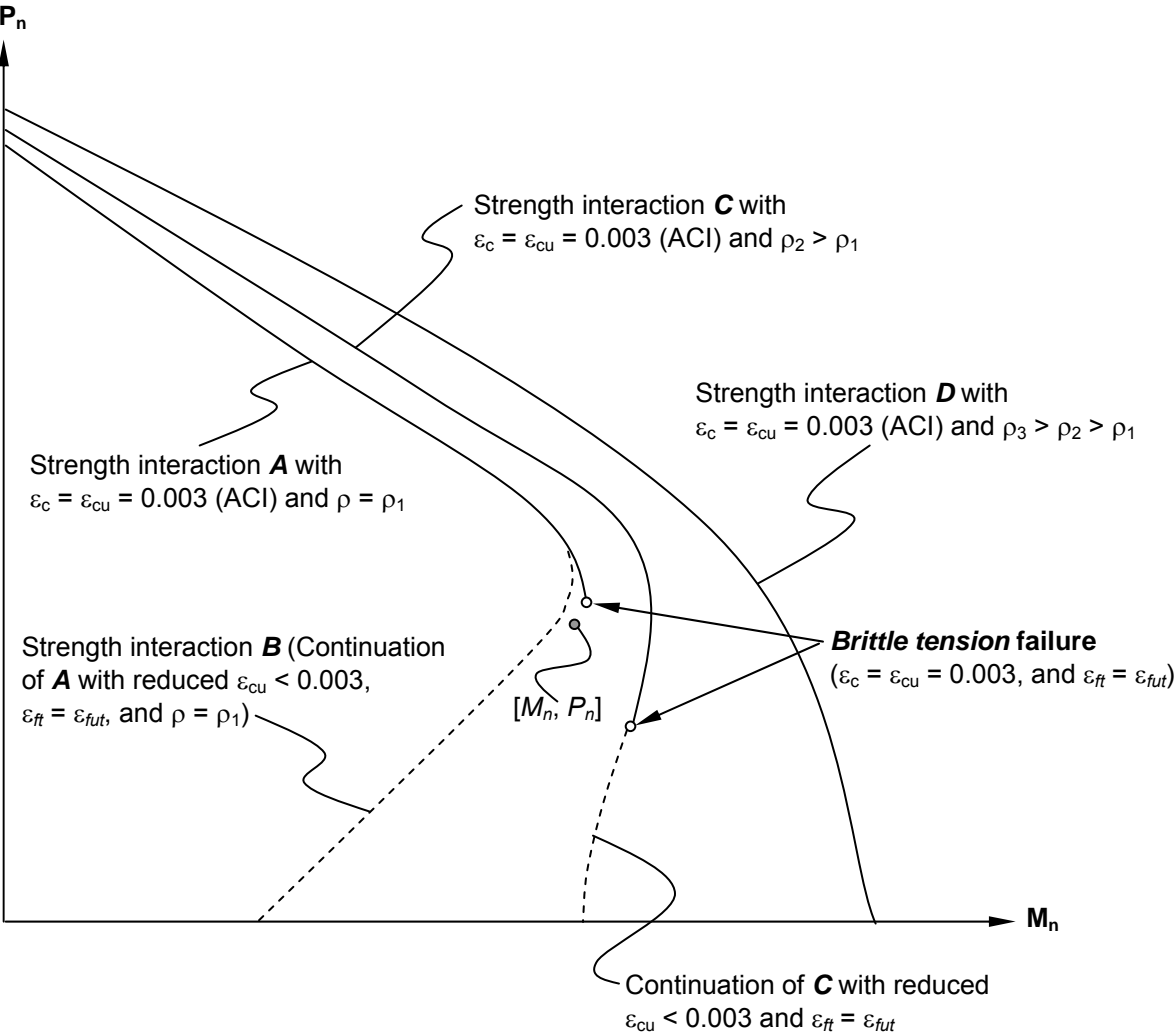


**Fig. 6.2 – Schematic strength interaction curves of columns reinforced with FRP rebars.**

One solution to the problem is to increase the amount of reinforcement used in the column. This will produce strength interaction curves **C** and **D** in Fig. 6.2. Note that increase of uniformly distributed column reinforcement *retards* the occurrence of *brittle-tension* failure (i.e.

$\rho_2 > \rho_1$  in strength interaction **C**). Further increase of reinforcement ratio prevents *brittle-tension* failure instead leading to failure controlled by concrete crushing (i.e.  $\rho_3 > \rho_2 > \rho_1$  in strength interaction **D**). A column cross section reinforced with GFRP rebars analyzed in Chapter 3 (see Fig. 3.6) is repeated in Fig. 6.3. Numerical example in Fig. 6.3 illustrates *brittle-tension* failure due to the small ultimate tensile strain ( $\epsilon_{fut}$ ) of the GFRP rebars (compared to the ultimate failure strains of steels such as ASTM A615 and A706 rebars which are commonly larger than 10 percent). The figure also demonstrates the consequence of increasing reinforcement ratio to avert *brittle-tension* failure.

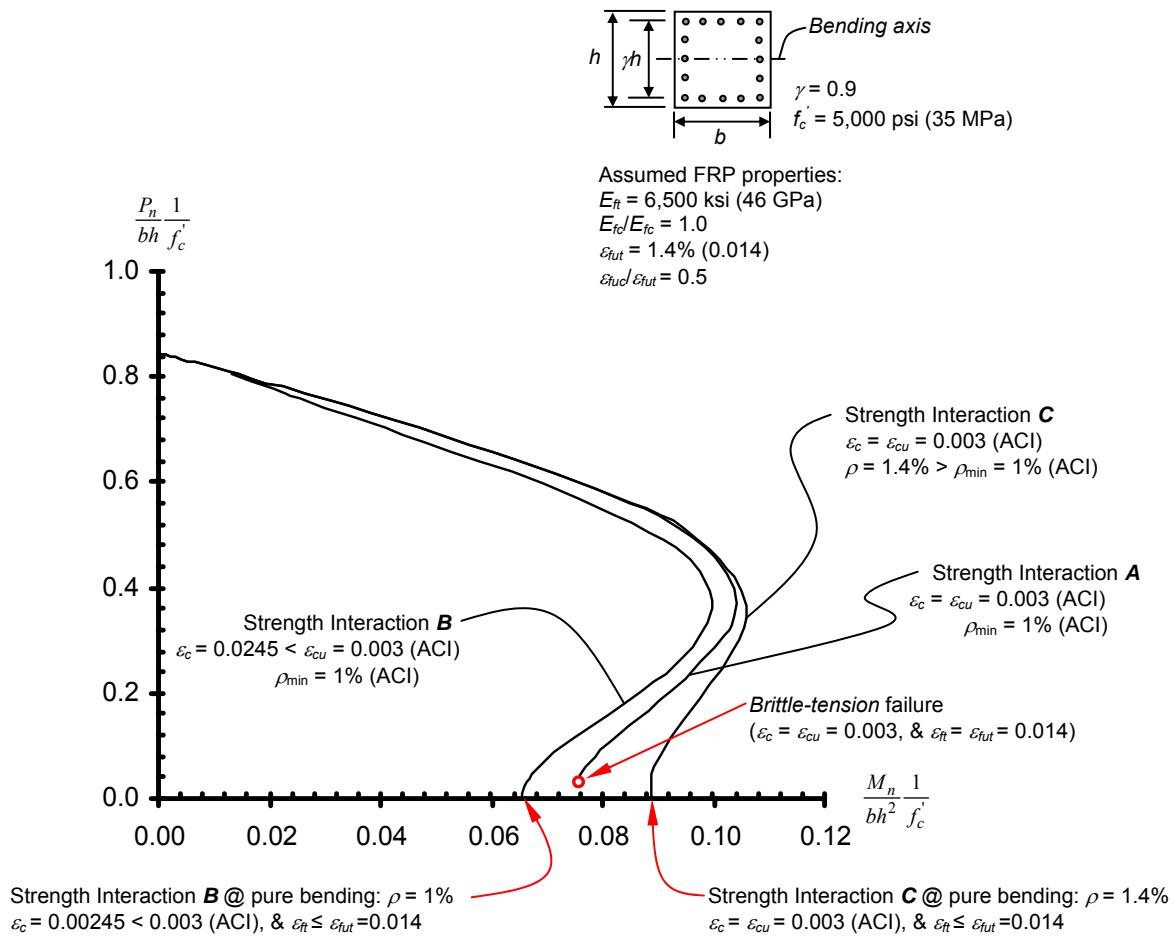


**Fig. 6.3 – Strength interactions of concrete columns reinforced with GFRP rebars (also see Fig. 3.6).**

### 6.3 Prevention of Brittle-Tension Failure

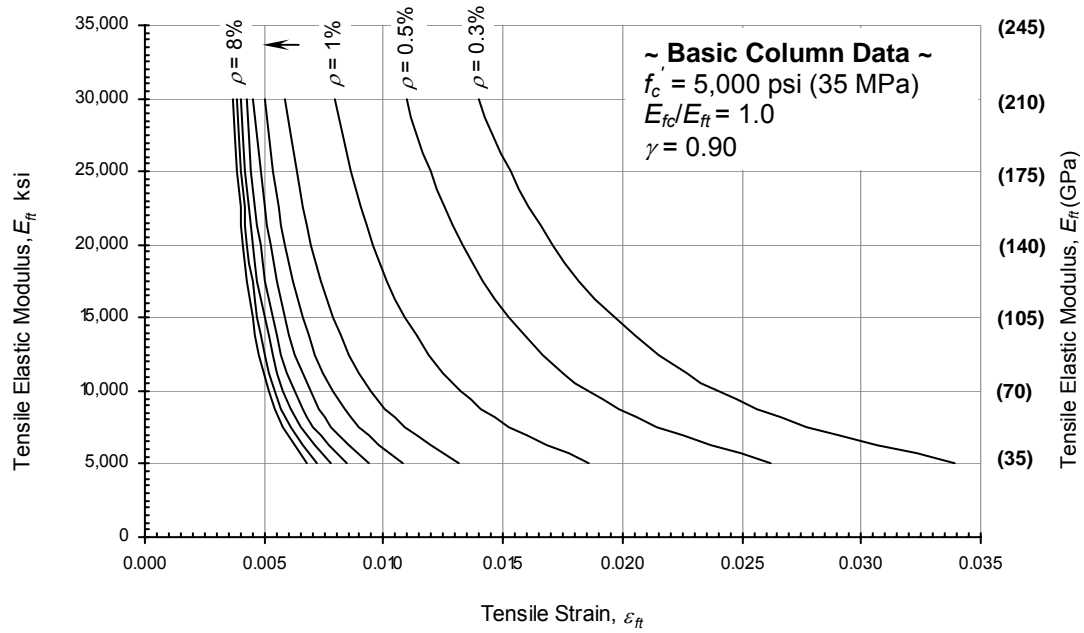
This section presents a rational approach to preventing the *brittle-tension* failure of a concrete column with FRP rebars and hence resulting in failure controlled by concrete crushing which presumably will be more progressive and less aggressive. From the foregoing it appears that concrete columns with FRP rebar can be safeguarded from *brittle-tension* failure by providing a reinforcement ratio ( $\rho$ ) larger than a minimum ratio designated as  $\rho_{f,\min}$ . The ACI 318-02 Code limits, particularly the minimum ( $\rho_{\min}$ ) of 1% on reinforcement ratio set for steel reinforced concrete columns may not apply to concrete columns reinforced with FRP rebars. The ACI Code (2002) reinforcement limits were set in the 1930s when medium strength materials were typically used. At that time nominal concrete compressive strengths ranged from 2,000 to 5,000 psi (14 to 35 MPa) and steel yield strengths ranged from 39 to 54 ksi (269 to 372 MPa) (Richart et al. 1933; Logeman et al. 1933; and Richart 1933). The maximum limit ( $\rho_{\max}$ ) of 8% remains applicable since the adoption is to prevent rebar congestion, though in everyday practice this limit is rarely reached.

In general, the strain in every reinforcing bar of a column cross section can be determined from an assumed strain distribution for a pre-defined ultimate concrete compression strain. Concrete and reinforcement stresses can then be calculated from the respective material constitutive laws. Subsequent resultant axial load and moment of the column cross section can then be found from statics. Explicitly, the maximum tensile reinforcement strain will be developed at the outermost tensile layer corresponding to a pure flexural condition ( $P_n = 0$  and  $M_n = M_{\max}$ ), and this value can be determined numerically. Given the material and cross sectional properties of a column, a reinforcement ratio ( $\rho_f$ ) can be found through an analytical process by matching the maximum tensile strain ( $\varepsilon_f$ ) developed to the FRP rebar fracture strain ( $\varepsilon_{f,ut}$ ), and hence establishing the ratio as the minimum ( $\rho_{f,\min}$ ). Once  $\rho_{f,\min}$  has been determined, a  $\rho_f$  larger  $\rho_{f,\min}$  can then be provided for that column to prevent *brittle-tension* failure. Naturally,  $\rho_{f,\min}$  varies and depends on a variety of factors. Further discussions of these factors are provided in the subsequent sections.

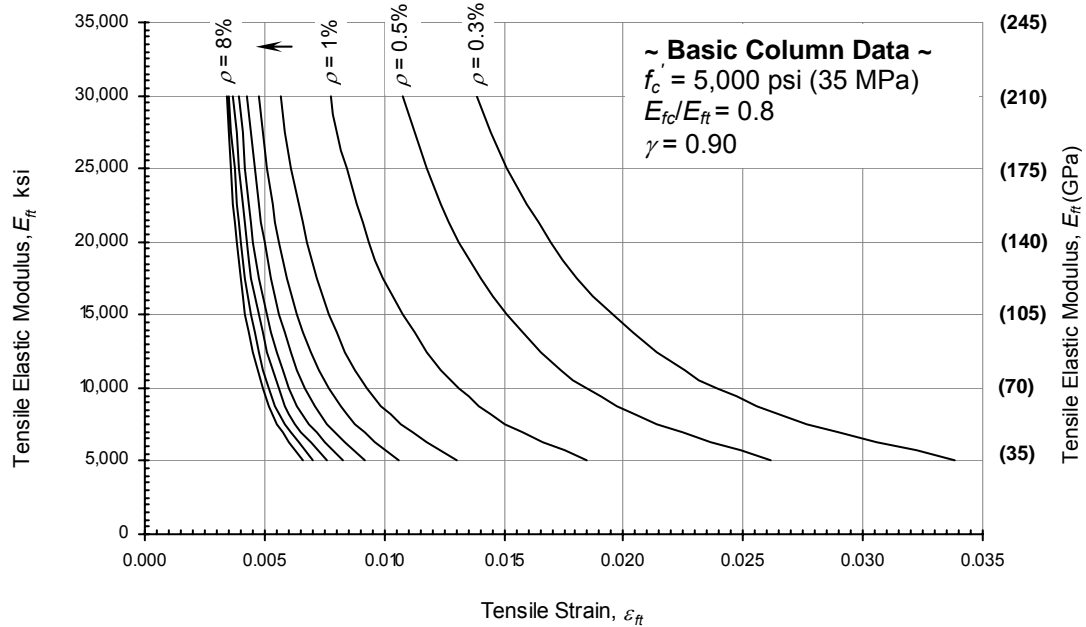


To expedite the determination of  $\rho_{f,\min}$ , the design aids shown in Fig. 6.4 have been developed. The graphs are applicable to any rectangular column cross section having dimensions of  $b$  by  $h$  (see Fig. 6.3) bent uni-axially, and with the FRP rebars symmetrically distributed. The ordinates represent the tensile elastic moduli ( $E_{ft}$ ) of FRP rebars ranging from 5,000 to 30,000 ksi (35 to 210 GPa), covering most available FRP rebars. The abscissas represent the tensile strains ( $\varepsilon_{ft}$ ) that will develop at the outermost tensile layers of the reinforcement at pure flexure.  $\varepsilon_{ft}$  is determined for a combination of  $E_{ft}$  and  $\rho$  as shown. The graphs were developed using an instantaneous concrete stress/strain model consisting of a parabolic ascending branch and a linear descending branch with ultimate strain of 0.003 in compression.

Since the compressive elastic modulus ( $E_{fc}$ ) is frequently lower than the tensile elastic modulus ( $E_{ft}$ ), graphs with  $E_{fc}/E_{ft}$  ratios of 1.0, 0.8, 0.6, 0.4, 0.2, and 0, respectively, were generated, although the differences are indiscernible. Other parameters such as the concrete compression strength ( $f'_c$ ) and the ratio of the distance between the outer layers of rebars to the height of the column cross section in the direction of bending ( $\gamma$ ) of Fig. 6.3 were kept constant. Note that  $E_{fc}/E_{ft}$  ratio of 0 implies that the compression contribution of FRP bars in the compression zone was neglected, similar to neglecting tensile force of concrete in tension zone, even though compression rebars were physically present.

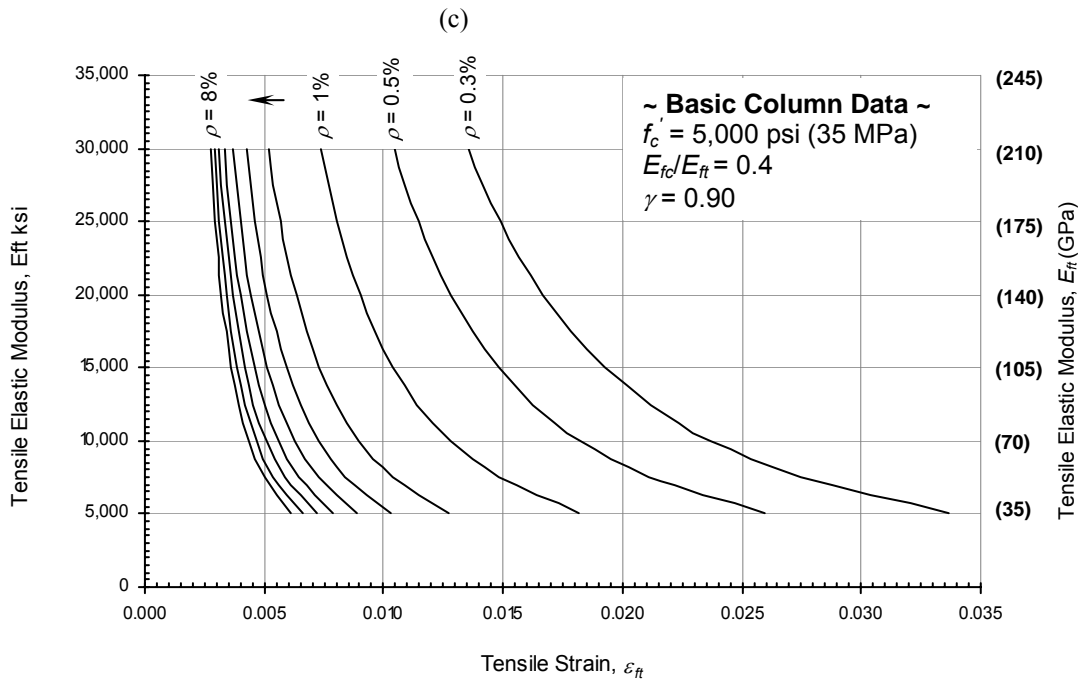
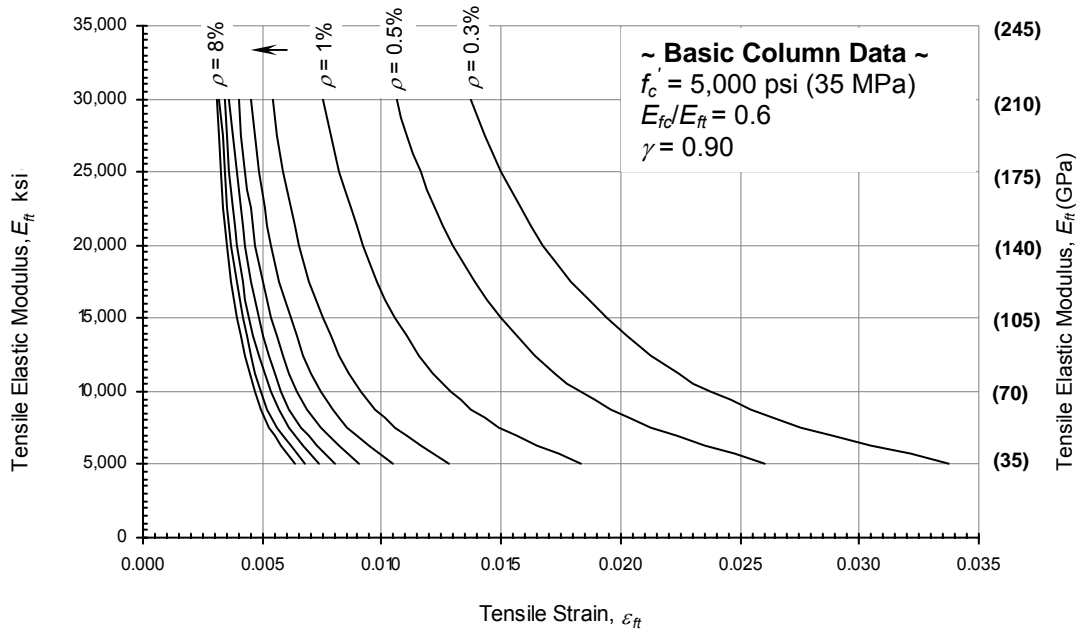


(a)



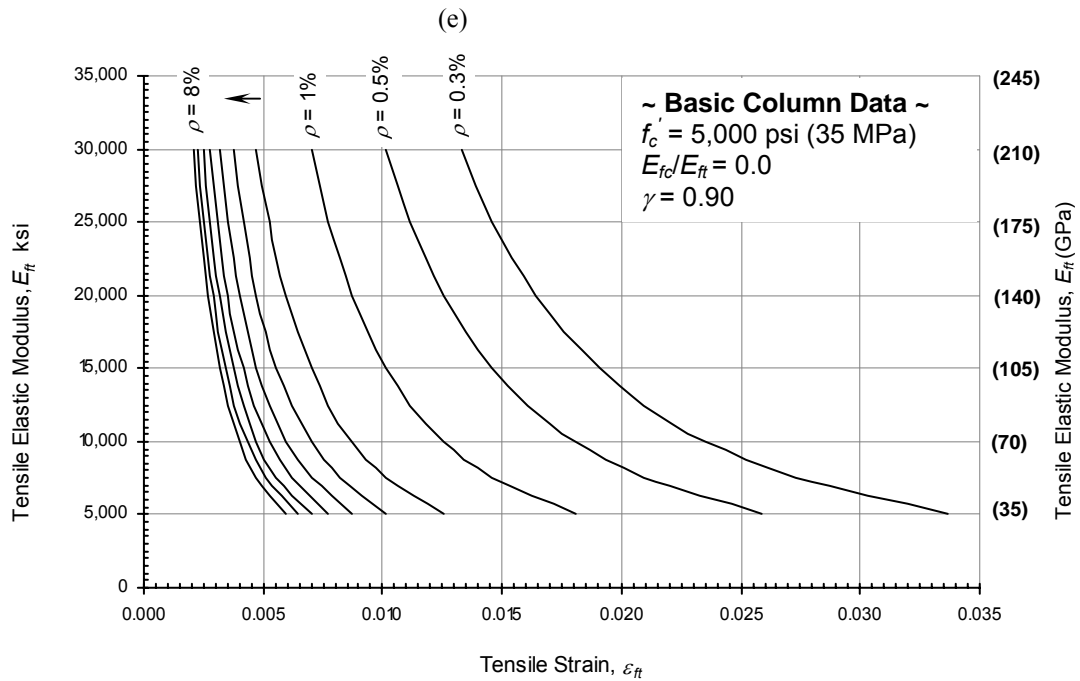
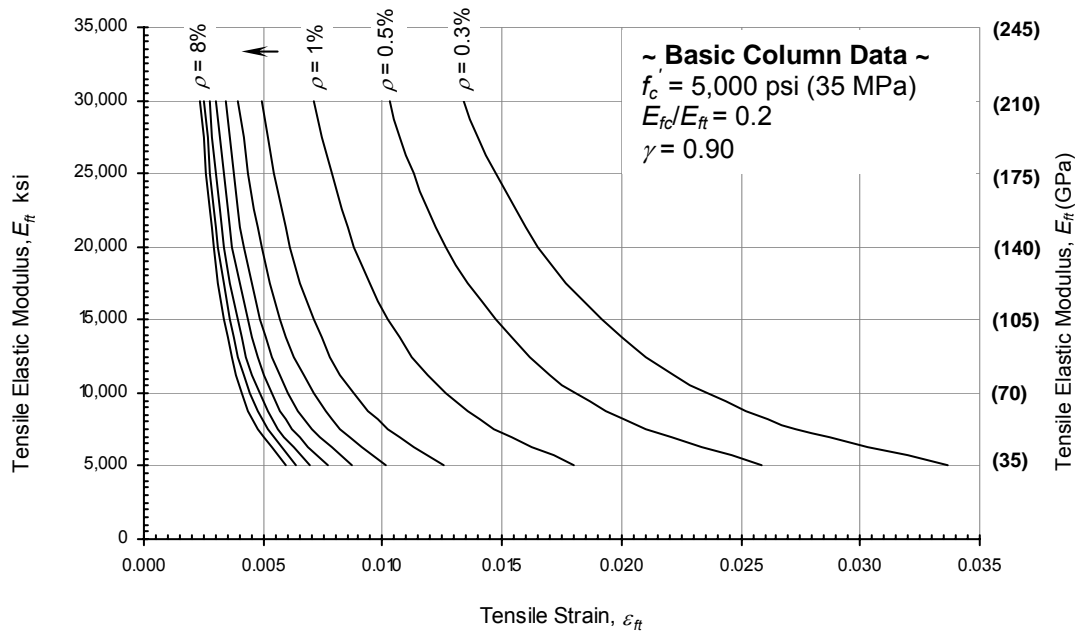
(b)

**Fig. 6.4 – Tensile elastic modulus-strain ( $E_{ft}$ - $\epsilon_{ft}$ ) interaction charts of concrete columns of rectangular shapes reinforced with FRP rebar having linearly-elastic stress/strain behavior.**



(d)

**Fig. 6.4 (Cont.) – Tensile elastic modulus-strain ( $E_{ft}$ - $\epsilon_{ft}$ ) interaction charts of concrete columns of rectangular shapes reinforced with FRP rebar having linearly-elastic stress/strain behavior.**



(f)

**Fig. 6.4 (Cont.) – Tensile elastic modulus-strain ( $E_{ft}$ - $\epsilon_{ft}$ ) interaction charts of concrete columns of rectangular shapes reinforced with FRP rebar having linearly-elastic stress/strain behavior.**

### 6.3.1 Influence of Concrete Compressive Strength ( $f_c'$ )

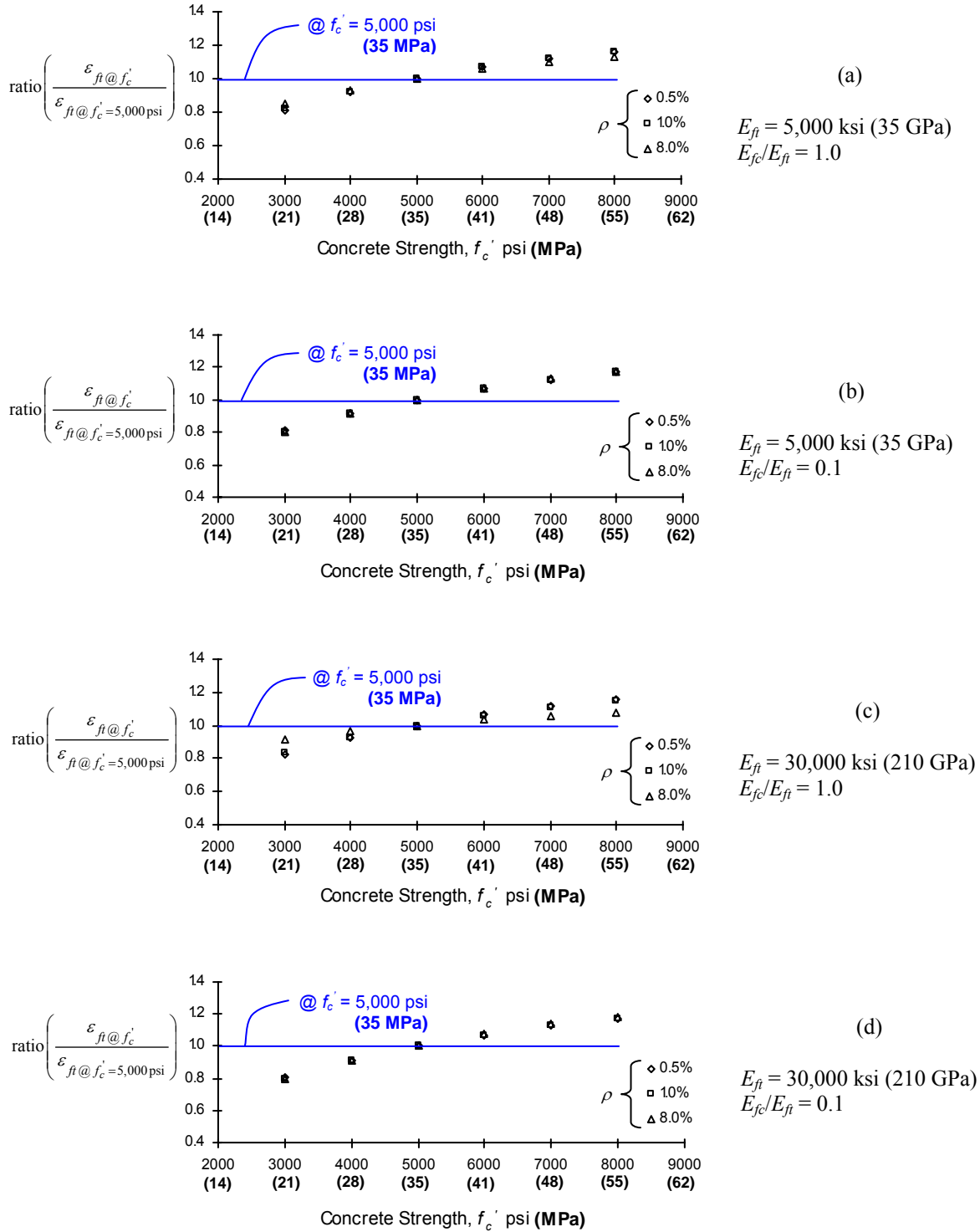
As indicated, the design aids provided in Fig. 6.4 are derived based upon two other parameters:  $f_c'$  and  $\gamma$ . The increase or decrease of concrete compression strength ( $f_c'$ ) has a significant effect on the magnitude of the tensile strain ( $\epsilon_{ft}$ ) developed at the outermost tensile reinforcement. For instance, when  $f_c'$  is reduced [with respect to  $f_c' = 5,000$  psi (35 MPa)], the tensile stresses and strains, and consequently forces, developed in the FRP rebar would also be reduced to maintain force equilibrium. In addition, reduction of  $f_c'$  results in reduction of the slope of the concrete stress-strain curve, and probable increase in creep.

Fig. 6.5 illustrates how concrete compression strength affects the magnitude of tensile strain at the outermost tensile layer of the reinforcement. The concrete compression strengths considered include 3,000 psi (21 MPa), 4,000 psi (28 MPa), 6,000 psi (41 MPa), 7,000 psi (48 MPa), and 8,000 psi (55 MPa), with 5,000 psi (35 MPa) as reference. The figure shows an increase in magnitude of tensile strain as concrete strength increases. Using 5,000 psi (35 MPa) concrete strength as a basis, a multiplier,  $\alpha_c$  can be developed for  $\epsilon_{ft}$  to accommodate concrete compression strengths other than 5,000 psi (35 MPa):

$$\begin{aligned} &\text{When } 3,000 \text{ psi} \leq f_c' < 5,000 \text{ psi} && \text{(or } 21 \text{ MPa} \leq f_c' < 35 \text{ MPa);} \\ \alpha_c = \frac{3,000 - 0.2f_c'}{2,000} \geq 1.0 && \text{or } \left( \frac{21 - 0.2f_c'}{14} \right) \geq 1.0 && (6.1) \end{aligned}$$

and

$$\begin{aligned} &\text{when } 5,000 \leq f_c' \leq 8,000 \text{ psi} && \text{(or } 35 \text{ MPa} \leq f_c' \leq 55 \text{ MPa)} \\ \alpha_c = \frac{3,750 - 0.15f_c'}{3,000} \leq 1.0 && \text{or } \left( \frac{25.25 - 0.15f_c'}{20} \right) \leq 1.0 && (6.2) \end{aligned}$$



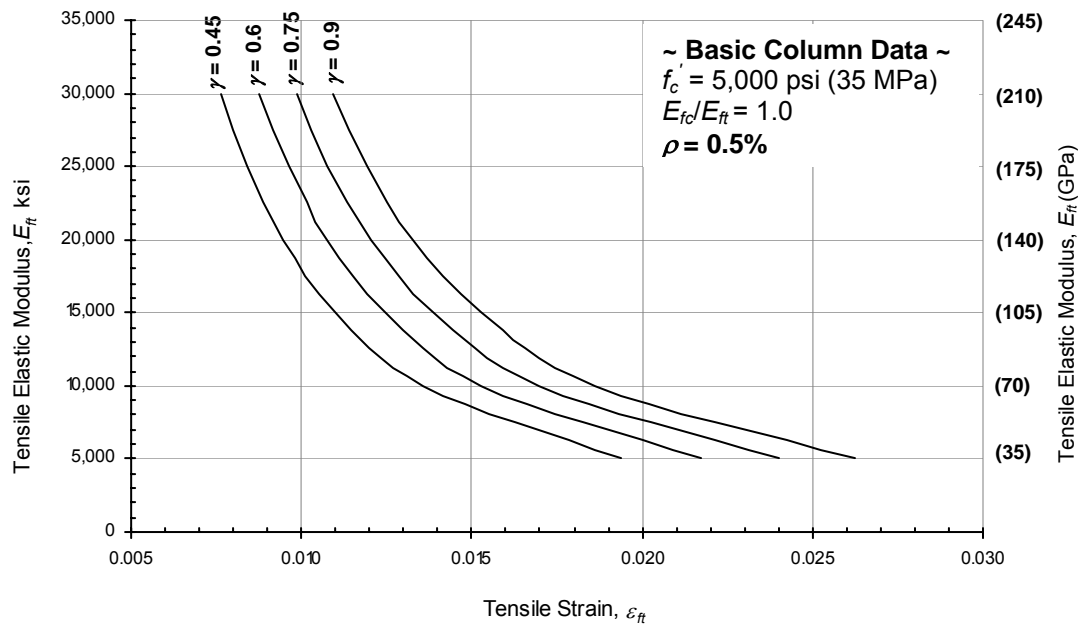
**Fig. 6.5 – The effect of concrete strength on reinforcement tensile strain.**

### 6.3.2 Influence of $\gamma$

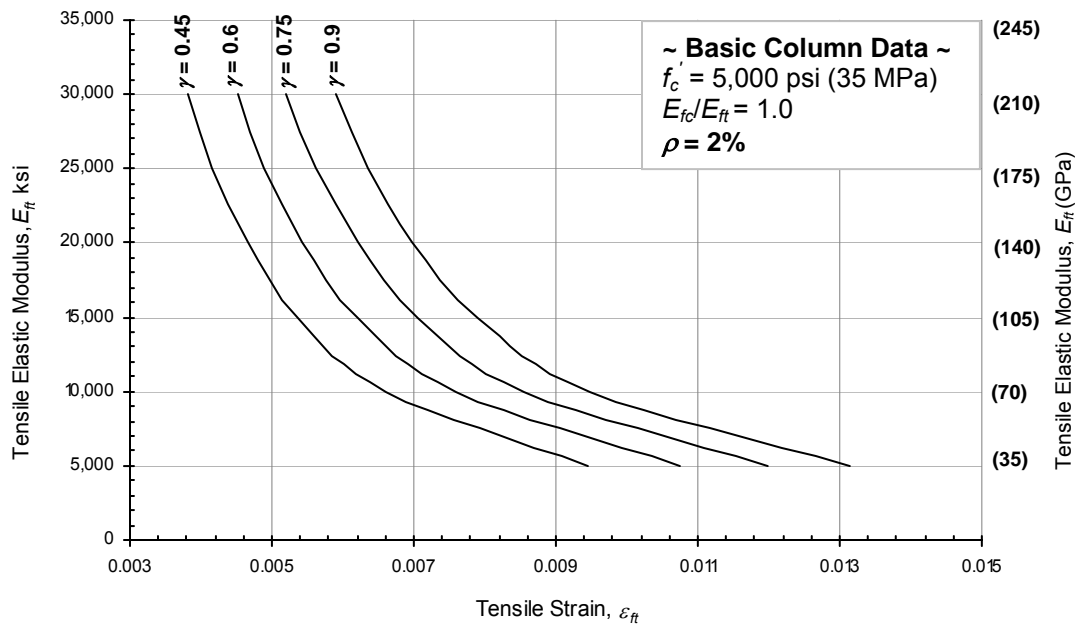
Fig. 6.6 shows how the  $E_{ft}$ - $\varepsilon_{ft}$  interaction curves are affected as  $\gamma$  varies from 0.9, 0.75, 0.6, to 0.45. The  $\gamma$  values chosen are the values used for steel reinforced column strength interactions in the ACI Committee 340 Design Handbook (1998).

As anticipated, with the other parameters held constant, the tensile strain ( $\varepsilon_{ft}$ ) at the outermost tensile layer of the reinforcement decreases as  $\gamma$  decreases. Graphically it can be observed that the  $E_{ft}$ - $\varepsilon_{ft}$  interaction curves shift to the left as  $\gamma$  decreases from 0.9 to 0.45 (Fig. 6.6). Eq. 6.3 can be used to relate the graphs of Figs. 6.4 with their  $\gamma$  value equal to 0.9 to other values of  $\gamma$ . Let  $\alpha_\gamma$  (Eq. 6.3) be a multiplier of  $\varepsilon_{fut}$  to obtain a modified  $\varepsilon_{fut}$  for use with Fig. 6.4:

$$\alpha_\gamma = 1.5 - 0.556\gamma \geq 1.0 \quad \text{when } 0.45 \leq \gamma \leq 0.9 \quad (6.3)$$



(a)  $\rho = 0.5\%$



(b)  $\rho = 2\%$

**Fig. 6.6 – The effect of  $\gamma$  on  $E_{ft}$ - $\epsilon_{ft}$  interaction.**



### 6.3.3 Influence of Long Term Concrete Loadings

The minimum reinforcement ratio of 1% set by ACI 318 was intended to prevent yielding of longitudinal steel rebar when load is transferred gradually from concrete to steel as concrete creeps under sustained axial load (ACI 318-02, Section R10.9.1). Similarly, the determination of  $\rho_{\min}$  in concrete columns with FRP rebar – a material that does not yield – must therefore include the long term effects such as creep and shrinkage. It has been shown in Chapter 3 that *brittle-tension* failures that do not occur when using short term load analyses may occur when long term effects are considered.

Two long term concrete loadings were introduced in Chapter 2. Detailed descriptions of both long term concrete models can be found in Chapter 2. In this section, only the *realistic long term* (RLT) concrete stress/strain model will be considered. The RLT model is intended to model *real* long term concrete behavior.

In general, long term concrete models postulate increase in concrete strain with time. The ACI maximum usable concrete compression strain ( $\epsilon_{cu}$ ) of 0.003 is almost doubled when the RLT model is considered with a maximum concrete shrinkage strain of 0.0012 (worst case scenario) and a concrete stress at service condition of  $0.45f'_c$ . Schematic stress-strain relationships for the instantaneous (ST) and the realistic long term (RLT) concrete loadings are repeated in Fig. 6.7. Analyses indicated that for concrete columns with low reinforcement ratio (e.g.  $\rho = 0.5\%$ ), the tensile strain would increase 17% to 23% for moduli of elasticity ranging from 5,000 to 30,000 ksi (35 to 210 GPa), and an increase of approximate 34% to 66% could be expected for high reinforcement ratio (e.g.  $\rho = 8\%$ ) using the same range of moduli of elasticity. This increase in strain, and hence stress, in FRP rebars is consistent with that occurs in steel reinforced concrete columns where creep and shrinkage cause stress redistribution leading to increase in the steel stress and a decrease in the concrete stress with time.

To estimate the change  $\alpha_L$  in  $\varepsilon_{fut}$  required due to the RLT concrete loading, the following expressions can be used:

For  $5,000 \text{ ksi} \leq E_{ft} \leq 30,000 \text{ ksi}$  (for  $35 \text{ GPa} \leq E_{ft} \leq 210 \text{ GPa}$ )

$$\alpha_L = 8 \times 10^{-11} E_{ft}^2 - 7 \times 10^{-6} E_{ft} + 0.764 \quad (\text{for } 2 \times 10^{-6} E_{ft}^2 - 1 \times 10^{-3} E_{ft} + 0.764) \quad (6.4)$$

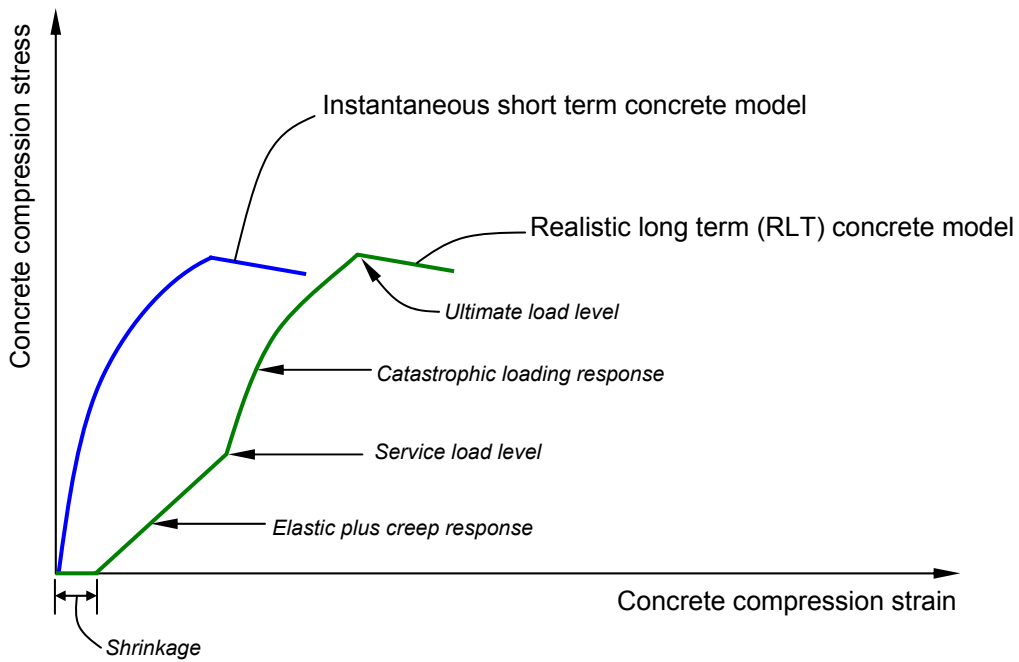


**Fig. 6.7 – Instantaneous (ST) and realistic long term (RLT) concrete stress/strain models.**

### 6.3.4 Application of the ( $E_{ft}$ - $\varepsilon_{ft}$ ) Interaction Design Aids

The  $E_{ft}$ - $\varepsilon_{ft}$  interaction aids shown in Fig. 6.4 can be used directly to obtain  $\rho_{f,min}$  for a column cross section given the materials (i.e. concrete and FRP rebars) and the cross sectional property (i.e.  $\gamma$ ) of a rectangular shape. To reflect the influence of the factors discussed previously, the ultimate tensile strain ( $\varepsilon_{fut}$ ) of a given FRP rebar shall be modified as follows:

$$\varepsilon_{fut}^* = \alpha_c \cdot \alpha_\gamma \cdot \alpha_L \cdot \varepsilon_{fut} \quad (6.4)$$

As noted, the  $\alpha_c$ ,  $\alpha_\gamma$ , and  $\alpha_L$  modification factors are unity when  $f_c'$  and  $\gamma$  are 5,000 psi (35 MPa) and 0.9, respectively, and when long term loading is not considered. The application of Eq. 6.4 coupled with the interaction design charts of Fig. 6.4 is demonstrated in Examples 6.1-6.3 in the following pages:

*Example 6.1:*

Using the appropriate  $E_{ft}$ - $\varepsilon_{ft}$  interaction aids in Fig. 3, determine the minimum reinforcement ratio required,  $\rho_{f,\min}$ , of a rectangular concrete column reinforced with GFRP rebars to prevent brittle-tension failure. Ignore long term loading.

Given:

$$f'_c = 5,000 \text{ psi (35 MPa)}$$

$$E_{fc} = 3.9 \times 10^3 \text{ ksi (28} \times 10^3 \text{ MPa)}$$

$$E_{ft} = 6.5 \times 10^3 \text{ ksi (46} \times 10^3 \text{ MPa)}$$

$$\varepsilon_{fuc} = 0.007 \text{ (0.7\%)}$$

$$\varepsilon_{fut} = 0.014 \text{ (1.4\%)}$$

$$\gamma = 0.9 \text{ (assumed)}$$

*Solution to Example 6.1:*

From the given material properties for GFRP rebars:

$$E_{fc}/E_{ft} = 3.9 \times 10^3 / 6.5 \times 10^3 = 0.6$$

The modification factors of  $\alpha_c$  and  $\alpha_\gamma$  are 1.0 and 1.0, respectively, or

$$\alpha_c = \frac{3,000 - 0.2f'_c}{2,000} = \frac{3,000 - 0.2(5,000)}{2,000} = 1.0 \quad \text{(from Eq. 6.1)}$$

or

$$\alpha_c = \frac{3,750 - 0.15f'_c}{3,000} = \frac{3,750 - 0.15(5,000)}{3,000} = 1.0 \quad \text{(from Eq. 6.2)}$$

$$\alpha_\gamma = 1.5 - 0.556(0.9) = 1.0 \quad \text{(from Eq. 6.3)}$$

$$\alpha_L = 1.0 \quad \text{(Ignored long term loading)}$$

The modified  $\varepsilon_{fut}^*$ :

$$\varepsilon_{fut}^* = \alpha_c \cdot \alpha_\gamma \cdot \alpha_L \cdot \varepsilon_{fut} = 1.0 \times 1.0 \times 1.0 \times 0.014 = 0.014$$

Based on  $E_{fc}/E_{ft}$ , Fig. 6.4.c is selected and is reproduced in Fig. 6.8:

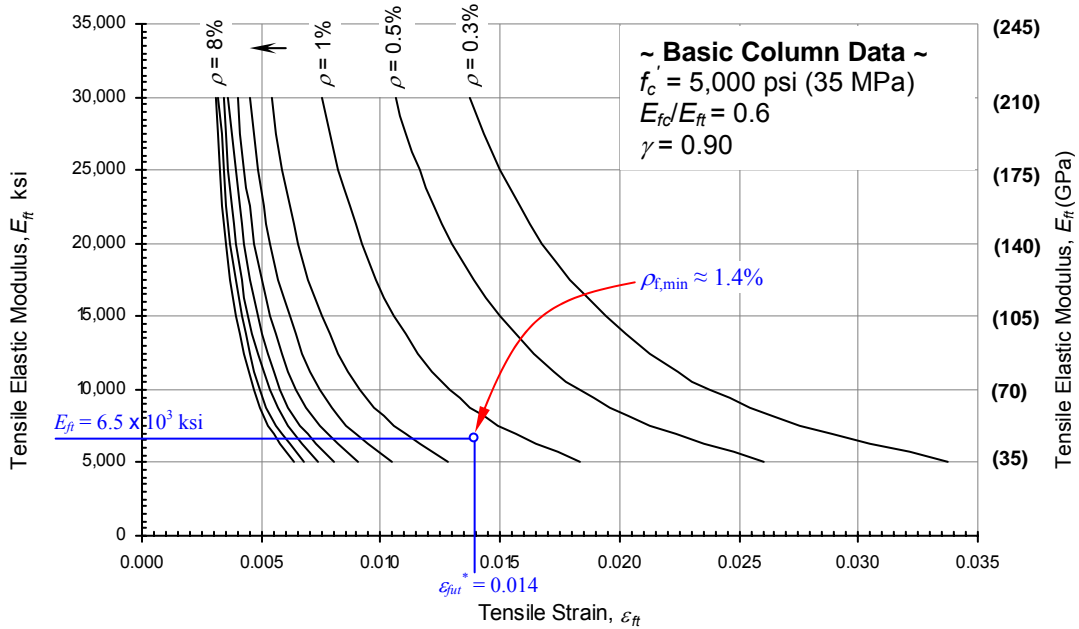


**Fig. 6.8 – (Fig. 6.4.c) Application of  $E_{ft}$ - $\varepsilon_{ft}$  graph for Example 6.1.**

Based on the combination of  $E_{ft} = 6.5 \times 10^3 \text{ ksi}$  ( $46 \times 10^3 \text{ MPa}$ ) and  $\varepsilon_{ft}^* = 0.014$ , enter Fig. 6.8:

$$\rho_{f,\min} \approx 1.40\% \text{ (from chart shown in Fig. 6.8)}$$

The minimum reinforcement ratio required can also be determined via analytical technique described in the text, which gives

$$\rho_{f,\min} \approx 1.35\% \text{ (Analytical solution).}$$

In this example, it can be concluded that direct interpolation of the interaction chart (with all modification factors equal unity in this case) produces accurate prediction of the minimum reinforcement ratio required.

*Example 6.2:*

Using the appropriate  $E_{ft}$ - $\varepsilon_{ft}$  interaction aids in Fig. 6.4, determine the minimum reinforcement ratio required,  $\rho_{f,\min}$ , of a rectangular concrete column in *Example 6.1* by replacing GFRP rebars with CFRP rebars to prevent *brittle-tension* failure. Ignore long term loading.

Given:

$$\begin{aligned}f_c' &= 6,000 \text{ psi (35 MPa)} \\E_{fc} &= 15.2 \times 10^3 \text{ ksi (108} \times 10^3 \text{ MPa)} \\E_{ft} &= 19.0 \times 10^3 \text{ ksi (135} \times 10^3 \text{ MPa)} \\ \varepsilon_{fuc} &= 0.008 \text{ (0.8\%)} \\ \varepsilon_{fut} &= 0.011 \text{ (1.1\%)} \\ \gamma &= 0.8 \text{ (assumed)}\end{aligned}$$

*Solution to Example 6.2:*

From the given material properties for CFRP rebars:

$$E_{fc}/E_{ft} = 15.2 \times 10^3 / 19.0 \times 10^3 = 0.8$$

The modification factors of  $\alpha_c$  and  $\alpha_\gamma$  are:

$$\alpha_c = \frac{3,750 - 0.15 f_c'}{3,000} = \frac{3,750 - 0.15(6,000)}{3,000} = 0.95 \quad \text{(from Eq. 6.2)}$$

$$\alpha_\gamma = 1.5 - 0.556(0.8) = 1.06 \quad \text{(from Eq. 6.3)}$$

$$\alpha_L = 1.0 \quad \text{(Ignored long term loading)}$$

The modified  $\varepsilon_{fut}^*$ :

$$\varepsilon_{fut}^* = \alpha_c \cdot \alpha_\gamma \cdot \alpha_L \cdot \varepsilon_{fut} = 0.95 \times 1.06 \times 1.0 \times 0.011 = 0.0111$$

Based on  $E_{fc}/E_{ft}$ , Fig. 6.4.b is selected and is reproduced in Fig. 6.9:

## 6.4 Effect of Internal Prestressing

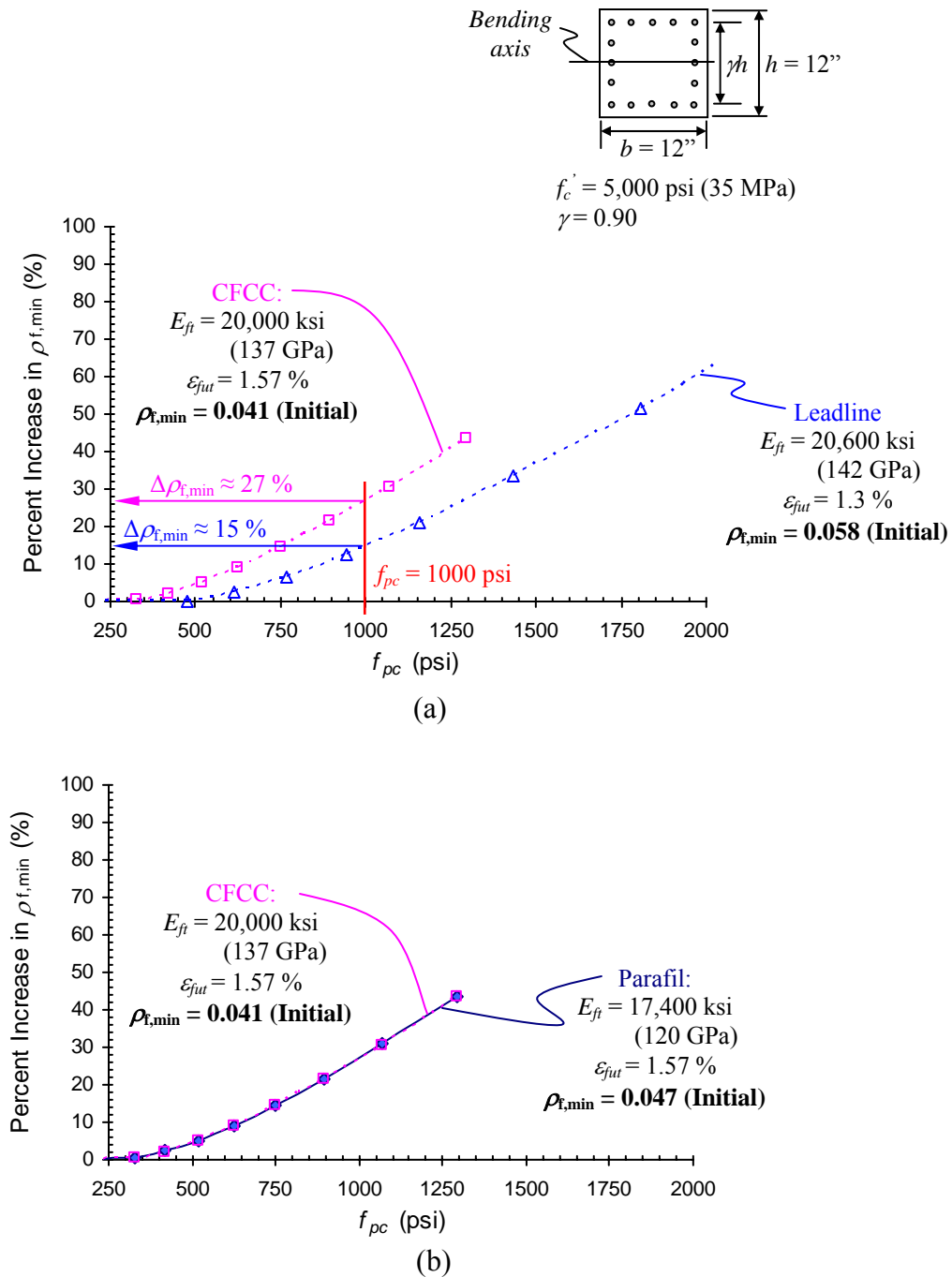


**Fig. 6.11 – Effect of prestressing on the minimum required reinforcement ratio.**

The strength interaction relations of concrete columns prestressed with FRP tendons were presented in Chapter 5. There it concluded that concrete columns prestressed with FRP tendons,

similar to concrete columns reinforced with FRP bars, could potentially experience *brittle-tension* failure. In addition, the likelihood of *brittle-tension* failure of such columns increased when the prestressing forces or stresses were increased. Therefore, to prevent *brittle-tension* failure for concrete columns prestressed with FRP tendons, a minimum required reinforcement ratio ( $\rho_{f,\min}$ ) should also be specified.

Fig. 6.11 is presented to show how prestressing affects the minimum required reinforcement ratio ( $\rho_{f,\min}$ ). The two CFRP tendons considered for illustrative purposes in Fig. 6.11.a are the CFCC and Leadline tendons (ACI 440.4R 2004). The initial  $\rho_{f,\min}$  of concrete columns prestressed with CFCC and Leadline tendons are 0.041 and 0.058, respectively. The initial  $\rho_{f,\min}$  for the columns were determined analytically based on the tendon properties (i.e.  $E_{ft}$  and  $\varepsilon_{fut}$ ) at zero internal pre-stress or zero concrete stress ( $f_{pc} = 0$ ). The initial  $\rho_{f,\min}$  must first be established because any subsequent increase in internal prestressing required a corresponding increase in the  $\rho_{f,\min}$  in order to preclude *brittle-tension* failure, and such phenomenon is illustrated in Fig. 6.11.

It is observed in Fig. 6.11.a that when concrete columns were internally-stressed with a minimum concrete stress of 250 psi (a minimum concrete stress required by ACI318-02), the required increases in the  $\rho_{f,\min}$  for concrete columns with CFCC and Leadline tendons were less than 1 %. It is worth pointing out that while both tendons have comparable modulus of elasticity of approximately 20,000 ksi ( $\approx 140$  GPa), the rates of increases for  $\rho_{f,\min}$  are markedly different. For example, at concrete stress ( $f_{pc}$ ) of 1,000 psi (6.895 MPa), the required increase of the initial  $\rho_{f,\min}$  for concrete column with CFCC tendons is approximately 27 %, whereas only approximately 15 % increase is required for concrete column with Leadline tendons (Fig. 6.11.a). In Fig. 6.11.b, while the modulus of elasticity for CFCC and Parafil tendons (ACI 440.4R 2004) are distinctly varied, the curves indicating the rates of increase for  $\rho_{f,\min}$  however are essentially the same, where both are overlapping.

Based on the above observations, it can therefore be concluded that internal prestressing not only will result in an increase to the minimum required reinforcement ratio ( $\rho_{f,\min}$ ) for



concrete columns prestressed with FRP tendons, the rate of increase for  $\rho_{f,\min}$  depends also on a multitude of factors such as FRP properties and the initial required reinforcement ratio. While no design aids were developed in this study, the analytical procedures for strength interactions presented in Chapter 5 can be used for the determination of  $\rho_{f,\min}$  for concrete columns prestressed with FRP tendons.

## 6.5 Summary and Conclusions

Strength interaction axial load-moment analyses were carried out on concrete columns with fiber reinforced polymer (FRP) rebars (see Chapters 3-6). They were performed based on equilibrium condition, strain compatibility, and material constitutive laws. One of the important findings related to these studies is the distinct possibility of these columns experiencing *premature compression* and/or *brittle-tension* failure. These failures occur when FRP reinforcements rupture prior to concrete reaches its pre-defined ultimate strain, and hence not realizing its full strength in compression. Predictably, either failure would result in loss of load bearing capacity, and worst of all, such failure would be sudden with not prior warning.

As stated in the introductory section of this chapter, the likelihood of *premature compression* failure is presumably smaller than that of *brittle tension* failure, since the ultimate compression strain ( $\varepsilon_{fuc}$ ) of a typical FRP rebar is generally many times larger than concrete ultimate strain ( $\varepsilon_{cu}$ ) in compression (i.e. ACI 318 (2002) assumes instantaneous ultimate concrete compression strain of 0.003). *Brittle tension* failure, on the other hand, would be more likely to occur since large tensile strain in rebars could develop particularly when columns are subjected to large bending.

Aiming at precluding potential *brittle tension* failure of concrete columns reinforced with FRP rebars, this chapter presents interaction design aids in form of tensile elastic modulus-tensile strain ( $E_{ft}$ - $\varepsilon_{ft}$ ) relations to determine the minimum required reinforcement ratio ( $\rho_{f,\min}$ ) to prevent such failure. The rational behind  $\rho_{f,\min}$  is to insure that the ultimate tensile strain ( $\varepsilon_{fut}$ ) of FRP rebars would not be exceeded at any time for any combination of axial load-moment ( $P$ - $M$ )

responses while allowing concrete to reach its pre-defined ultimate strain in compression (i.e. 0.003). Conceivably, if a reinforcement ratio ( $\rho_f$ ) greater than the minimum reinforcement ratio ( $\rho_{f,\min}$ ) is provided for the column then *brittle tension* failure can be averted.

Generally,  $\rho_{f,\min}$  is unique which depends on several controlling factors as previously described. Hence, to facilitate the determination of  $\rho_{f,\min}$ , interaction aids such as the ones shown in Fig. 6.4 have been developed for columns of rectangular shapes. The design aids were developed for tensile elastic moduli ( $E_{ft}$ ) of FRP rebars ranging from 5,000 to 30,000 ksi (35 to 210 GPa), covering most available FRP rebars. In addition, accounting for the prevailing factors that govern the finding of  $\rho_{f,\min}$ , modification factors (Eqs. 6.2-6.4) considering the concrete compressive strength ( $f'_c$ ), reinforcement layout ( $\gamma$ ), and long term concrete loading, have also been developed to be coupled with the use of these aids. Examples illustrating the use of these aids and factors were subsequently presented (see Examples 6.1-6.3).

The proposed aids offer the following advantages:

- Since the aids were developed based on ACI ultimate concrete compression strain, the analysis and design of concrete columns reinforced with FRP rebars once  $\rho_{f,\min}$  is determined can be carried out similarly to steel reinforced concrete columns without alteration to existing provisions (i.e. ACI 318-02).
- The aids provide a convenient mean of selecting the appropriate type of FRP rebars for specific use. For instance, if a particular type of FRP rebar requires a  $\rho_{f,\min}$  of greater than 6% of its columns, it implies that this specific FRP rebar type may lead to rebar congestion and other constructability related issues.

The following are the findings and reminders pertained to the use of design aids and modification factors ( $\alpha_\gamma$ ,  $\alpha_c$  and  $\alpha_L$ ):

- Direct use (adhering to the physical conditions presented in the aids) of the  $E_{ft}$ - $\epsilon_{ft}$  charts will provide accurate prediction of  $\rho_{f,\min}$ .

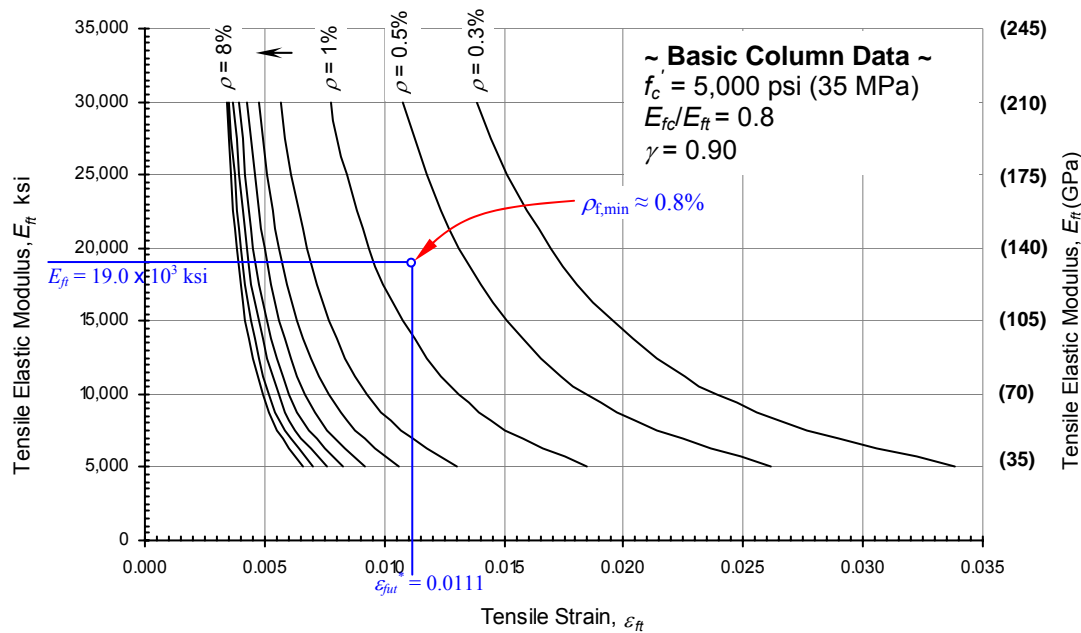


**Fig. 6.9 – (Fig. 6.4.b) Application of  $E_{ft}$ - $\varepsilon_{ft}$  graph for Example 6.2.**

Based on the combination of  $E_{ft} = 19.0 \times 10^3$  ksi ( $135 \times 10^3$  MPa) and  $\varepsilon_{ft}^* = 0.0111$ , enter Fig. 6.9:

$$\rho_{f,min} \approx 0.80\% \text{ (from chart shown in Fig. 6.9)}$$

The minimum reinforcement ratio required can also be determined via analytical technique described in the text, which gives

$$\rho_{f,min} \approx 0.76\% \text{ (Analytical solution).}$$

It can be observed that the use of the interaction chart and modification factors produces accurate estimate of the minimum reinforcement ratio required.

It should also be noted that the minimum reinforcement ratio required for concrete column reinforced with this particular CFRP rebar type is lower than the minimum specified in the ACI code for steel reinforced concrete columns.

Example 6.3:

Reconsider Example 6.2. Using the appropriate  $E_{ft}$ - $\epsilon_{ft}$  interaction aids in Fig. 6.4, determine the minimum reinforcement ratio required,  $\rho_{t,\min}$ , of a rectangular concrete column in Example 6.1 by replacing GFRP rebars with CFRP rebars to prevent *brittle-tension* failure. Long term loading is to be included.

Given:

$$\begin{aligned} f'_c &= 6,000 \text{ psi (35 MPa)} \\ E_{fc} &= 15.2 \times 10^3 \text{ ksi (108} \times 10^3 \text{ MPa)} \\ E_{ft} &= 19.0 \times 10^3 \text{ ksi (135} \times 10^3 \text{ MPa)} \\ \epsilon_{fuc} &= 0.008 \text{ (0.8\%)} \\ \epsilon_{fut} &= 0.011 \text{ (1.1\%)} \\ \gamma &= 0.8 \text{ (assumed)} \end{aligned}$$

Solution to Example 6.3:

From the given material properties for CFRP rebars:

$$E_{fc}/E_{ft} = 15.2 \times 10^3 / 19.0 \times 10^3 = 0.8$$

The modification factors of  $\alpha_c$  and  $\alpha_\gamma$  are:

$$\alpha_c = \frac{3,750 - 0.15 f'_c}{3,000} = \frac{3,750 - 0.15(6,000)}{3,000} = 0.95 \quad \text{(from Eq. 6.2)}$$

$$\alpha_\gamma = 1.5 - 0.556(0.8) = 1.06 \quad \text{(from Eq. 6.3)}$$

$$\begin{aligned} \alpha_L &= 8 \times 10^{-11} E_{ft}^2 - 7 \times 10^{-6} E_{ft} + 0.764 \\ &= 8 \times 10^{-11} (19,000)^2 - 7 \times 10^{-6} (19,000) + 0.764 = 0.66 \quad \text{(from Eq. 6.4)} \end{aligned}$$

The modified  $\epsilon_{fut}^*$ :

$$\epsilon_{fut}^* = \alpha_c \cdot \alpha_\gamma \cdot \alpha_L \cdot \epsilon_{fut} = 0.95 \times 1.06 \times 0.66 \times 0.011 = 0.0073$$

Based on  $E_{fc}/E_{ft}$ , Fig. 6.4.b is selected and is reproduced in Fig. 6.10:

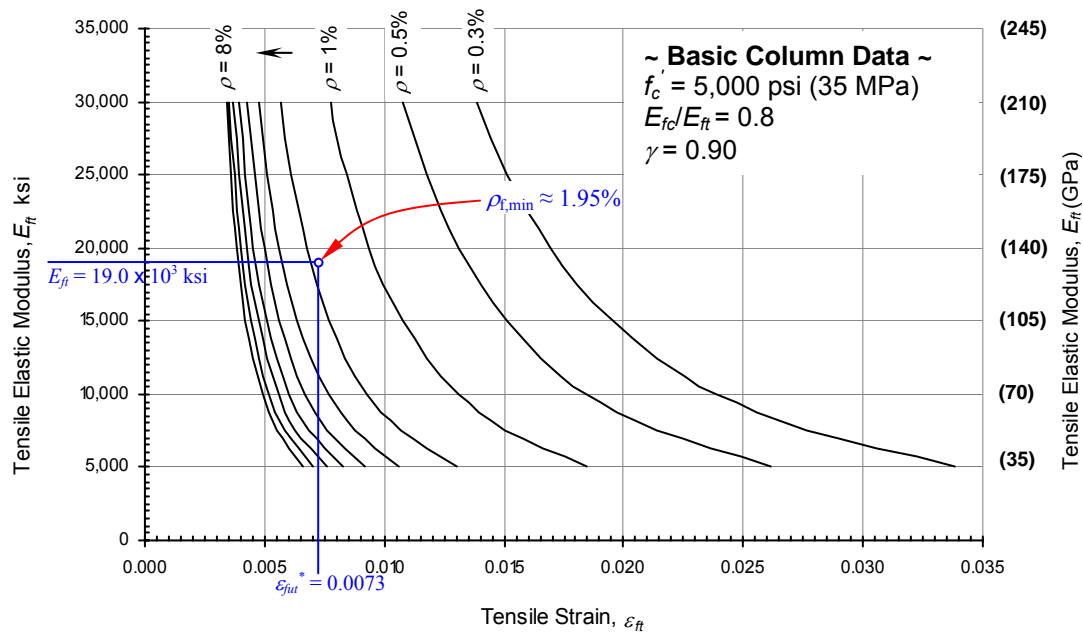


**Fig. 6.10 – (Fig. 6.4.b) Application of  $E_{ft}$ - $\epsilon_{ft}$  graph for Example 6.3.**

Based on the combination of  $E_{ft} = 19.0 \times 10^3$  ksi ( $135 \times 10^3$  MPa) and  $\epsilon_{ft}^* = 0.0073$ , enter Fig. 6.10:

$$\rho_{f,\min} \approx 1.95\% \text{ (from chart shown in Fig. 6.10)}$$

The minimum reinforcement ratio required can also be determined via analytical technique described in the text, which gives

$$\rho_{f,\min} \approx 1.15\% \text{ (Analytical solution).}$$

It can be observed that the use of the interaction chart and modification factors produce conservative estimate of the minimum reinforcement ratio required.

- The use of the  $\alpha_\gamma$  and  $\alpha_c$  modification factors or combination, which are related to the specific concrete compression strength and rebar layout, will produce reasonable estimate of  $\rho_{f,\min}$ . This is because the expressions (Eqs. 6.2 and 6.3) presented for estimating these particular changes were obtained at the lower bounds of variable data.
- The use of the  $\alpha_L$  reduction factor and/or in combination with other modification factors, will generally yield conservative estimate of  $\rho_{f,\min}$  because of the fact that the formulation of Eq. 6.4 was based on an assumed reinforcement ratio ( $\rho > 5\%$ ). As indicated previously, a relatively large reinforcement ratio would generally result in a greater increase in tensile strain. Additionally, because of highly unpredictability of creep and shrinkage in concrete, such conservatism is essential and desired in order to maintain a greater margin of safety from design standpoint.

Though it is rare, based on standard ACI assumptions, to have *premature-compression* rebar failure, the compression strain in the FRP rebar in columns should always be verified – the compression strain ( $\epsilon_{fc}$ ) developed at the reinforcement level should be much less than the ultimate compression strain ( $\epsilon_{fuc}$ ) of the FRP rebar to allow for creep and shrinkage. As a conservative measure, it is recommended that the ultimate compression strain ( $\epsilon_{fuc}$ ) of the FRP rebar should be at least twice and perhaps three times as large as the ACI maximum usable concrete compression strain (0.003).

The study of concrete columns prestressed with FRP tendons in prior section concluded that introducing internal prestressing to such columns required a corresponding increase in the minimum reinforcement ratio. It has also been demonstrated that such an increase depends largely on the material properties and the initial required minimum reinforcement ratio. While no design aids have been developed, the ones that derived for rectangular concrete columns reinforced with FRP bars, the analytical formulas presented in Chapter 5 can be used to evaluate and analyze the required reinforcement ratio of such columns.

## **CHAPTER 7**

### **SUMMARY AND CONCLUSION**

#### **7.1 Introduction**

The emergence of fiber reinforced polymer (FRP) composites as construction materials that are high-strength, light-weight, non-conductive and non-magnetic, etc., allows the engineers and designers to flexibly create new structures that are durable, and more importantly structures that devoid of inherent problems associated with steel construction such as corrosion. In addition to designing new structures, FRP composites are also becoming a popular choice for strengthening damaged structural components and upgrading structures.

#### **7.2 Summary and Conclusion of Chapters**

FRP composites in concrete construction are proving to be successful in a number of structural applications: as primary flexural and shear reinforcement in concrete beam elements, as concrete slab or bridge deck reinforcement, as prestressing reinforcement in concrete beams, slabs, and piles, as confinement reinforcement for column and pier in seismic applications, etc. Additional information on various other applications can be easily found in the literatures. For instance, ACI Committee 440 (2001) has compiled an impressive record of such information. There are also several guides readers can refer to for analysis, design, and testing of such materials. Chapter one of this dissertation compiles a list of applications involving FRP composites.

Albeit that massive effort has been devoted to research and promote the use of FRP composites, there is a lack of encouragement in regard to using FRP composites as compression reinforcements (i.e. as compression reinforcement in beams and columns). For instance, FRP rebars are not recommended (ACI 440 2001) for use as compression reinforcement, in part because the direct effect of compression reinforcement on the ultimate bending strength of concrete members is frequently small as in case of concrete beams, and therefore often ignored. Additionally, compression properties of FRP rebars are difficult to predict, and difficulties in

testing such as gripping and alignment, are hard to overcome. Moreover, lack of stability of individual fibers in rebar complicates testing and can produce erroneous measurements of compression properties. General information on material properties and testing of FRP composites is presented in Chapter Two of this dissertation.

Improved testing method and better understanding of compression behavior of FRP composites will eventually lead to their use as main compression reinforcement in concrete beams and columns. One of the objectives of this research study is to examine the behavior of concrete columns reinforced and/or prestressed with FRP rebars or tendons. Understanding and results of the analytical effort will lead to the other objective of this study which is to formulate design guide for such column members.

To accomplish the first objective, analytical approaches were presented in Chapters 3-5. These approaches were used to examine and understand the strength ( $P$ - $M$ - $\phi$ ) interaction of short and slender concrete columns with FRP rebars. Observations and findings in Chapters 3-5 related to the research effort are as follows:

Chapter 3: Column cross sectional (also referred to as short columns) strength ( $P$ - $M$ ) interaction analyses, based on equilibrium condition, strain compatibility, and material constitutive laws, were conducted. Analyses included examination of instantaneous column behavior and also consideration of concrete creep and shrinkage effects. The analytical results revealed that the strength interaction behavior of reinforced concrete reinforced with FRP rebars do not exhibit a “*balanced*” point (a point where a compression-controlled region transitions into tension-controlled region, or in the case of steel reinforced concrete columns, a point where concrete reaches its predefined ultimate strain in compression and steel reaches its yield simultaneously) similar to those of steel reinforced concrete columns based on current ACI specification. This is understandably so since FRP rebars in tension and in compression behave linearly-elastic until rupture, unlike steel which exhibits a well-defined yield point and plateau. In addition, the study also identified the possibility of FRP reinforced concrete columns experiencing



*pre-mature compression* or *brittle-tension* failure. These failures are associated with rupture of FRP in compression and tension before the concrete reached its pre-determined ultimate strain and hence not capitalizing its strength in compression. Furthermore, the tendency of either failure occurring grew increasingly great when concrete creep and shrinkage were considered. One significant advantage, in the absence of either failure, is the considerable gain in moment resistance by concrete columns reinforced with FRP rebars when compared to steel rebars of similar stiffness. This is especially beneficial for columns that are subjected to large bending.

Chapter 4: A numerical approach was presented in this chapter to study slender concrete columns reinforced with FRP rebars. The approach was first verified and applied to examine concrete columns reinforced with FRP rebars. Comparisons were made with concrete columns reinforced with steel rebars. While there were variations in column stiffness due to different FRP rebar types, the axial load-deflection and axial load-bending interaction pattern were nonlinear in nature and were in general very similar to that of steel reinforced concrete columns. As expected, the strength interactions of these columns were governed by the column length than other factors.

Chapter 5: The analytical procedures presented in Chapter 3 and 4 were extended with proper modification to include the effect of initial prestress to the study of prestressed concrete columns with FRP tendons. Parametric studies were carried out by considering the influence of effective prestress, concrete compression strength, reinforcement ratio, and long-term load effects. Similar to reinforced concrete columns, the study on prestressed concrete columns with FRP tendons identified two similar failure modes: *pre-mature compression* and *brittle-tension* failure. Previous studies in the literature have demonstrated that one significant advantage of concrete columns prestressing with steel tendons (e.g. 250 K and/or 270 K strands) was the gain of moment resistance at lower axial load level while sacrificing minimal axial capacity. This is viewed as positive when considerable

bending exists in the column. In the case of concrete columns with FRP tendons, such introduction of pre-strain may not be beneficial at times as it will reduce the overall capacity of such columns.

An attempt to formulate a design guide for concrete columns reinforced with FRP rebars was made in Chapter Six. In keeping with the philosophy that ACI 318 has established for years, design aids have been developed consistent with the assumptions used for steel reinforced concrete columns. One of such characteristics is the adoption of ACI ultimate concrete compression strain (or maximum usable strain) of 0.003 in deriving these aids. Another important feature in concrete compression member design according to the ACI code is the establishment of reinforcement ratio limits. For instance, the minimum reinforcement ratio [a ratio of reinforcement area over gross concrete area ( $\rho = A_s/A_g$ ) of 1%] is specified to ensure adequate resistance is provided for bending and for creep and shrinkage effects (ACI 318 2002). The maximum reinforcement ( $\rho = 8\%$ ) is specified for constructability reason where rebar congestion and concrete placement related issues are avoided. Developed along the same line of reasoning and taking into consideration the fact that FRP rebars are linearly-elastic, the following findings and observations are obtained:

Chapter 6: Design aids in the forms of tensile elastic modulus-tensile strain ( $E_{fr}-\varepsilon_{fr}$ ) charts have been developed for conveniently determine the minimum required reinforcement ratio ( $\rho_{f,min}$ ). The proposed approach using  $\rho_{f,min}$  aims at precluding *brittle-tension* failure, and resulting in a failure governs by concrete crushing (concrete strain in the outermost compression fiber reaches its ultimate). As documented in various research studies, FRP reinforced concrete elements which fail in concrete crushing exhibit more ductility and failure is more gradual. The design aids generated for rectangular shape column cross sections account for FRP rebars having tensile elastic moduli ranging from from  $5 \times 10^6$  psi to  $30 \times 10^6$  psi ( $35 \times 10^3$  MPa to  $210 \times 10^3$  MPa), covering most available FRP rebars. Several modification factors affecting the determination  $\rho_{f,min}$  of have also been developed to be coupled with the use of these design aids. Some of the

advantages of these aids are: (1) since the aids were developed with the use of assumptions consistent with ACI code, the analysis and design of concrete columns reinforced with FRP rebars once  $\rho_{f,\min}$  is determined can be carried out similarly to steel reinforced concrete columns without alteration to existing provisions; and (2) the aids provides an expedient mean of selecting the appropriate type of FRP rebars for use to meet design specifications. In general the use of design aids and modification factors would yield accurate estimate of the required  $\rho_{f,\min}$ . To account of unpredictability of creep and shrinkage in concrete, conservative estimate of  $\rho_{f,\min}$  using these aids is obtained. Such conservatism is warrant in order to maintain a greater margin of safety from design standpoint.

While no design aids were developed for concrete columns prestressed with FRP tendons, it has been concluded in the chapter that the analytical procedures presented in Chapter 5 can be used to evaluate the required reinforcement ratio for such columns.

### **7.3 Financial Viability of Fiber Reinforced Polymer**

Because of the inherent benefits (i.e. high-strength, corrosion resistance, low maintenance, long term durability, low thermal conductivity, etc.) and a wide variety of practical applications, the use of FRP in construction industry is expected to continually grow. Busel (2000) reported that the composites industry has grown approximately 460 % over the past 30 years; from 360,000 tons in 1970 to 1.68 million tons in 2000. And construction industry occupied approximately 21 % of the total volume of the composites shipments in the states (Busel 2000).

Applications that use FRP are expected to have higher construction costs than traditional concrete constructions; due to the high material cost of the FRP composites (Busel 2000; Hastak and Halpin 2000; and Ehlen 1999). As reported, the material, amongst others such as assembly, shipment, installation, etc., reflects the largest cost in most applications involving FRP

composites. Nystrom et al. (2003) reported that, at present state, the life-cycle costs of this material cannot be quantified with a great level of precision, due to the fact that most applications of FRP are still in their introductory phase. Nystrom et al. (2003) also pointed out that presently the applications of FRP in construction will only be limited to those applications where intangible benefits such as longer service life, reduced maintenance costs, reduced field installation, etc., can be justified.

#### **7.4 Future Research**

Part of the study was aimed towards understanding and characterizing the structural responses and failure mechanisms of concrete columns reinforced with FRP bars or prestressed with FRP tendons. The other part of the study represented an attempt towards establishing guidelines and design recommendations first of its kind. There are other related areas of research that need exploration and reinforcement. Other areas of research interests can be expanded to include, but not limited to, are:

- Experimental work supplementing the results and findings of current analytical investigation is desired; specifically, the failure mechanism from a brittle tension failure to concrete crushing through the alteration or modification of reinforcement ratio.
- While the focus of current investigation is affixed on rectangular shapes concrete columns, similar methodologies are believed to be equally applicable and can be extended to include concrete columns of irregular shapes.
- The buckling effect of individual bars in a concrete column may be examined along with spacing requirements for lateral reinforcement (i.e. ties and spirals).
- The nonlinear concrete stress/strain relations and the ACI-318 stress block used in current study are for normal-strength concrete (i.e. concrete strength in the range of 3,000 psi to 8,000 psi). Consideration and proper modification to current recommendations may be made to include higher-strength concrete (i.e. concrete strength in excess of 8,000 psi).

## Bibliography

ACI Committee 105. Reinforced Concrete Column Investigation – Tentative Final Report of Committee 105. ACI Journal, Proceedings V. 29, No. 5, Feb. 1933, pp. 275-282.

ACI Committee 318. Building Code Requirements for Structural Concrete (ACI 318-02) and Commentary (318R-02). American Concrete Institute, Farmington Hills, Mich., 2002. 443 pp.

ACI Committee 340, “ACI Design Handbook – Design of Structural Reinforced Concrete Elements in accordance with the Strength Design Method of ACI 318-95,” SP-17, 6<sup>th</sup> Ed., American Concrete Institute, Farmington Hills, Michigan. 1998.

ACI Committee 440. Prestressing Concrete Structures with FRP Tendons (ACI 440.4R-04). American Concrete Institute, Farmington Hills, Mich., 2003. 35 pp.

ACI Committee 440. Guide for the Design and Construction of Concrete Reinforced with FRP Bars (ACI 440.1R-03). American Concrete Institute, Farmington Hills, Mich., 2003. 42 pp.

Alagusundaramoorthy, P., Harik, I.E., and Choo, C.C., “Flexural Behavior of RC Beams Strengthened with Carbon Fiber Reinforced Polymer Sheets or Fabric,” *Journal of Composites for Construction*, American Society of Civil Engineers (ASCE), Vol. 7 No. 4, November 2003, pp. 292-301.

Alsayed, S.H., Al-Salloum, Y.A., Almusallam, T.H., and Amjad, M.A., “Concrete Columns Reinforced by GFRP Rods,” Fourth International Symposium – *Fiber Reinforced Polymer Reinforcement for Reinforced Concrete Structures*, ACI SP-188, 2000, pp. 103-112.

Amer, A., Arockiasamy, M., Shahawy, M., “Ultimate Strength of Eccentrically Loaded Concrete Columns Reinforced with CFRP Bars,” *Proceedings of the Conference on Advanced Composite Materials in Bridges and Structures*, Canada, 1996. pp. 209-216.

Ando, N., Matsukawa, H., Hattori, A., and Mashima, M., “Experimental Studies on the Long Term Properties of FRP Tendons,” *Non-Metallic (FRP) Reinforcement for Concrete Structures – Proceedings of the Third International Symposium on Non-Metallic (FRP) Reinforcement for Concrete Structures*, Vol. 2, Sapporo, Japan, October 14-16, 1997. pp. 203-210.

Arockiasamy, M. and Amer, A., “Studies on CFRP Prestressed Concrete Bridge Columns and Piles in Marine Environment,” Technical Report to Florida Department of Transportation, Tallahassee, FL, July 1998.

ASTM D695-2a “Standard Test Method for Compressive Properties of Rigid Plastic,” ASTM International, Vol. 08.01. 2003.

Branson, D.E. *Deformation of Concrete Structures*. The McGraw-Hill Companies, Inc., New York, N.Y., 1977.

Brown, M.C., “Corrosion Protection Service Life of Epoxy Coated Reinforcing Steel in Virginia Bridge Decks,” Doctoral Dissertation, Virginia Polytechnic Institute and State University, Blacksburg, Virginia. 2002.

Busel, J.P., ed. *Product Selection guide: FRP Composite Products for Bridge Applications*. Harrison, New York. 2000.

CALTRANS. *Seismic Design Criteria*. Department of Transportation, California, CA, 1999.

Choo, C.C., Gesund, H., and Harik, I.E., “Influence of Long Term Loads on Concrete Column Strength,” *Practice Periodical on Structural Design and Construction – American Society of Civil Engineers (ASCE)*, Vol. 8, No. 1, Feb. 2003, pp. 57-60.

Clemeña, G.G., “Investigation of the Resistance of Several New Metallic Reinforcing Bars to Chloride-Induced Corrosion in Concrete,” Interim Report (Report No. VTRC 04-R7), Virginia Transportation Research Council, Charlottesville, Virginia. Dec. 2002.

Clemeña, G.G., “Testing of Selected Metallic Reinforcing Bars for extending the Service Life of Future Concrete Bridges: Summary of Conclusions and Recommendations,” Final Report (Report No. VTRC 03-R7), Virginia Transportation Research Council, Charlottesville, Virginia. 2002.

Deitz, D.H., Harik, I.E., and Gesund, H., “One-way Slabs Reinforced with Glass Fiber Reinforced Polymer Reinforcing Bars,” *Fourth International Symposium – Fiber Reinforced Polymer Reinforcement for Reinforced Concrete Structures*, ACI International SP-188, Farmington Hills, MI. 1999.

Deitz, D.H., Harik, I.E., and Gesund, H., “Physical Properties of Glass Fiber Reinforced Polymer Rebars in Compression,” *Journal of Composites for Construction*, American Society of Civil Engineers (ASCE), Vol. 7 No. 4, November 2003, pp. 363-366.

Deniaud, C. and Cheng, J.J.R., “Reinforced Concrete T-Beams Strengthened in Shear with Fiber Reinforced Polymer Sheets,” *Journal of Composites for Construction*, American Society of Civil Engineers (ASCE), Vol. 7 No. 4, November 2003, pp. 302-310.

Dortzbach, J., “Carbon Fiber Reinforcing Polymers as Negative Moment Reinforcing in Repair of Composite Steel Parking Deck,” *Fourth International Symposium – Fiber Reinforced Polymer Reinforcement for Reinforced Concrete Structures*, ACI SP-188, 2000, pp. 417-428.

Ehlen, M.A., “Life-Cycle Costs of Fiber-Reinforced Polymer Bridge Decks,” *Journal of Materials in Civil Engineering*, American Society of Civil Engineers (ASCE), Vol. 11, No. 3, Aug. 1999, pp. 224-230.

El-Hacha, R., and Rizkalla, S.H., “Fundamental Material Properties of MMFX Steel Rebars,” Report submitted to MMFX Steel Corporation of America, July 2002, 59 p.

Ford, J.S., Chang, D.C., and Breen, J.E., "Behavior of Concrete Columns under Controlled Lateral Deformation," *ACI Journal*, V. 78, No. 1, Jan-Feb. 1981, pp. 3-20.

Fuyukama, H., Suzuki, H., and Nakamura, H., "Seismic Retrofit of Reinforced Columns by Fiber Sheet Wrapping without Removal of Finishing Mortar and Side Wall Concrete," *Fourth International Symposium – Fiber Reinforced Polymer Reinforcement for Reinforced Concrete Structures*, ACI SP-188, 2000, pp. 205-216.

Guadagnini, M., Pilkoutas, K., and Waldron, P., "Shear Design for Fiber Reinforced Polymer Reinforced Concrete Elements," *Fourth International Symposium – Fiber Reinforced Polymer Reinforcement for Reinforced Concrete Structures*, 1999, pp. 11-22.

Hamilton, H.R., Holberg, A., Caspersen, J., and Dolan, C.W., "Strengthening Concrete Masonry with Fiber Reinforced Polymer," *Fourth International Symposium – Fiber Reinforced Polymer Reinforcement for Reinforced Concrete Structures*, ACI SP-188, 2000, pp. 1103-1116.

Harik, I.E., and Gesund, H., "Reinforced Concrete Column in Biaxial Bending," *Concrete Frame Structures – Stability and Strength*, Elsevier Applied Science Publishers, London and New York. 1986.

Harik, I.E., Zhao, T., and Choo, C.C., "Preservation of Existing Bridges in Kentucky using Advanced Composites," *US-Japan Conference Paper*, Oct. 31 – Nov. 2, 2003, Japan.

Hastak, M., and Halpin, D.W., "Assessment of Life-Cycle Benefit-Cost of Composites in Construction," *Journal of Composites for Construction*, American Society of Civil Engineers (ASCE), Vol. 4, No.3, Aug. 2000, pp. 103-111.

Hill, C., Choo, C.C., and Harik, I.E., "Reinforcement Alternatives for Concrete Bridge Decks" *Research Report (KTC-03-19/SPR-215-00-1F)*, Kentucky Transportation Center and University of Kentucky, July 2003.



Hurley, M.F. and Scully, J.R., "Chloride Threshold Levels in Clad 316L and Solid 316LN Stainless Steel Rebar," CORROSION 2002, National Association of Corrosion Engineers (NACE), Paper No. 02224. 2002.

Iacobucci, R.D., Sheikh, S.A., and Bayrak, O., "Retrofit of Square Concrete Columns with Carbon Fiber-Reinforced Polymer for Seismic Resistance," *ACI Structural Journal*, Vol. 100, No. 6, Nov.-Dec. 2003. pp. 785-798.

Iyer, S.L. 1995. "Demonstration of Advanced Composite Cables for use as Prestressing in Concrete Waterfront Structures," Final Report submitted to U.S. Army Corps of Engineers, Construction Engineering Res. Lab. In Champaign, IL.

Iyer, S.L. and Lampo, R.G., "Demonstration of Advanced Composite Cables for Prestressing Applications in Concrete Waterfront Structures," *Construction Productivity Advancement Research (CPAR) Program*, US Army Corps of Engineers, USACERL Technical Report 98/33, 1998.

Iyer, S.L., Lampo, R., Hoy, D., and McCarthy, N., "First Navy Pier built in the USA using FRP Cables for Prestressing," Proceedings of the International Conference on FRP in Civil Engineering at IIT Madras, December 18-20, pp. 490-498, 1996.

Jaeger, L.G., Mufti, A., and Tadros, G., 1997, "The Concept of the Overall Performance Factor in Rectangular Section Reinforced Concrete Beams," Proceedings of the Third International Symposium on Non-Metallic (FRP) Reinforcement for Concrete Structures (FRPRCS-3), Japan Concrete Institute, Sapporo, Japan, V. 2, pp. 551-558.

Kawaguchi, N., "Ultimate Strength and Deformation Characteristics of Concrete Members Reinforced with AFRP Rods under Combined Axial Tension or Compression and Bending," *Fiber Reinforced Plastic Reinforcement for Concrete Structures*, ACI SP-138, MI, 1993. pp. 671-685.

Knoll, H., "NRC Studies Corrosion Inhibitors for Reinforcing Steel in Concrete," *The Ottawa Construction News*, Vol. 12 No. 11, IRC – National Research Council Canada. 2002.

Laoubi, K., "Compressive Properties of Isorod Glass Bars (#6) used as Reinforcement for Morristown Concrete Bridge Deck Slab (Morristown, Vermont, USA)," Summary Report. Dept. of Civil Engr., University of Sherbrooke, Quebec, Canada. 2002.

Logeman, R., Wheeler, W., Mensch, L., and Di Stasio, J., 1933, Discussion of "Report of Committee 105: Reinforced Concrete Column Investigation – Tentative Final Report of Committee 105, and Minority Recommendations for Design Formula of Reinforced Concrete Columns," *ACI Journal*, Proceedings V. 30, Sep.-Oct. 1933, pp. 78-90.

MacGregor, J.G. *Reinforced Concrete Mechanics and Design*. Prentice Hall, Upper Saddle River, New Jersey, N.J., 1997.

Masuo, K., "Seismic Retrofitting of Reinforced Concrete Columns with Wing Walls using Carbon Fiber Reinforced Plastic Walls," *Fourth International Symposium – Fiber Reinforced Polymer Reinforcement for Reinforced Concrete Structures*, ACI SP-188, 2000, pp. 193-204.

Mirmiran, A., Yuan, W.Q., and Chen, X.B., "Design for Slenderness in Concrete Columns Internally Reinforced with Fiber Reinforced Polymer Bars," *ACI Structural Journal*, Vol. 98, No. 1, Jan.-Feb. 2001, pp. 116-125.

Mutsuyoshi, H., Ishibashi, T., Okano, M., and Katsuki, F., "New Design Method for Seismic Retrofit of Bridge Columns with Continuous Fiber Sheet – Performance-Based Design," *Fourth International Symposium – Fiber Reinforced Polymer Reinforcement for Reinforced Concrete Structures*, ACI SP-188, 2000, pp. 229-242.

Nanni, A., "Flexural Behavior and Design of Reinforced Concrete Using FRP rods," *Journal of Structural Engineering*, V. 119, No. 11, pp. 3344-3359, 1993.

Nawy, E.G. Reinforced Concrete – A Fundamental Approach. 3<sup>rd</sup> Ed. Prentice Hall, Upper Saddle River, New Jersey, N.J., 1996.

Nawy, E.G. Prestressed Concrete: A Fundamental Approach. 2<sup>nd</sup> Ed. Prentice Hall, Inc., Upper Saddle River, NJ., 1996.

Nilson, A.H. Design of Concrete Structures. The McGraw-Hill Companies, Inc., New York, N.Y., 1997.

Nystrom, H.E., Watkins, S.E., Nanni, A., and Murray, S., (2003), “Financial Viability of Fiber-Reinforced Polymer (FRP) Bridges,” *Journal of Management in Engineering*, American Society of Civil Engineers (ASCE), Vol. 19, No. 1, Jan. 2003, pp. 2-8.

Pape, J. and Fanous, F., “Impact of Bridge Deck Cracking on Durability,” *Transportation Conference Proceedings*. 1998.

Paramanatham, N.S., “Investigation of the Behavior of Concrete Columns Reinforced with Fiber Reinforced Plastic Re-bars,” MS thesis, Lamar University, Beaumont, TX, 1993.

PCI Industry Handbook Committee. PCI Design Handbook – Precast and Prestressed Concrete. 5<sup>th</sup> Ed. Precast/Prestressed Concrete Institute. 1999.

Richart, F., 1933, Discussion of “Report of Committee 105: Reinforced Concrete Column Investigation – Closure by Chairman, Committee 105,” *ACI Journal*, Proceedings V. 30, Nov.-Dec. 1933, pp. 153-156.

Richart, F., Bertin, R., and Lyse, I., 1933, “Reinforced Concrete Column Investigation – Tentative Final Report of Committee 105, and Minority Recommendations for Design Formula of Reinforced Concrete Columns,” *ACI Journal*, Proceedings V. 29, No. 6, Feb. 1933, pp. 275-284.

Rosenberg, A., "How to Prevent Corrosion in Precast Concrete," Technical Section – *Manufactured Concrete*, National Precast Concrete Association, Indianapolis, IN. 1999.

Schiebel, S., and Nanni, A. 2000. "Axial and Flexural Performance of Concrete Piles Prestressed with CFRP Tendons," Proceedings of the Third International Conference on Advanced Composite Materials in Bridges and Structures, Ottawa, Canada, August, pp. 471-478.

Seki, H., Sekijima, K., and Konno, T., "Test Method on Creep of Continuous Fiber Reinforcing Materials," Non-Metallic (FRP) Reinforcement for Concrete Structures – Proceedings of the Third International Symposium on Non-Metallic (FRP) Reinforcement for Concrete Structures, Vol. 2, Sapporo, Japan, October 14-16, 1997. pp. 195-202.

Schiebel, S. and Nanni, A., "Axial and Flexural Performance of Concrete Piles Prestressed with CFRP Tendons," Proceedings of the Third International Conference on Advanced Composite Materials in Bridges and Structures, Ottawa, Canada, August 2000, pp. 471-478.

Sheikh, S.A., and Yau, G., "Seismic Behaviour of Concrete Columns Confined with Steel and Fiber-Reinforced Polymers," *ACI Structural Journal*, Vol. 99, No. 1, Jan.-Feb. 2002. pp. 72-80.

Singhvi, A., and Mirmiran, A., "Creep and durability of Environmentally Conditioned FRP-RC Beams Using Optic Sensors," *Journal of Reinforced Plastics and Composites*, V. 21, No. 4, 2002. pp. 351-373.

Sohanghpurwala, A.A. and Scannell, W.T., "Condition and Performance of Epoxy-Coated Rebars in Bridge Decks," *Public Roads*, Federal Highway Administration, Washington D.C. 1999.

Tacchino, J.b. and Brown, V.L., "Design of T-Beams with Internal Fiber Reinforced Concrete Elements," *Fourth International Symposium – Fiber Reinforced Polymer Reinforcement for Reinforced Concrete Structures*, 1999, pp. 1-10.

Tavakkolizadeh, M. and Saadatmanesh, H., "Repair of Damaged Steel-Concrete Composite Girders using Carbon Fiber-Reinforced Polymer Sheets," *Journal of Composites for*

*Construction*, American Society of Civil Engineers (ASCE), Vol. 7 No. 4, November 2003, pp. 311-322.

Theriault, M. and Benmokrane, B., 1998, "Effect of FRP Reinforcement Ratio and Concrete Strength on Flexural Behavior of Concrete Beams," *Journal of Composites for Construction*, V. 2, No. 1, pp. 7-16.

Thomas, M., "Determining the Corrosion Resistance of Steel Reinforcement for Concrete," Correspondence note to MMFX Technologies, University of New Brunswick, Fredericton, NB, Canada. 2002.

Vandeveldade, C.E. The Behavior of Long, Hinged End Reinforced Concrete Columns under Sustained Axial Load and Biaxial Bending. MS Thesis, University of Kentucky, Lexington, KY. 1968.

Wang, C.K. and Salmon, C.G. (1998). *Reinforced Concrete Design*. 6<sup>th</sup> Ed. Addison-Wesley Longman, Inc.

Wiolet, A. P., Weyers, R.E., Weyers, R.M., Mokarem, D.W., Zemajtis, J., Sprinke, M.M., and Dillard, J.G., "Field Performance of Epoxy-Coated Reinforcing Steel in Virginia Bridge Decks," Final Report (VTRC 00-R16), Virginia Transportation Research Council, Charlottesville, Virginia. 2000.

Yamaguchi, T., Kato, Y., Nishimura, T., and Uomoto, T., "Creep Rupture of FRP Rods Made of Aramid, Carbon and Glass Fibers," *Non-Metallic (FRP) Reinforcement for Concrete Structures – Proceedings of the Third International Symposium on Non-Metallic (FRP) Reinforcement for Concrete Structures*, Vol. 2, Sapporo, Japan, October 14-16, 1997. pp. 179-186.

Zhao, T., Zhang, C.J., and Xie, J., "Study and Application on Strengthening the Cracked Brick Walls with Continuous Carbon Fibre Sheet," *Advanced Polymer Composites for Structural Applications in Construction*, Proceedings of the 1<sup>st</sup> International Conference, University of Southampton, UK. 2002.

Zou, X.W.P., "Long-Term Properties and Transfer Length of Fiber-Reinforced Polymers," *Journal of Composites for Construction*, American Society of Civil Engineers (ASCE), Vol. 7 No. 4, February 2003, pp. 10-19.

Zou, X.W.P., "Flexural Behavior and Deformability of Fiber Reinforced Polymer Prestressed Concrete Beams," *Journal of Composites for Construction*, American Society of Civil Engineers (ASCE), Vol. 7 No. 4, November 2003, pp. 275-284.

## VITA

Name: Ching Chiaw Choo

Date of Birth: November 21, 1972

Place of Birth (City, State, Country): Kuching, Sarawak, Malaysia

Educations: Inti College Sarawak (1993-1995)  
Sarawak, Malaysia

B.S. in Civil Engineering (1995-1997)  
University of Kentucky  
Lexington, KY

M.S. in Civil Engineering (1997-1999)  
University of Kentucky  
Lexington, KY

*Ching Chiaw Choo*

March 23, 2005